FINAL TECHNICAL REPORT

NASA GRANT NAG3-869

STUDIES OF THE KINETICS AND MECHANISMS OF PERFLUOROETHER REACTIONS ON IRON AND OXIDIZED IRON SURFACES

Mary E. Napier
Peter C. Stair

Department of Chemistry
Northwestern University
Evanston, Illinois 60208-3113

ABSTRACT

Polymeric perfluoroalkylethers are being considered for use as lubricants in high temperature applications, but have been observed to catalytically decompose in the presence of metals. X-ray photoelectron spectroscopy (XPS) and temperature programmed desorption (TPD) were used to explore the decomposition of three model fluorinated ethers on clean polycrystalline iron surfaces and iron surfaces chemically modified with oxygen. Low temperature adsorption of the model fluorinated ethers on the clean, oxygen modified and oxidized iron surfaces was molecular.

Thermally activated defluorination of the three model compounds was observed on the clean iron surface at remarkably low temperatures, 155 K and below, with formation of iron fluoride. Preferential C-F bond scission occurred at the terminal fluoromethoxy, CF_3O, of perfluoro-1-methoxy-2-ethoxy ethane and perfluoro-1-methoxy-2-ethoxy propane and at CF_3/CF_2O of perfluoro-1,3-diethoxy propane. The reactivity of the clean iron toward perfluoroalkylether decomposition when compared to other metals is due to the strength of the iron fluoride bond and the strong electron donating ability of the metallic iron.

Chemisorption of an oxygen overlayer lowered the reactivity of the iron surface to the adsorption and

decomposition of the three model fluorinated ethers by blocking active sites on the metal surface. Incomplete coverage of the iron surface with chemisorbed oxygen results in a reaction which resembles the defluorination reaction observed on the clean iron surface.

Perfluoro-1-methoxy-2-ethoxy ethane reacts on the oxidized iron surface at 138 K, through a Lewis acid assisted cleavage of the carbon oxygen bond, with preferential attack at the terminal fluoromethoxy, CF_3O. The oxidized iron surface did not passivate, but became more reactive with time. Perfluoro-1-methoxy-2-ethoxy propane and perfluoro-1,3-diethoxy propane desorbed prior to the observation of decomposition on the oxidized iron surface.

Acknowledgments

First I would like to thank my research advisor, Peter Stair for his support, advice and guidance. From start to finish, it has been a long and winding road. Thanks for keeping me pointed in the right direction, for the most part.

Next I want to thank all of my coworkers, past and present, who have provided the support and friendship I needed to see me through the good times and the bad. Special mention most certainly has to go to Michele, who showed me how to eat like a kid again, to Karen and Simon for all of the wonderful meals and hours of conversation, to my old neighbor to the North, Paul, who tried moving a thousand miles away to no avail. We still track you down and make you listen to all of our problems. You can run, but you cannot hide. To the comedy team of Mitch and Vic, I just have one thing to say, ***Be Quiet!!!*** To Howard, please slow down because you are making me dizzy. To the new group members, Karen and Michelle, hang in there. If I made it, you can to. Additional thanks have to go to Mitch, who is a great friend and provided a much welcomed shoulder to cry on, especially while Mike was in California. I wish you and Debbie all the best. You deserve it and much more.

My graduate school support group, Susan, Wade, Jack, Julie, Diana, Pete and the newest member, Vickie deserve

heaps of praise for their ability to listen, to discuss and to solve the problems of the world or at least Northwestern. Some members of the group were better at the listening part than others, but I wont mention any names. My favorite memories of graduate school will be about you and the great times we had. Special thanks also have to go to Julie, who has had to put up with me for the last few months. Julie you are a saint.

Thanks to my grandparents, Marion and Steve, my parents, Don and Carol, to my sisters, Karen, Susan and Lori and my brother, Mike. You always believed in me and I truly appreciate your love and understanding.

I do not possess the ability to make the written word express the strength of my love for and the depth of my gratitude to my husband Mike. With out his support, love and understanding none of this would have been possible and the future would not look as promising. Thank you for standing by me.

Table of Contents

List of Tables

List of Figures

CHAPTER I

INTRODUCTION

A. ORGANIZATION OF THE THESIS

Chapter I is a brief introduction describing the model fluorinated ether/metal systems studied and the objectives of the thesis work. Also included is a brief review of the relevant polymeric perfluoroalkylether and model fluorinated ether literature. Chapter II describes the surface characterization techniques used in the thesis research. Chapter III discusses the effect of x-ray flux on model fluorinated ether layers adsorbed on iron surfaces. Chapter IV and V describe the thermally activated decomposition of the three model fluorinated ethers on atomically clean iron surfaces and iron surfaces chemically modified with oxygen, respectively. Chapter VI describes the experimental results for two additional model fluorinated ether compounds adsorbed on room temperature nickel, chromium and iron surfaces. Chapter VII gives a general summary of the work described in this thesis. Given in Appendix A is a description of the Teknivent software used to control the Balzer mass spectrometer.

B. PREPARATION OF PERFLUOROALKYLETHERS

1. Polymeric compounds

The most widely known and used, commercially available polymeric perfluoroalkylethers are Fomblin Z, Fomblin Y, Krytox and Demnum. Representative structural formulae are

shown in Figure 1.1. Fomblin Y and Z are prepared by photo-oxidation of tetrafluoroethylene and hexafluoropropylene, respectively.[1-3] Individual oxide units are randomly distributed within each linear chain, in the ratios indicated in Figure 1.1 a and b. Krytox and Demnum are synthesized through a base catalyzed polymerization of perfluoropropylene oxide and trifluoromethylene oxide, respectively.[3,4]

2. Model Compounds

The model fluorinated ethers investigated in this research were prepared by direct fluorination of the corresponding hydrocarbon ether, using the LeMar process.[5,6] The hydrogen containing material is placed in a reaction chamber and the chamber is then purged with an inert atmosphere such as helium or nitrogen. Fluorine gas is introduced in the reaction chamber in a low concentration relative to the inert environment. The temperature is monitored to determine the extent of fluorination. The fluorine concentration is gradually increased over time, until total fluorination is achieved. The LeMar process allows for control of the highly exothermic fluorination reaction. By limiting the amount of fluorine available, the reaction is slowed, heat evolution controlled and heat dissipation is possible. This minimizes the thermal degradation and skeletal fragmentation of the material.

a) Fomblin Z

$$CF_3-O-(CF_2-CF_2-O)_m-(CF_2-O)_n-CF_3$$

m/n=2/3

b) Fomblin Y

$$CF_3-O-(\underset{\displaystyle F}{\overset{\displaystyle CF_3}{C}}-CF_2-O)_m-(CF_2-O)_n-CF_3$$

m/n=40/1

c) Krytox

$$CF_3-CF_2-CF_2-O-(\underset{\displaystyle F}{\overset{\displaystyle CF_3}{C}}-CF_2-O-)_m-CF_2-CF_3$$

d) Demnum

$$CF_3-CF_2-CF_2-O-((CF_2)_3-O)_m-CF_2-CF_3$$

Figure 1.1 Representative structural formulae for commercially available polymeric perfluoroalkylethers a) Fomblin Z b) Fomblin Y c) Krytox and d) Demnum.

C. POLYMERIC PERFLUOROALKYLETHERS

This discussion is a general review of the properties and the reactivity of the commercially available, polymeric perfluoroalkylether materials.

1. Properties of Polymeric Materials

Polymeric perfluoroalkylethers possess physical and chemical properties, which make them attractive for use as lubricants in high temperature applications. The desirable properties are excellent thermal, chemical and oxidative stabilities, wide liquid range, good lubricity, excellent shear stability and nonflammablity.[1,2,4,7,8] The undesirable properties are a bulk modulus significantly less than other functional fluids, a density double that of other lubricants, incompatibility with many metals and the inability to dissolve conventional anti-wear and anti-oxidant additives.[1-4,7-11] Typical, commercially used polymeric materials are shown in Figure 1.1.

2. Compatibility with Metal Oxides/Lewis Acids

The oxidative, chemical and thermal stabilities of these polymeric materials were initially evaluated using micro-oxidation corrosion tests.[1-3,7-9] The following is a description of a micro-oxidation test. A degradation tube containing a specified volume of a polymeric fluid and a metal coupon, if applicable, was evacuated. Depending upon the desired information, the test could be run under vacuum

or under a specified atmosphere of known pressure. The degradation tube was inserted into a preheated box furnace or oil bath for a set amount of time. After removal from the heat source, the tube is allowed to cool to room temperature, attached to a high vacuum line and opened. Liquid nitrogen condensibles and non-condensibles were collected, weighed and analyzed using the appropriate techniques. Production of volatiles, oxygen consumption, metal corrosion, changes in the fluid viscosity and the fluid molecular weight were the criteria applied to determine the extent of degradation. The metal coupons used were polished and cleaned prior to insertion into the tube, but had an oxide layer due to room temperature, atmospheric exposure.

In an inert, metal-free environment, the branched fluids are stable to approximately 380°C and the linear fluids to approximately 320°C.[1-3,7-9] In an oxidative, metal-free environment, the branched fluids are stable to approximately 320°C and the linear fluids to approximately 260°C.[1-3,7-9] The branched fluids possess better oxidative and thermal stabilities than the linear fluids, but have a liquid range which is significantly smaller. The branched fluids show poor viscosity properties at low temperatures and excessive evaporation at high temperatures.[8] Both the linear and the branched fluids possess characteristics which

limit their usefulness in a high temperature lubrication situation. In the absence of metals, the degradation mechanism is a free radical type.[1] The initiation reaction is followed by β scission and propagation. The C-C bond is the weakest in the molecule and when broken the whole molecule decomposes with evolution of gaseous products. Under oxidizing conditions the main product is COF_2. The physical properties of the bulk of the fluid remain unchanged after heating.

The degradation of both the linear and branched polymeric fluorinated ethers is accelerated by the presence of metal coupons in the micro-oxidation corrosion tests, under both inert and oxidizing environments.[1-3,7-9] The metal coupons were polished and cleaned prior to insertion into the micro-oxidation tube, but had an oxide layer due to room temperature, atmospheric exposure. Just as in the metal free test, the degradation in the presence of metals is more severe in an oxidizing environment, although an oxygen environment is not required for the decomposition of the polymeric materials to occur in the presence of the metal coupons.

For the polymeric structures shown in Figure 1.1, there were several constants in the micro-oxidation results in the presence of metal coupons. The decomposition was characterized by the evolution of reactive degradation

products, weight change in the metal coupon and formation of metal fluoride on the coupon surface.[1-3,7-9,12] The branched polymeric materials were less reactive than the linear, under the same reaction conditions.[12] The volatile degradation products converted the metal oxide to the more reactive fluoride, and the rate of degradation increased with time.

Fomblin Z (Fig 1.1a) has been reported to react with both iron oxide and aluminum oxide at 185°C, approximately 100°C lower than the decomposition temperature reported in the metal free, oxidizing environment.[12,13] The micro-oxidation test was carried out under evacuated conditions. During the initial stage of the reaction, the induction period, a slow breakdown by the weakly acidic sites on the metal oxide surface resulted in the formation and evolution of CO_2, COF_2, CF_3CFO and lower molecular weight fluorocarbon fragments. Reaction with the COF_2 converted the metal oxide to the corresponding metal fluoride. Rapid degradation occurs in the second stage catalyzed by Lewis acid sites on the FeF_3 and AlF_3 surfaces. When the PFAE is in contact with AlF_3, FeF_3 or a sulfate promoted Fe_2O_3 superacid, the reaction proceeds rapidly with no induction period.[12-14]

Decomposition of polymeric perfluoroalkylethers in contact with Lewis acids at elevated temperatures has been

reported to occur through a cleavage of the ether carbon oxygen bond.[15,16] The Lewis acid catalyzed, intramolecular disproportionation mechanism, shown in Figure 1.2, has been proposed for the decomposition of Fomblin Z in the presence of metal oxides and fluorides.[13] A bidentate linkage is formed between the Lewis acid sites on the metal surface and the basic oxygen atoms of the Fomblin Z chain. A fluorine atom transfer occurs from the adjacent CF_2 to the acetal carbon, which causes scission of the carbon oxygen bond with formation of a methoxy end group and either an acyl fluoride $CFO-CF_2$ or a fluoroformate $CFO-O-CF_2$. The acetal unit, $O-CF_2-O$, is very reactive toward the Lewis acid assisted cleavage of the carbon oxygen bond. In hydrocarbon ethers, the same phenomena was observed with increased reactivity toward C-O bond cleavage by Lewis acids, when an acetal group was present in the hydrocarbon chain.[12] The three other polymers, shown in Figure 1.1, do not decompose when in contact with the aluminum and iron oxides up to 205 °C.[12,13] Fomblin Y has significantly fewer acetal groups and Krytox and Demnum do not have any.

The metal oxide is not a strong enough Lewis acid to initiate a reaction of the polymeric materials, which do not contain the reactive acetal group. More severe conditions are necessary, either higher temperature, a stronger Lewis acid or a combination of both. FeF_3 and AlF_3 have been

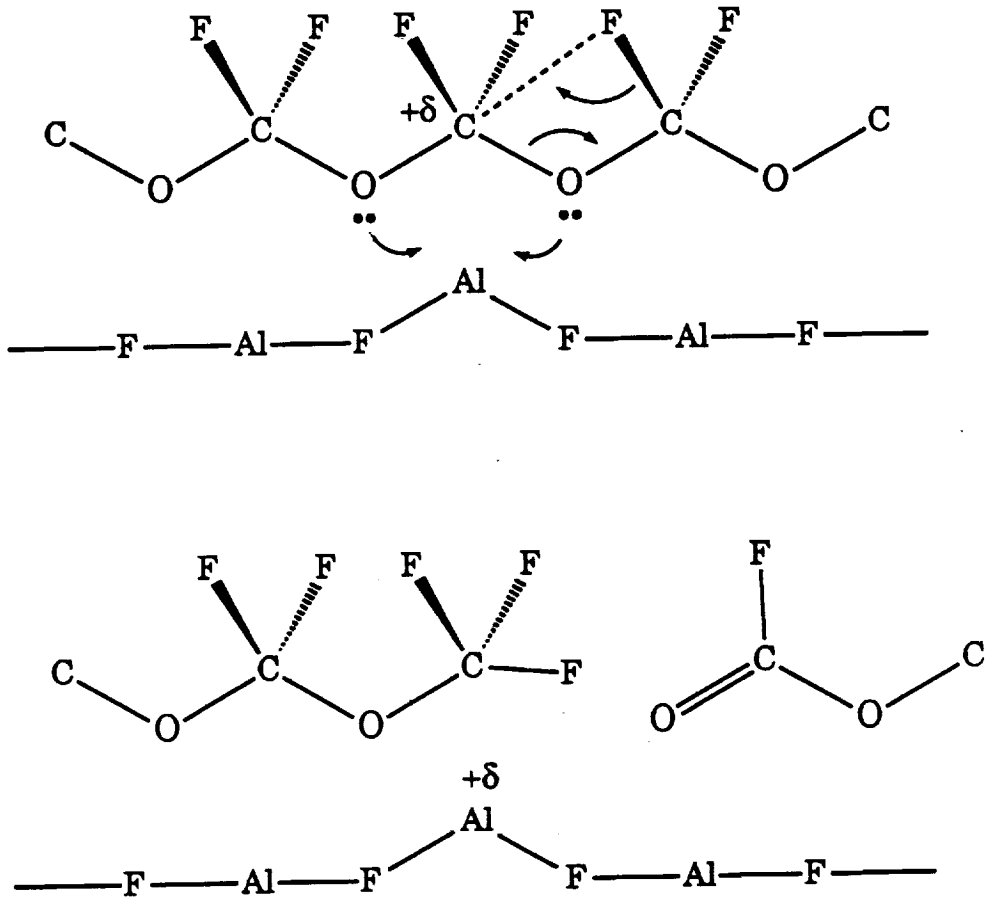

Figure 1.2 Reaction mechanism proposed for the decomposition of Fomblin Z in the presence of metal oxides. Data taken from Reference 13.

reported to cleave the primary and secondary carbon oxygen bonds of Krytox at 350°C forming acyl fluoride and ketone degradation products.[7,14] The mechanism for decomposition of the branched Krytox, shown in Figure 1.3, has been proposed.[7] The acidic metal on the surface and the acidic carbon on the molecular chain complex with basic fluorines, with partial electron density transfer. A FeF_4^- intermediate is formed, with fluorine transfer, causing chain scission at either a primary or secondary carbon oxygen bond. The polymeric material with the acetal unit are much more reactive. Both fluorine and oxygen are Lewis bases with abundant electron density, but oxygen, because it is less electronegative is more willing to share its electron density. For Krytox, the pendant perfluoromethyl group is thought to protect the oxygen atoms from attack.

3. Compatibility with Nascent Metal Surfaces

Under atmospheric conditions, metal surfaces are covered with an oxide layer and organic contaminants. During tribological processes the surface oxide layer and the hydrocarbon contaminants are removed and nascent surfaces are formed. The freshly formed, nascent metal surfaces show high chemical activity.[17,18] For example, the adsorption and decomposition of benzene has been studied on well defined, single crystal surfaces.[19] Irreversible C-H bond scission was observed at 150°C, 100° and 100°C on

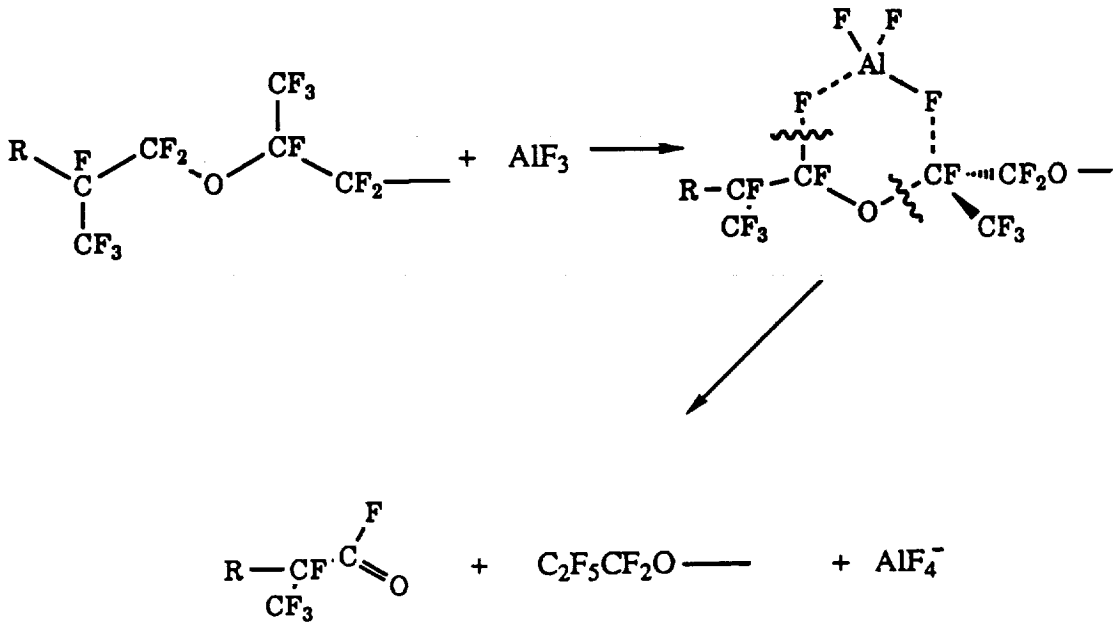

Figure 1.3 Reaction mechanism proposed for the decomposition of polymeric materials which do not contain the reactive acetal group, $O\text{-}CF_2\text{-}O$. Data taken from Reference 7.

Ni(100), Ni(111) and Ni(110), respectively.[19] Up to the decomposition temperatures reported for each crystal face, the benzene chemisorption was fully associative.[19] Benzene has been reported to decompose, in vacuum, on freshly formed, room temperature nickel surfaces, significantly lower than the decomposition temperature reported for the single crystal nickel.[18] The mechanically formed, nickel surface was much more reactive than the clean, single crystal because of the highly defective nature of the surface.[18,20,21]

Stainless steel surfaces freshly formed in vacuum were also found to be very reactive toward polymeric perfluoroalkylether decomposition.[22-25] Krytox, Demnum and Fomblin Z decompose at ambient temperatures with the formation of a cross-linked, polymeric fluorocarbon layer and metal fluorides in the wear track.[22-24] Gas evolution, in particular COF_2, was reported during sliding for Fomblin Z, only.[22,23] Gas evolution was not reported for Demnum or Krytox. The evolution of COF_2 continued, after sliding stopped, attesting to the catalytic nature of the metal fluoride in the wear track.[22,23]

The decomposition temperature, predicted from the micro-oxidation corrosion tests, is significantly higher than the ambient temperature reported for decomposition on

the nascent steel surfaces. Nascent metal surfaces produced during grinding, cutting and frictional processes can be studied using atomically clean surfaces as models.

D. MODEL COMPOUNDS

1. Atomically Clean Iron Surfaces

Halogens have been reported to dissociatively adsorb on room temperature iron surfaces.[26-30] LEED patterns observed upon halogen adsorption are interpreted as a regular overlayer net of chemisorbed halogen atoms, which are not necessarily coincident with the substrate.[26-28] Penetration of halogen atoms below the upper layer of metal atoms has been reported at 300°C for I and Cl atoms and at 20°C for F atoms.[29] Since 20°C was the lowest temperature investigated,[29] the minimum temperature for fluorine penetration is not known. Fluorine atoms may be penetrating into the subsurface regions of the metal at temperatures below 20°C.

Various chloro/fluoro methanes dissociatively adsorb on room temperature iron surfaces forming a random array of carbon atoms in four fold sites covered by a square net array of chlorine atoms, which are not necessarily coincident with the iron substrate.[28,31-33] The exact location of the fluorine atoms is not known, but the fluorine is believed to reside below the chlorine overlayer.[33] The Cl

overlayer is stabilized by the underlying carbon and fluorine and resembles the overlayer formed upon adsorption of Cl_2, at low coverages.[28,33] The fragmentation is terminated with the completion of the chlorine overlayer.[28,33]

Halogenated methanes molecularly adsorb on low temperature (90-100 K) iron surfaces. CCl_4, $CFCl_3$ and CF_2Cl_2 undergo thermally activated decomposition with carbon-halogen bond scission and iron-halogen bond formation, at temperatures below 180 K.[34-37] Iron aggressively attacks CCl_4 to break C-Cl bonds with production of a variety of reaction products, CCl_3, C_2Cl_4, C_2Cl_6, $:CCl_2$, a gas phase free radical and $FeCl_2$.[36] Iron aggressively attacks CF_2Cl_2 to preferentially break C-F bonds with selective production of $:CCl_2$ and iron fluorides.[37] Fluorine containing gas phase radicals, $:CF_2$ and :CClF and radical recombination products reported from CCl_4 decomposition were not reported for CF_2Cl_2 decomposition.[37] Selective $:CCl_2$ production indicates that the molecule preferentially interacts with the Fe(110) surface via the fluorine end. The decomposition of CCl_4 and CF_2Cl_2 has been proposed to occur at the defect sites on the iron surface.[36-38] The desorption yield of $:CCl_2$ can be increased by the creation of additional defect sites with argon ion sputtering.[38] The driving force behind the carbon-halogen bond scission, in particular C-F bond scission, is

the formation of iron fluoride.[37] This reaction should be thermoneutral on iron.

There have been relatively few studies of model halocarbon ethers on transition metal surfaces. The most comprehensive body of work to date has been an investigation of the bonding and reactions of model fluorinated monoethers and diethers and the corresponding hydrocarbon ethers on Ru(001) and Ru(100) surfaces.[39-41] Hydrogenated ethers bond to metal surfaces via two types of interactions. The stronger interaction consists of electron donation from the oxygen lone pair to the metal, which contributes approximately 40 kJ/mol.[42,43] The second component of the hydrocarbon ether metal bond is an attractive interaction between the methylene groups and the surface, which contributes 5 to 6.5 kJ/mol, per CH_2 group.[42] Fluorination is expected to weaken both of these attractive interactions.[39,41] The electronegative fluorines inductively deplete electron density from the oxygen atom. The net interaction of a CF_2 group is probably less favorable because the C-F bond is longer than the C-H bond,[44] holding the carbon further away from the surface and the fluorine is more electron rich than the hydrogen, increasing the repulsive interaction. Model fluorinated ethers bond more weakly to Ru(001), when compared to hydrogenated ethers.[40,41]

The hydrocarbon ethers are reported to decompose on the ruthenium surfaces, via C-H bond breaking at an α-carbon.[40] For the case of fluorinated ether decomposition, the C-F bond is stronger than the C-H bond[44] and would require a higher substrate temperature to activate the bond scission. Fluorination weakens the chemisorption bond strength to the ruthenium surface and the ether desorbs prior to decomposition.[39-41] Differences in the bonding geometries could also account for the fluorocarbon stability. Due to the repulsion between the electron rich fluorine and the metal surface the alkyl side chains may not approach the surface as closely as the alkyl group of the hydrogenated ether resulting in a lower propensity for C-F bond scission.[40]

2. Metal Surfaces Chemically Modified with Oxygen

Only a few studies of the interaction of halocarbons and oxygenated halocarbons on oxygen modified metal surfaces have been undertaken. Preadsorption of a chemisorbed oxygen overlayer deactivates an iron surface toward CCl_4 decomposition due to blocking of the active sites.[45] Halogenation of Al_2O_3, SiO_2, TiO_2, Fe_2O_3 and Fe_3O_4 was found with exposure to gaseous halocarbons.[28] A sudden sharp decrease in the metal/oxygen ratio due to CO_2 production and oxide halide exchange was reported.[28] The reaction always

occurred very sharply above an onset temperature related to the stability of the oxide and the deposited reaction product layer containing C, F and Cl.[28] Perfluorodiethyl ether, $CF_3CF_2OCF_2CF_3$, adsorbs reversibly on ZrO_2 thin films.[46] Fluorination reduced the chemisorption bond strength, so that the fluorinated ether desorbs from the ZrO_2 surface prior to decomposition.

E. OBJECTIVE

Polymeric perfluoroalkylethers show reduced chemical, oxidative and thermal stabilities in the presence of many metals, both oxidized and nascent metal surfaces. The mechanism for decomposition on the oxidized and the freshly formed metal surfaces, as well as the importance of the atomic structure of the fluorinated ether on the reactivity has not been thoroughly assessed. The objective of this research is to study the adsorption and thermally activated decomposition of three model fluorinated, diether lubricants on polycrystalline iron surfaces, atomically clean and chemically modified with oxygen, using X-ray photoelectron spectroscopy (XPS) and temperature programmed desorption (TPD). The model structures investigated were perfluoro-1-methoxy-2-ethoxy ethane, $CF_3OCF_2CF_2OCF_2CF_3$, mPFAE1, perfluoro-1-methoxy-2-ethoxy propane, $CF_3OCF_2CF(CF_3)OCF_2CF_3$, mPFAE2, and perfluoro-1,3-diethoxy propane, $CF_3CF_2OCF_2CF_2CF_2OCF_2CF_3$,

mPFAE3. The model structures are monomer units of polymeric PFAE materials being considered for use as high temperature lubricants.

XPS can be used to monitor the reaction on the surface and TPD to monitor the temperature dependent evolution of gas phase reaction products. XPS can differentiate atoms, which exist in non-equivalent chemical environments, making it a particularly useful technique for the study of the model fluorinated ether surface reactions. Each of the model fluorinated ethers has at least two carbons which can be resolved using XPS, allowing for the study of the effect of atomic structure on the thermal stability. Additionally, C-F bond breaking and Fe-F bond formation are easily monitored because of the substantial shifts observed in the carbon, oxygen and fluorine XPS binding energies, with loss of electronegative fluorine from the molecular chain and metal halide bond formation. XPS and TPD provide a strong combination for the study of the thermally activated decomposition of the model fluorinated ethers on polycrystalline iron surfaces.

CHAPTER II

EXPERIMENTAL METHODS

A. INTRODUCTION

This chapter will describe the UHV techniques used in this research. The XPS and SIMS measurements were conducted in a VG Scientific ESCALAB/SIMSLAB Mk. II. The XPS chamber was equipped with a twin anode x-ray source, Al Kα and Mg Kα, an Al monochromatic x-ray source, an Ar ion gun, a stainless steel leak valve controlled doser and a sample manipulator. The SIMS chamber was equipped with an Ar ion gun, a quadrupole mass analyzer and a sample manipulator. The TPD experiments were conducted in a turbomolecular pumped, stainless steel UHV chamber equipped with a water cooled, Ti sublimation pump, an apertured UTI-100C mass spectrometer, an Auger spectrometer with retarding field energy analyzer and integral electron gun, an Ar ion gun, a bakeable glass/teflon gas handling system and a sample manipulator.

B. SURFACE ANALYTICAL TECHNIQUES

1. X-ray Photoelectron Spectroscopy

A diagram of the photoelectric process, on which x-ray photoelectron spectroscopy is based, is shown in Figure 2.1.[1] A number of detailed references are available which provide an in-depth review of x-ray photoelectron spectroscopy (XPS).[1-3] A solid surface in vacuum, is irradiated with x-rays of known energy, exciting core level

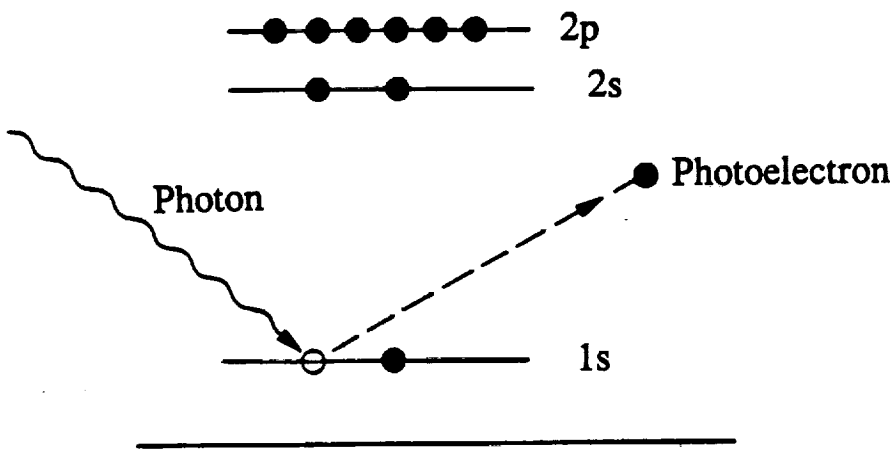

Figure 2.1 Diagram of the photoelectric process. Adapted from Reference 1.

electrons. The ejected photoelectrons have kinetic energies given by,

$$E_K = h\upsilon - E_B - \Phi_s \qquad (2.1)$$

where E_K is the kinetic energy of the ejected electron, $h\upsilon$ is the energy of the incident radiation, E_B is the binding energy of the electron and Φ_s is the work function of the spectrometer. The equation can also be solved for binding energy,

$$E_B = h\upsilon - E_K - \Phi_s \qquad (2.2)$$

The spectrum obtained is a plot of the number of emitted electrons per energy interval versus their kinetic or binding energy.

Most commonly used x-ray sources are the twin anode, non-monochromatic Mg $K\alpha_{1,2}$ (1253.6 eV) and Al $K\alpha_{1,2}$ (1486.6 eV). Also available is a monochromatic Al $K\alpha$ source. Due to the radiation sensitivity of the model fluorinated ethers, the Al monochromatic x-ray source was used exclusively to study their surface chemistry. The ejected photoelectrons are detected using an electron spectrometer and analyzed according to their energy. For the experiments conducted in this research, the spectrometer was operated in the constant analyzer energy (CAE) mode. In the CAE mode the spectrometer accepts only those electrons having an energy within a specified range (pass energy). Scanning through a region of energies larger than the pass energy is

accomplished by applying a variable electrostatic field to a retarding lens. The voltage on the lens may be varied from zero up to the x-ray photon energy, controlling the energy of the emitted electrons. The work function of the spectrometer is measured with reference to known photoelectron lines of standard materials, typically clean Pd, Au, Ag, and Cu.

Figure 2.2 shows a survey XPS spectrum of a clean, iron surface obtained using the twin anode, Al x-ray source. The primary structure of Figure 2.2 will be discussed. A series of peaks are observed on a background, which increases to higher binding energy. The peaks reflect the core level electronic structure of the atom being probed. The core level from which the electron originates is indicated on the spectrum. As can be seen in Figure 2.2, the core levels have variable intensities and widths and all non s levels are doublets.[1-3] The relative intensity of the core level peaks is determined by their atomic photoemission cross section. The doublets arise from spin orbit coupling (j-j). The two possible states in the doublet are defined by the quantum number j (j=l+s), when l>0 for the p, d, f, etc. subshells. The doublet observed for the iron 2p subshell, l=1, and s=1/2 and -1/2, for quantum number j equivalent to 3/2 and 1/2, respectively, corresponds to $Fe(2p_{3/2})$ at 706.8 eV and $Fe(2p_{1/2})$ at 720.0 eV. The energy

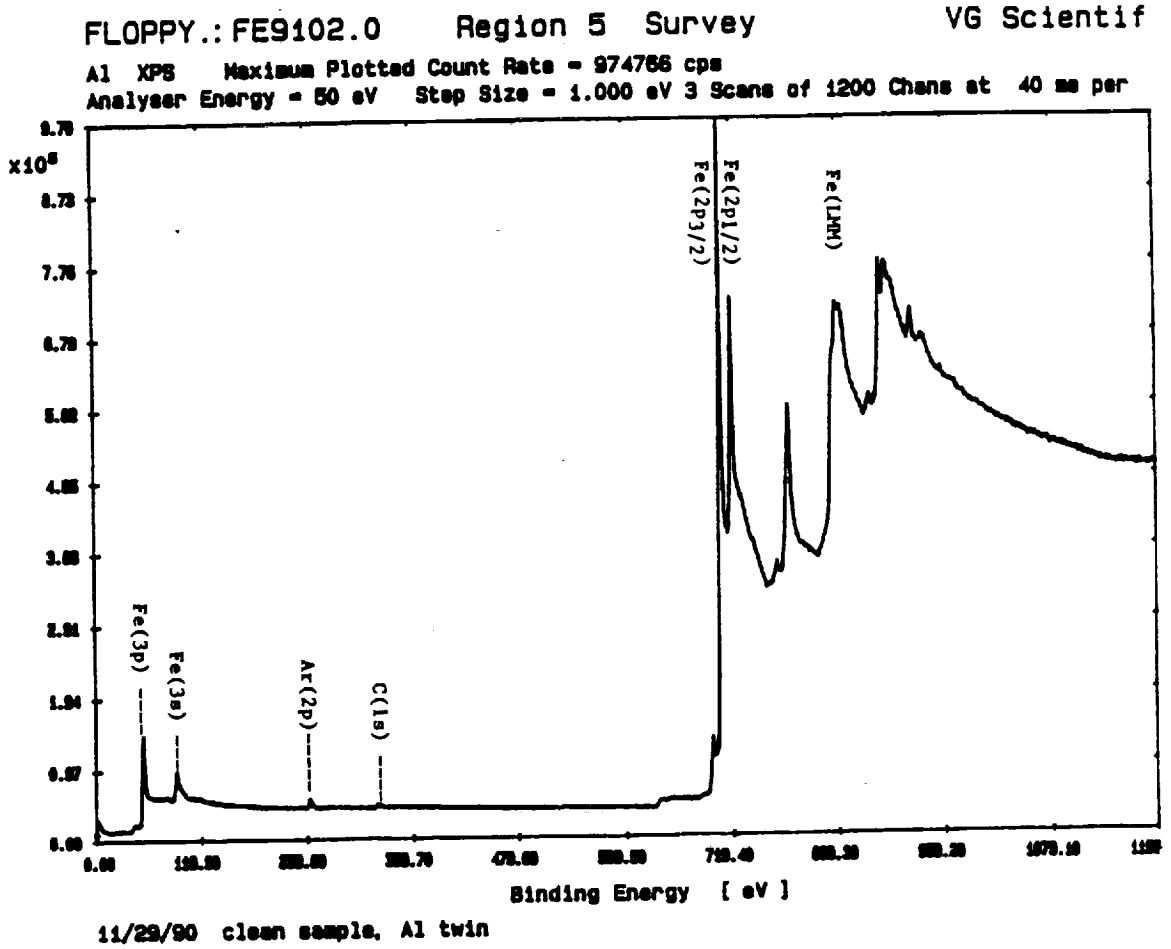

Figure 2.2 Survey scan of a clean iron surface using the Al twin anode x-ray source and a 50 eV pass energy. The photoelectron peaks and the Auger transitions are marked appropriately on the spectrum.

splitting of the two states reflects the parallel or antiparallel nature of the spin and orbital angular momentum. The magnitude of the energy difference is dependent upon the spin orbit coupling. The ratio of the degeneracy, 2j+1, determines the ratio of the relative intensities of the doublets. In addition to the photoelectrons emitted in the photoelectric process, Auger electrons are emitted due to relaxation of the energetic ions left after photoemission. The Auger transition for iron is appropriately marked on Fig. 2.2.

The absorption length of a photon in a solid is on the order of micrometers and ionization occurs to that depth.[1] The path length of an electron in a solid is on the order of tens of Angstroms, significantly less than the path length of a photon.[1] Only those electrons that originate within the first few atomic layers escape without energy loss and it is these photoelectrons which produce the peaks in the spectra. The restricted mean free path of an electron in a solid provides the basis for the surface sensitivity of XPS. The electrons that interact with the solid escape with energy loss and contribute to the background.

One of the most important applications of XPS is the determination of the oxidation state or the chemical environment of the elements at the surface. Non-equivalent atoms of the same element give rise to core level peaks with

measurably different binding energies.[2,3] Non-equivalence most commonly arises from a change in the formal oxidation state or a change in the molecular environment. The energy shifts are related to charge transfer in the outer electronic levels, which induces changes in the binding energy of the core level electrons. The direction of the shift in the binding energy, depends on the direction of the charge transfer. This binding energy increase is very clearly seen for the case of the changing carbon environment with electronegative substitution. Indicated on the perfluoro-1-methoxy-2-ethoxy ethane C(1s) spectrum, shown in Figure 2.3, are the peak positions for the two non-equivalent carbons in diethyl ether.[4] Substitution of the hydrogens by the electronegative fluorines shifts the C(1s) binding energy to significantly higher values.

Use of a quartz crystal monochromator acts to remove satellite interference, improve signal to background through the elimination of Bremsstrahlung radiation and improve the resolution through the selection of an individual line from the unresolved principal line doublet.[2] The model fluorinated ethers are electron sensitive and degrade upon exposure to the twin anode (non-monochromatic) x-ray source. The monochromator acts to remove extraneous sources of electron production. The monochromator allows only a selected small portion of the total Kα emission to fall on

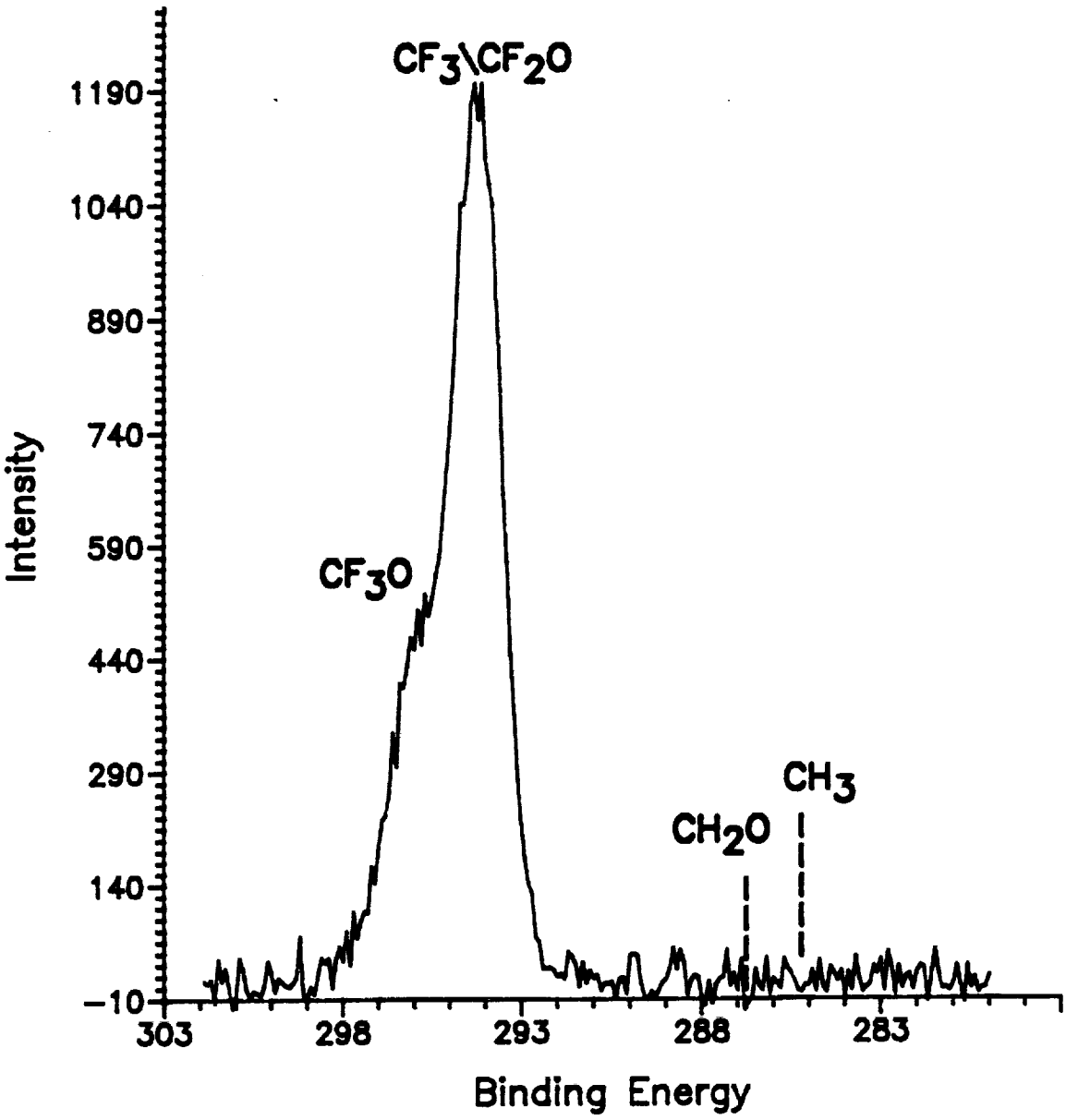

Figure 2.3 C(1s) spectrum for perfluoro-1-methoxy-2-ethoxy ethane. Indicated on the spectrum are the peak positions for the two non-equivalent carbons in diethyl ether, to illustrate the effect of the changing chemical environment of carbon due to fluorination.

the sample significantly reducing the count rate, as well as the production of internal secondary electrons. The monochromatic x-ray window is far removed from the sample surface, so electrons generated at the window are not likely to reach the surface.

2. Auger Electron Spectroscopy

Auger electron spectroscopy is another commonly used technique to study the composition of surfaces.[2,3] References are available which provide a detailed review of Auger Electron Spectroscopy (AES).[2,3] The Auger electron emission process is shown in Figure 2.4.[2] An energetic beam of electrons, typically 1-5 keV, impinges on a surface. A core level electron (K shell in Fig. 2.4) is ejected by the incident electron, whose energy must be greater than the binding energy of the core level electron and for efficient ionization needs to be approximately five times greater. The atom may relax to fill the core level hole by an electronic transition from a higher shell (L_I shell in Fig. 2.4). As a result of the transition, the energy difference becomes available as excess kinetic energy, which may be emitted as a photon or transferred to another electron (from the L_{III} shell in Fig. 2.4). If the binding energy of this electron is less than the energy transferred in the deexcitation, then this electron will be ejected into the vacuum. The Auger transition shown in Figure 2.4 is denoted

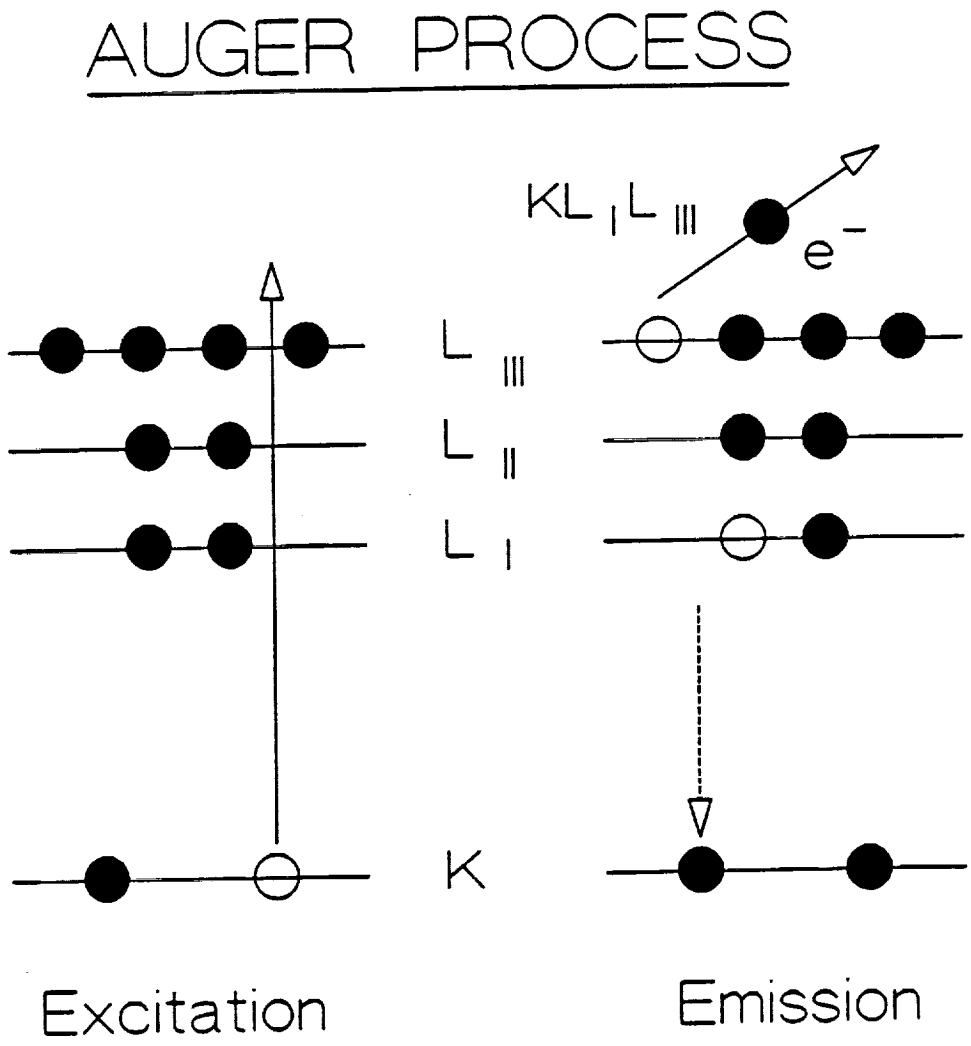

Figure 2.4 Diagram of the Auger process. Adapted from Reference 2.

as KL_IL_{III}.

The energy of the emitted Auger electron is a function of atomic energy levels and is independent of the energy of the ionizing radiation, so for each element there is a unique set of Auger energies.[2,3] The emitted Auger electrons of interest have energies between 10-1000 eV. The absorption length of an electron in a solid is on the order of tens of Angstroms, so only those electrons that originate within the first few atomic layers escape without energy loss and provide the basis for the surface sensitivity of Auger electron spectroscopy.[1] In addition to Auger electrons, a large number of inelastically scattered electrons are emitted in this energy range. Thus if one were to plot N(E) versus E, where N is the number of electrons emitted at an energy E, the Auger electrons would appear as small peaks on a large sloping background of inelastically scattered electrons. To extract the Auger peaks from the background, dN(E)/dE versus E is typically plotted.

Due to the electron sensitivity of the model fluorinated ethers, AES was used only to check the cleanliness of the iron surface prior to mPFAE exposure. AES was never used to probe the adsorbed fluorinated ether layer.

3. Temperature Programmed Desorption

Temperature programmed desorption (TPD) can be used to study the desorption and the reaction of adsorbed gases on a variety of surfaces.[2,5-7] Typically a clean surface in vacuum is held at a specified temperature and exposed to an adsorbing gas. The sample is then heated at a controlled rate to desorb the gas and a mass spectrometer is used to detect the species evolving from the surface. The specific rate of desorption will depend on the surface population (coverage), bond strength of the adsorbate to the surface and the energy available to the system (temperature) and can be expressed in the following equation,

$$\frac{dc}{dt} = N = \upsilon c^{n} \exp\left(-\frac{E(c)}{RT}\right) \qquad (2.3)$$

where N is the rate of desorption or decomposition, υ is the preexponential factor, c is the surface coverage per unit area, n is the order of the reaction, E(c) is the activation energy and T is the surface temperature. The temperature programmed desorption spectrum is a plot of N, the rate of desorption of the evolving gas versus either temperature or time. The temperature is increased with time at a constant rate.

Analysis of the temperature programmed desorption spectra can proceed in several ways. The activation energy of desorption for zero, first and second order reactions can be determined from the peak temperature and the analytical

techniques determined by Redhead.[6] Assuming υ and E are independent of the adsorbate concentration, that the temperature ramp is linear and the order of the reaction is known, the following equations can be used to obtain the activation energy of desorption,

$$\frac{E_0}{RT_p} = \frac{\upsilon_0}{c\beta} \exp\left(-\frac{E_0}{RT_p}\right) \qquad (2.4)$$

$$\frac{E_1}{RT_p^2} = \frac{\upsilon_1}{\beta} \exp\left(-\frac{E_1}{RT_p}\right) \qquad (2.5)$$

$$\frac{E_2}{RT_p^2} = \frac{\upsilon_2 c}{\beta} \exp\left(-\frac{E_2}{RT_p}\right) \qquad (2.6)$$

where E is the activation energy of desorption, T_p is the peak temperature, υ is the preexponential factor, c is the initial coverage and β is the heating rate. Subscripts 0, 1, or 2 denote the zero, first or second order desorption processes, respectively. As can be seen from the equations, the peak temperature, T_p, is independent of coverage for first order, increases for zero order and decreases for second order desorption processes. The heat of adsorption can be approximated by E, the activation energy for desorption, if the adsorption is a nonactivated process.

A more detailed analysis of the temperature programmed desorption data can be made using the desorption rate isotherm method developed by Falconer and Madix.[7] The

desorption rate isotherm method can be used to obtain reaction order, n and the activation energy for desorption, E, without making all of the assumptions needed to use Redhead's equations. Each point of the desorption curve corresponds to a measurement of the desorption rate at a given temperature, surface coverage and surface composition. A series of desorption curves at an initial coverage, ranging from low coverage up to saturation, are obtained. At a specified temperature, the desorption rate and the surface coverage can be measured for each desorption curve, corresponding to a different initial coverage. The rate of desorption is proportional to the curve amplitude at that temperature. The area under the portion of each curve, to the right of the specified temperature, is proportional to the surface coverage at that temperature. Plot of ln N versus ln c, at constant temperature, where N is the rate of desorption and c is the surface coverage, should yield a straight line slope of n, the order of the reaction if the activation energy is independent of coverage. Deviations in the slope are an indication of a coverage dependent activation energy.

The activation energy can be obtained by plotting a number of desorption rate isotherms at specified temperatures over the entire desorption range. Then at a given coverage, the desorption rate measurements at

different temperatures can be obtained from the desorption rate isotherms. A plot of ln N against 1/T at constant coverage yields a straight line with a slope equal to the activation energy.

4. Secondary Ion Mass Spectrometry

SIMS provides mass analysis for surface species ejected from the surface after collision with an energetic ion.[2,8] Bombardment of a surface with energetic argon ions imparts collisional energy to the atoms in the first few monolayers of the surface. Atoms which acquire enough energy escape the sample surface and a small percentage of these atoms will be ionized. The secondary ions are collected and mass analyzed using a quadrupole analyzer. Knowledge of cluster masses allows the chemical composition of the surface to be investigated.

SIMS has several advantages when compared to XPS and AES. Because SIMS is a mass analysis technique, the full range of elements can be analyzed. The detection limits are several orders of magnitude lower than the other techniques. SIMS is inherently destructive, removing a portion of the sample surface through sputtering.

CHAPTER III

EFFECT OF X-RAY EXPOSURE ON MODEL FLUORINATED ETHERS

A. INTRODUCTION

Low energy photons and electrons have been reported to fragment halocarbon molecules.[1-4] Before x-ray photoelectron spectroscopy could be used to investigate the surface chemistry of the model fluorinated ethers on polycrystalline iron surfaces, it was necessary to study the effect of the probing photon beam. The model compound investigated was perfluoro-1-methoxy-2-ethoxy ethane, $CF_3OCF_2CF_2OCF_2CF_3$, mPFAE1 on cooled iron and gold, and room temperature iron surfaces. The model compound is a monomer unit of one of the polymeric perfluoroalkylether materials being considered for use as a high temperature lubricant. Unlike iron, gold is inert toward perfluorinated ether decomposition and was investigated to separate surface reactions from x-ray induced reactions.

Perfluoro-1-methoxy-2-ethoxy ethane was observed to readily decompose upon exposure to the Al twin anode (non-monochromatic) x-ray source. In contrast, the Al monochromatic source could be used to analyze the adsorbed mPFAE1 layer with no degradation due to the probing photon beam over the experimental time frame.

B. EXPERIMENTAL

XPS measurements were conducted in a VG Scientific ESCALAB/SIMSLAB Mk. II, with typical base pressures of 1x10

10^{-10} torr. The system was equipped with a twin anode x-ray source, Al Kα (1486.6 eV) and Mg Kα (1253.6 eV), an Al monochromatic x-ray source, an Ar ion gun, a stainless steel leak valve controlled doser and a sample manipulator.

The polycrystalline iron foils (10 mm x 10 mm x 0.5 mm) were polished, using standard metallographic techniques, to a surface finish of 1.0 μm, followed by ultrasonic cleaning, in acetone, to remove the polishing residue. The iron foils were atomically cleaned in UHV, with cycles of Ar^+ bombardment and annealing. The iron foils were considered clean when contaminants, in particular carbon, oxygen, sulfur and nitrogen, could not be detected using XPS. The temperature was measured using a chromel-alumel, Type K, thermocouple spotwelded to an edge of the front face of the sample.

The polycrystalline gold foils, 0.25 mm thick and 99.99% pure, were obtained from Aldrich and ultrasonically cleaned in acetone prior to use. The gold foils were atomically cleaned in UHV, with cycles of Ar^+ bombardment and were considered clean when contaminants could not be detected using XPS. The gold foils were affixed to a standard VG sample stub using silver paint. No provisions were made for sample annealing nor temperature measurement. The temperature of the cooled gold surface was estimated to be at a minimum 165 K. This temperature was estimated from

the minimum temperature achievable using the VG manipulator and a modified sample stub.

Perfluoro-1-methoxy-2-ethoxy ethane, mPFAE1, was obtained from Exfluor Research Inc. and used as received. A GC/MS analysis showed mPFAE1 to be at a minimum 98 % pure, with higher molecular weight ethers present as impurities. Prior to introduction into the vacuum chamber, mPFAE1 was further purified by repeated freeze-pump-thaw cycles. The fluorinated ether exposures were calculated from uncalibrated ion gauge readings and are reported in Langmuir (1 L = $1x10^{-6}$ torr-sec).

The clean iron surfaces, at 110 K and ambient temperatures and cooled, gold surfaces were exposed to mPFAE1. XPS spectra were acquired using the Al twin anode (non-monochromatic) and the Al monochromatic x-ray sources monitoring the changes in the carbon, oxygen and fluorine XPS spectra with increasing x-ray exposure.

C. RESULTS

Shown in Figure 3.1 are the F(1s) spectra for mPFAE1 adsorbed onto a room temperature iron surface, with increasing Al non-monochromatic x-ray exposure. Exposure of the adsorbed mPFAE1 layer to the non-monochromatic x-ray source, caused the conversion observed in the fluorine XPS spectra from a covalently bonded fluorine (CF) at 689.0 eV

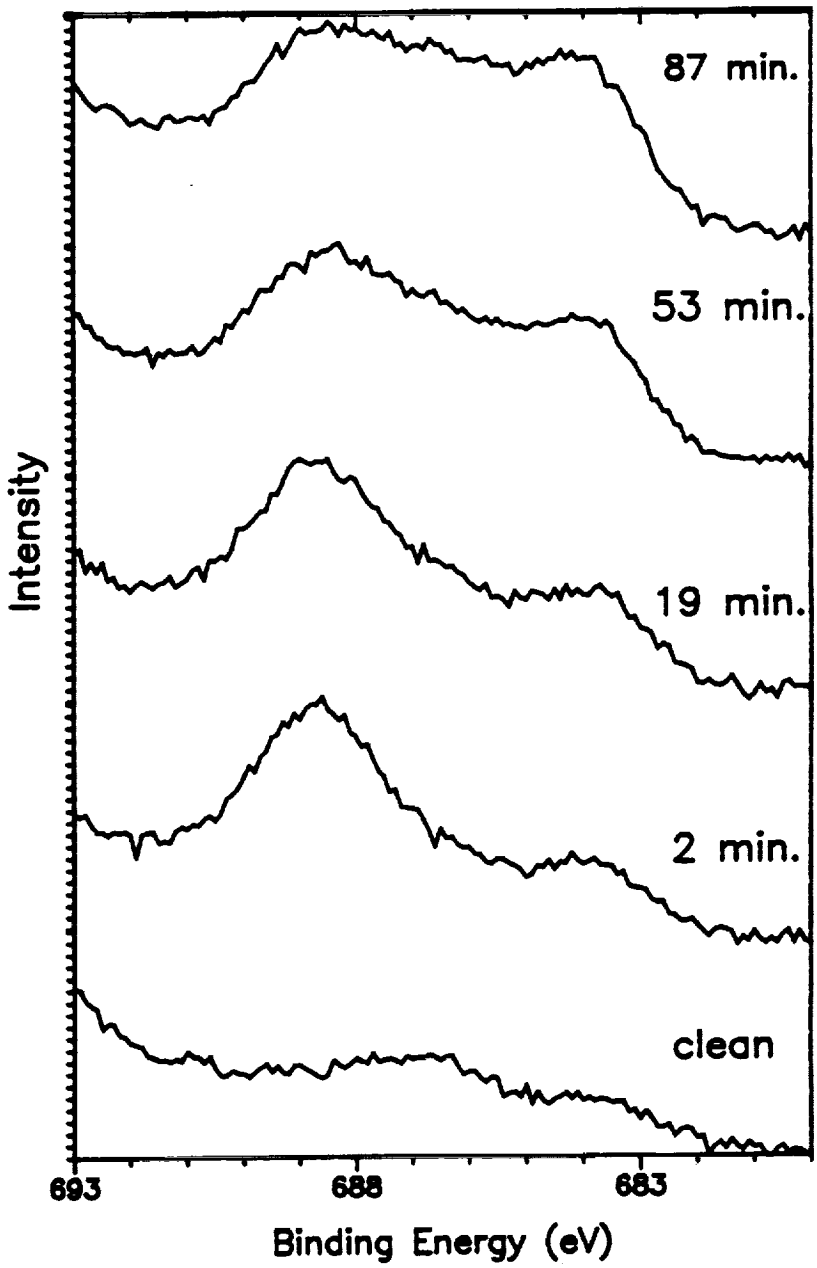

Figure 3.1 Perfluoro-1-methoxy-2-ethoxy ethane adsorbed onto a room temperature, polycrystalline iron surface. F(1s) spectra is monitored with increasing Al non-monochromatic x-ray exposure.

to an inorganic fluoride (FeF) at 684.0 eV. This conversion is indicative of C-F bond breaking and Fe-F bond formation.

Perfluoro-1-methoxy-2-ethoxy ethane dissociatively adsorbs on room temperature iron surfaces, but these surface effects can be distinguished from the effects of the x-ray flux. Shown in Figure 3.2 is the F(1s) spectrum for adsorbed mPFAE1 in contact with the room temperature iron surface for 102 minutes, prior to the acquisition of the fluorine XPS spectra. The F(1s) spectrum in Figure 3.2 resembles the F(1s) spectrum in Figure 3.1 at the lowest x-ray exposure. The conversion of the covalently bonded fluorine to an inorganic fluoride cannot be ascribed to time dependent contact with the room temperature iron surface or to the presence of mPFAE1 in vacuum.

Shown in Figure 3.3 are the F(1s) spectra for mPFAE1 adsorbed onto a cooled gold surface with increasing monochromatic x-ray exposure. Gold is not reactive toward mPFAE decomposition and molecular adsorption of mPFAE1, in the submonolayer regime, is observed on the cooled gold surface. The fluorine peak shape and C/F peak area ratio remained constant with increasing monochromatic x-ray exposure. A slight decrease in the fluorine peak area was observed (less than 5%), but attributed to variations in temperature. The temperature of the gold foil could not be monitored, so temperature variations could not be detected.

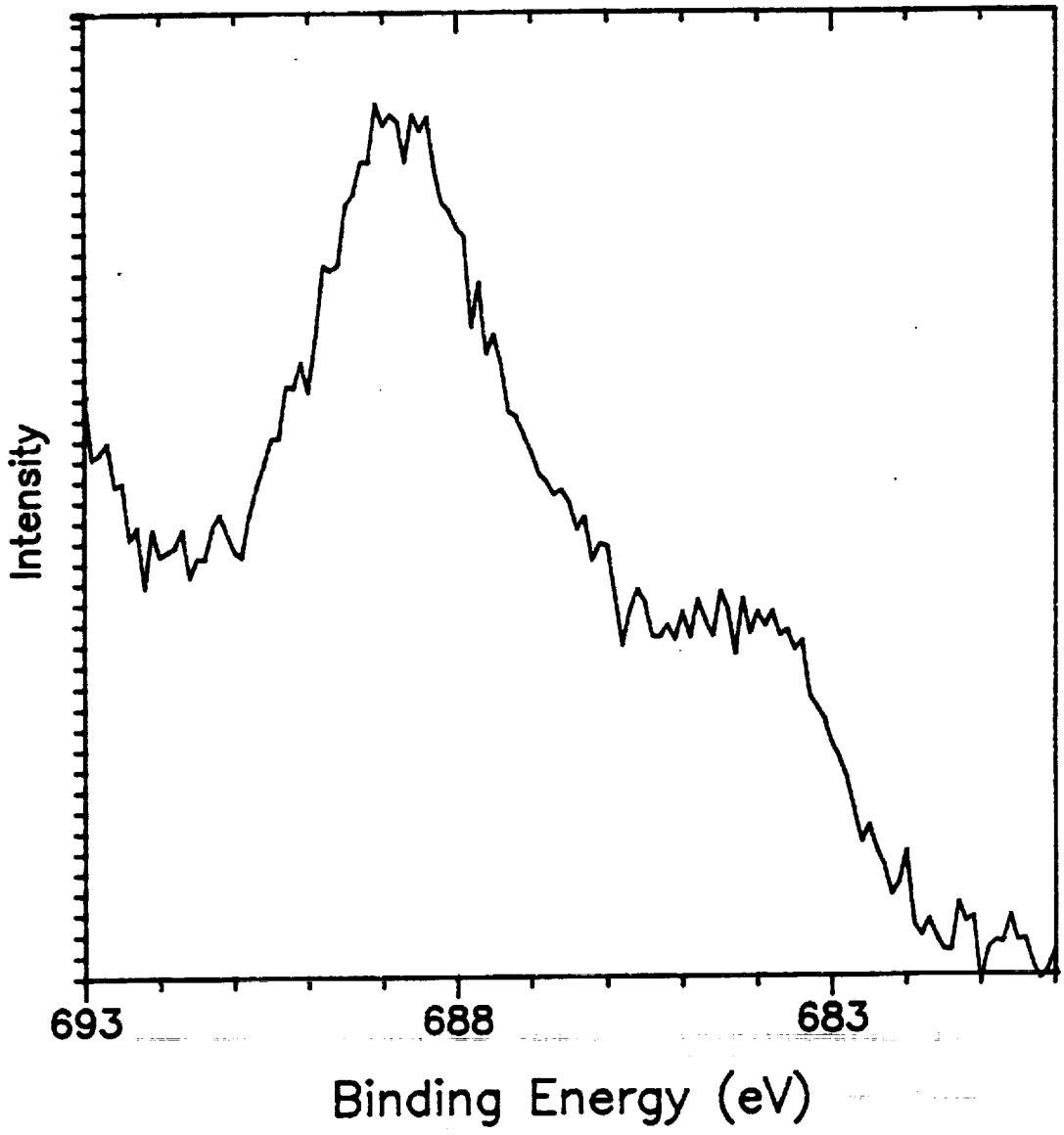

Figure 3.2 F(1s) spectrum for perfluoro-1-methoxy-2-ethoxy ethane, in contact with the polycrystalline iron surface, for 102 minutes prior to non-monochromatic x-ray exposure.

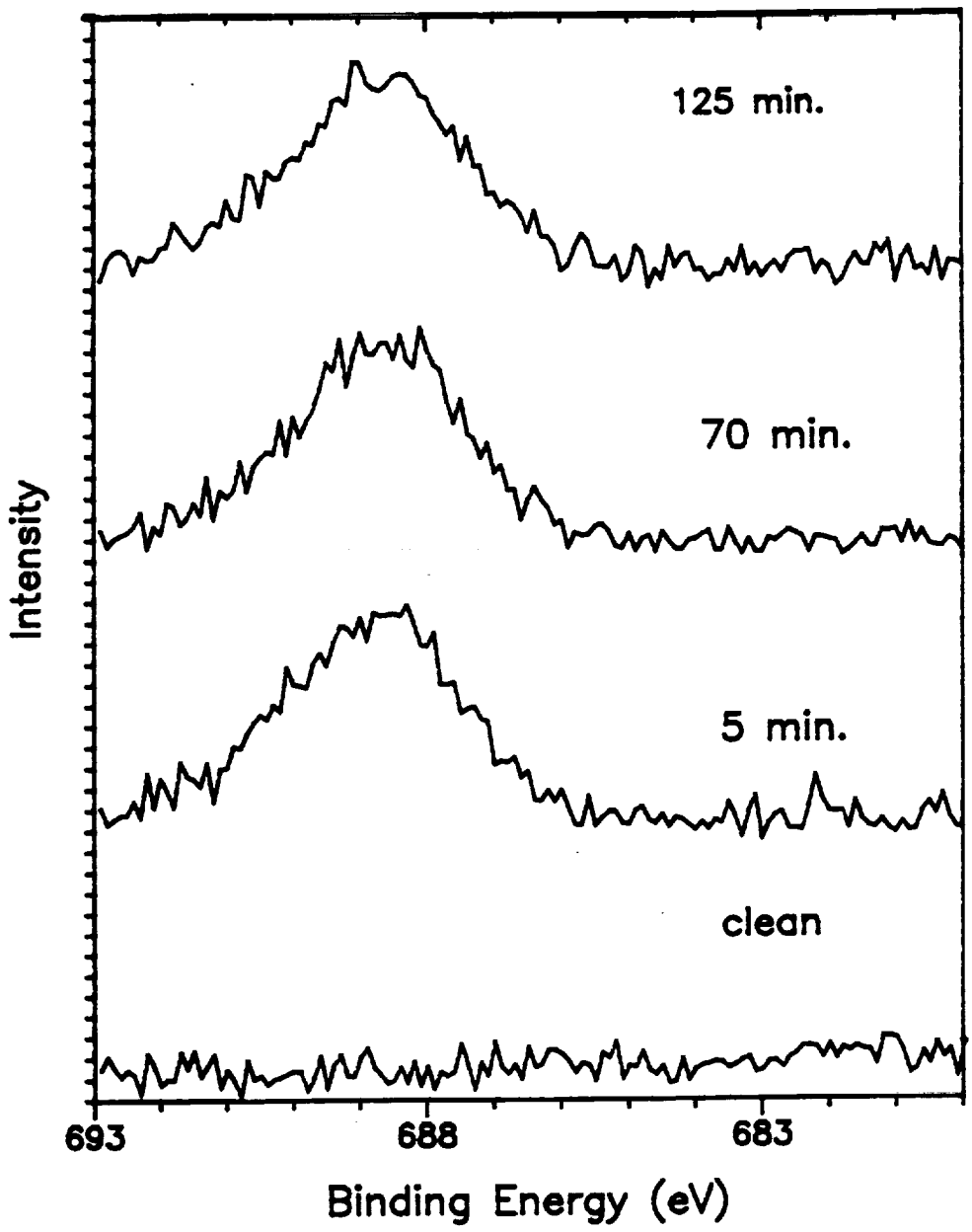

Figure 3.3 Perfluoro-1-methoxy-2-ethoxy ethane adsorbed onto a cooled, gold surface. F(1s) spectra monitored with increasing Al monochromatic x-ray source.

It is known through monitoring of the iron surface temperature, that over longer periods of time, temperature variations do occur. The adsorbed mPFAE1 layer on the cooled gold was not adversely affected by exposure to the monochromatic x-ray source.

Shown in Figure 3.4 are two F(1s) spectra for mPFAE1 adsorbed onto 115 K, polycrystalline iron surface, at Al monochromatic x-ray exposures of 20 minutes and 495 minutes. Molecular adsorption of mPFAE1 on the polycrystalline iron is observed at temperatures below 134 K. The temperature of the iron foil varied slightly over the eight hour period, but always remained well below the clean iron surface reaction temperature of 138 K, so that any changes observed in the fluorine, carbon and oxygen spectra can be attributed to x-ray exposure only. Continuous exposure of the molecularly adsorbed mPFAE1 to monochromatic x-rays does not result in conversion of the covalently bonded fluorine to an inorganic fluoride and does not result in growth in low binding energy carbon and oxygen species. Additionally, the carbon, oxygen and fluorine ratios do not deviate from parent stoichiometric ratio, with increasing monochromatic x-ray exposure. The defluorination of the mPFAE1 observed upon exposure to the non-monochromatic x-rays was not observed when the monochromatic x-ray source was used.

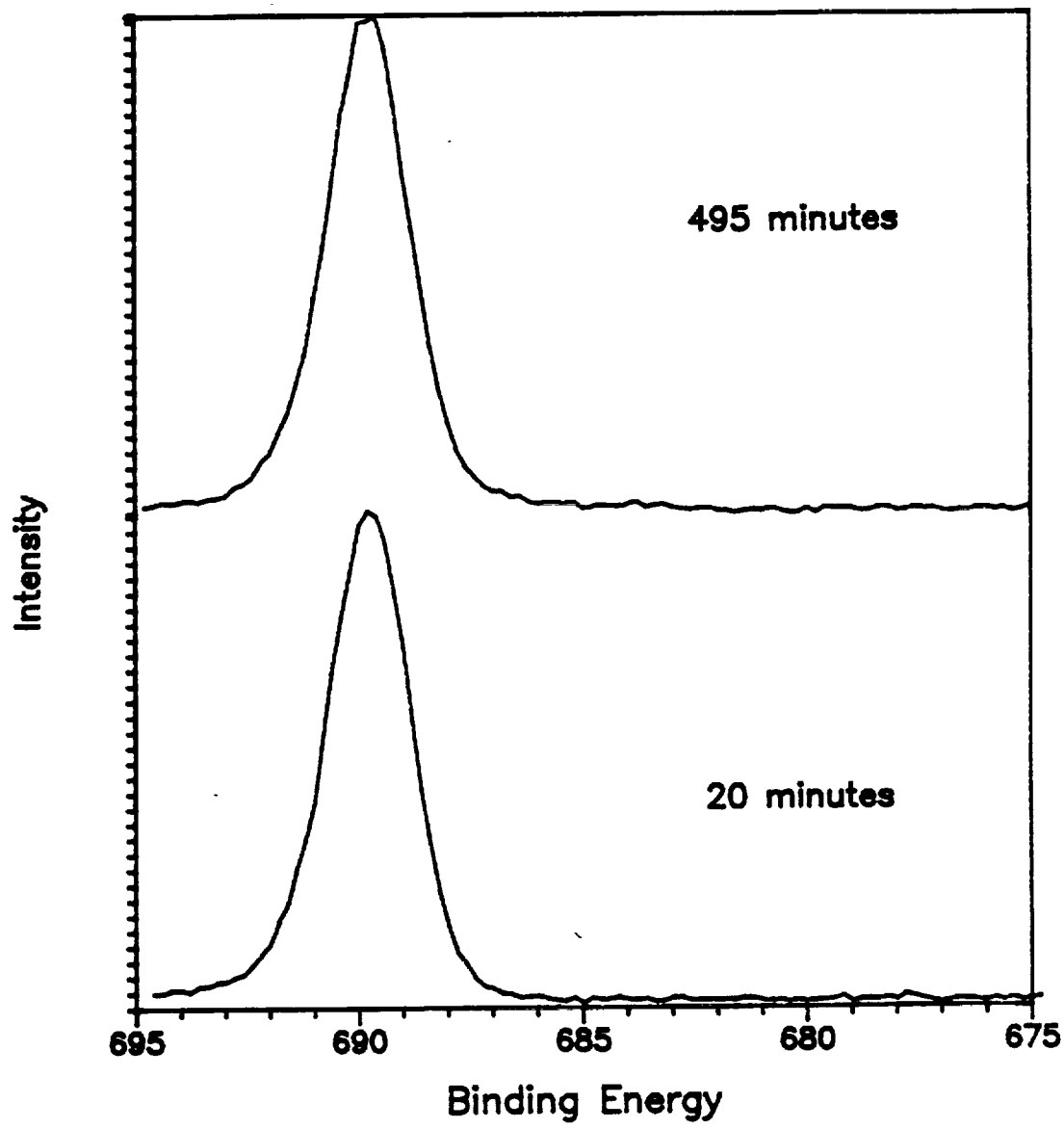

Figure 3.4 Perfluoro-1-methoxy-2-ethoxy ethane adsorbed onto a 115 K polycrystalline iron surface. F(1s) spectra at Al monochromatic x-ray exposures of 20 and 495 minutes.

D. DISCUSSION

The photon and electron induced fragmentation of gaseous halocarbons has been extensively studied, because of the link to the destruction of the stratospheric ozone layer.[1-4] When a carbon halogen bond is broken, the newly formed atomic chlorine radical reacts with an ozone molecule, O_3, to form O_2 and ClO. The tendency of photons and electrons to stimulate the dissociation of halocarbons requires that the effect of photon and electron beams used to probe an adsorbed halocarbon layer needs to be investigated.

Continuous exposure of a model fluorinated ether layer, adsorbed on a room temperature, polycrystalline iron surface, to the Al non-monochromatic x-ray source caused a conversion in the fluorine XPS spectra from the covalently bonded fluorine to an inorganic fluoride. This conversion was indicative of C-F bond breaking and Fe-F bond formation. The dissociation in the adsorbed layer could be distinguished from the thermally activated decomposition. PTFE, polytetrafluoroethylene, a linear polymer structure with repeating CF_2 units, has also been reported to be unstable upon exposure to ionizing radiation.[5-9] Irradiation of the polymer lowers the molecular weight of the polymer chain through chain scission. Primary radicals are formed when C-C bonds break and secondary and highly mobile

fluorine radicals are formed when C-F bonds break. The highly reactive and mobile radicals recombine forming branched and cross-linked polymeric structures and short chain, low molecular weight, saturated fluorocarbons terminated with CF_3 groups.[5-9] The low molecular weight fluorocarbons fragments evolve from the surface.[5-9]

The degradation observed upon exposure of the PTFE and the model fluorinated ethers to the non-monochromatic x-ray source could be caused by either x-ray photons or secondary electrons, produced internally and externally. Exposure to an electron beam and to x-rays induced the same type of damage in the PTFE.[8] Low energy electrons are reported to be more effective for the fragmentation of chlorofluoromethane, $CFCl_3$, than photons.[3] The cross section for dissociative electron attachment, resulting in Cl^-, is 10^4 times larger than the cross section for photodecomposition resulting in Cl.[3] Dissociative electron attachment is possible for zero electron kinetic energy for $CFCl_3$, with slightly higher impact energies needed for CF_2Cl_2 and CF_3Cl.[3] The electrons produced at the x-ray window or internally are thought to be primarily responsible for the C-C bond scission and the defluorination of the PTFE and perfluoro-1-methoxy-2-ethoxy ethane.

Use of the Al monochromatic x-ray source eliminated the

degradation of the perfluoro-1-methoxy-2-ethoxy ethane, over the experimental time frame. The monochromatization of the emitted x-rays removes satellite interference, improves the signal-to-background by eliminating the Bremsstrahlung continuum and improves the resolution through selection of an individual line from the unresolved principle line doublet.[10] Only a selected small portion of the total Kα emission falls on the sample, significantly reducing the production of internal secondary electrons. The Al monochromatic source x-ray window is far removed from the sample, so unlike the twin anode source, electrons generated at the x-ray window are unlikely to interact with the sample surface. By eliminating the extraneous sources for electron generation, XPS can be safely used to probe an adsorbed halocarbon layer.

CHAPTER IV

MODEL FLUORINATED ETHERS ON CLEAN IRON

A. INTRODUCTION

While polymeric perfluoroalkylether (PFAE) fluids are stable to approximately 400°C in an inert, metal free environment and to approximately 300°C in an oxidizing metal free environment, they catalytically decompose in the presence of many metals.[1-8] The interaction of halogens and halocarbons with metal surfaces has been previously investigated under ultra-high vacuum conditions.[9] Halogens dissociatively adsorb on metal surfaces in the monolayer regime, with multilayer formation of the molecular species at low temperatures and high exposures.[9-13] Halocarbons dissociatively adsorb on many transition metals with carbon halogen bond scission and metal halide bond formation.[9,14-16] Iron has been shown to attack both C-Cl bonds and C-F bonds of CCl_4, $CFCl_3$, CCl_2F_2 and $CF_3OCF_2CF_2OCF_2CF_3$ at relatively low temperatures of 180 K and below.[9,15-21]

The goal of this research is to investigate the metal enhanced decomposition of fluorinated ether lubricants, using model structures and atomically clean, polycrystalline iron surfaces. X-ray photoelectron spectroscopy (XPS) and temperature programmed desorption (TPD) were used to explore the surface chemistry of three model fluorinated ethers on clean polycrystalline iron surfaces. The model structures investigated were perfluoro-1-methoxy-2-ethoxy ethane,

$CF_3OCF_2CF_2OCF_2CF_3$, mPFAE1, perfluoro-1-methoxy-2-ethoxy propane, $CF_3OCF_2CF(CF_3)OCF_2CF_3$, mPFAE2, and perfluoro-1,3-diethoxy propane, $CF_3CF_2OCF_2CF_2CF_2OCF_2CF_3$, mPFAE3. The model structures are monomer units of polymeric PFAE materials being considered for use as high temperature lubricants. These low molecular weight structures have the same functional units as the polymeric materials, but yield results which are simpler to interpret. Defluorination of the model fluorinated ethers was observed at low temperatures, 155 K and below. Based on the XPS results, decomposition was initiated at approximately 140 K for mPFAE1 and mPFAE2, with preferential attack at the C-F bond of the terminal fluoromethoxy and at 155 K for mPFAE3, with preferential attack at the C-F bond of either CF_3 or CF_2O. Iron fluoride formation, observed at the reaction temperature for the three model fluorinated ethers, is considered to be the driving force for the reaction. The reactivity of iron toward mPFAE decomposition is due to the strength of the iron fluoride bond and the strong electron donating ability of metallic iron.

B. EXPERIMENTAL

The XPS measurements were conducted in a VG Scientific ESCALAB/SIMSLAB Mk.II, with a typical base pressure of $1x10^{-10}$ torr. The system was equipped with a twin anode x-ray

source, Al Kα (1486.6 eV) and Mg Kα (1253.6 eV), an Al Kα monochromatic x-ray source, an Ar ion gun, a stainless steel leak valve controlled doser and a sample manipulator.

The TPD experiments were conducted in a turbomolecular pumped stainless steel UHV chamber, with a typical base pressure of $2x10^{-10}$ torr. The system was equipped with a water cooled, Ti sublimation pump, an apertured UTI-100C quadrupole mass spectrometer, an Auger spectrometer with retarding field energy analyzer and integral electron gun, an Ar ion gun, a bakeable glass/teflon gas handling system and a sample manipulator. The sample could be reproducibly positioned in direct line-of-site to the mass spectrometer aperture and ionizer, approximately 40 mm removed from the ionizer. The mass spectrometer ionizing region was open to the chamber.

Exposure to electrons, as either secondaries from a photon source or as an energetic beam of electrons, can cause dissociation of molecularly adsorbed, halogenated hydrocarbons.[15,22] To avoid electron induced damage of the adsorbed model fluorinated ether layer, the Al monochromatic source was used exclusively. The Al monochromatic x-ray source significantly reduced the Kα flux and the exposure to continuum radiation (Bremsstrahlung), through the use of a quartz crystal monochromator, as well as, eliminating the exposure of the adsorbed layer to electrons generated at the

twin anode x-ray window. AES was never used to probe the adsorbed mPFAE layer, but only to check cleanliness of the iron surface prior to mPFAE exposure.

The polycrystalline iron foils (10 mm x 10 mm x 0.5 mm) were polished using standard metallographic techniques to a surface finish of 0.3 μm, followed by ultrasonic cleaning in acetone to remove the polishing residue. The iron foils were cleaned in UHV, with cycles of Ar^+ bombardment and annealing. The iron surface was considered atomically clean when contaminants, in particular carbon, oxygen, sulfur and nitrogen, could not be detected using either XPS or Auger. In the XPS chamber, the sample could be cooled to 100 K with liquid N_2 and heated to 900 K by radiation from a 0.2 mm tungsten filament located approximately 5 mm behind the sample. In the TPD chamber, the sample could be cooled to 115 K with liquid N_2 and heated to 1000 K using electron bombardment. During a TPD run, when perfluoro-1-methoxy-2-ethoxy ethane was adsorbed on the iron crystal, sample heating was by radiation from the heater filament, with a 200 V positive bias imposed on the filament to prevent stray electrons from interfering with the adsorbate. The sample could be heated linearly with time, through the temperature region of interest, up to 400 K. Typically a heating ramp of 15 +/- 2 K/s was used. The temperature was measured using a chromel-alumel, Type K, thermocouple spotwelded to

an edge of the front face of the sample.

Gases were admitted to the XPS chamber, with no directionality, through a stainless steel variable leak valve. Gases were admitted to the TPD chamber undirected through a leak valve or directed to the sample surface through a glass capillary with a 10 μm constriction to control the flow of gases into the chamber. The dosing capillary extends into the chamber to allow for positioning of the front face of the sample 1.5 - 2.0 mm from the end of the capillary.

The three perfluoroalkylethers investigated were obtained from Exfluor Research Inc. and used as received. A GC/MS analysis showed mPFAE1 and mPFAE2 to be at a minimum 98 % pure and mPFAE3 to be at a minimum 95 % pure, with higher molecular weight ethers present as impurities. Prior to introduction into the vacuum chamber, the mPFAEs were further purified by repeated freeze-pump-thaw cycles.

In both the XPS and TPD chambers, the fluorinated ether exposures were calculated from uncalibrated ion gauge readings and are reported in Langmuir (1 L = 1×10^{-6} torr sec). In the XPS chamber, adsorbate coverages were obtained by C(1s) and O(1s) XPS measurements calibrated using the known saturation coverage of CO on Fe(110).[23] The coverages reported in reference to the polycrystalline iron XPS data are approximate.

XPS spectra of unreacted mPFAE, shown in Figure 4.1, were obtained following exposure of a clean iron surface, at 100 K to a nominal 3 L exposure of the model fluorinated ether. The approximate coverage of the fluorinated ether on the 100 K iron surface, for the 3 L exposure, is 8 ML (monolayer), based on the CO/Fe(110) calibration. The approximate thickness of the model fluorinated ether overlayer on the clean iron surface was calculated using the expression:

$$d=(\lambda/\cos\theta)\ln(I_o/I), \qquad (4.1)$$

where θ is the emission angle with respect to the surface normal (θ is near zero for our experiments), I is the substrate signal intensity, I_o is the substrate signal intensity in the absence of an overlayer and λ is the electron mean free path. I and I_o were obtained by measuring the $Fe(2p_{3/2})$ signal intensity with an ether overlay and in the absence of an overlayer, respectively. An estimated published value of 13 Å was used to approximate the electron mean free path.[24] An upper limit to the molecular diameter was estimated to be 4.7 Å, based on carbon and fluorine atomic radii of 0.77 and 0.68 Å, respectively and a C-F bond length of 1.3 Å.[25] The thickness estimated by this procedure is 6.25 ML. The ether overlayer and substrate were heated to a series of temperatures between 120 and 160 K, with no additional exposures to

mPFAE, and immediately cooled using liquid N_2. The rate at which the final temperature was approached varied from 0.4 to 1.1 K/s and the ramps applied were not linear nor was any effort made to exactly reproduce the ramps from run to run. Detailed scans of the carbon XPS region were acquired, using both 20 and 50 eV pass energies, after each heat treatment. Detailed scans of the oxygen, fluorine and iron regions were also acquired, using a 50 eV pass energy.

TPD spectra were acquired following the exposure of a clean, 115 K iron substrate to a directed dose of mPFAE1. A linear temperature ramp was applied to the substrate and evolving species were detected as a function of increasing temperature. All mass spectra were obtained with the energy of the ionizing electrons set at 70 eV and the filament current at 2.0 mA. Prior to the start of each experiment, the iron substrate was cleaned by Ar^+ sputtering at 650 K for approximately 20 minutes.

Slight temperature differences were noted in the onset of mPFAE1 decomposition based on the XPS and the TPD results. Onset of decomposition using XPS was found to be 138 K and using TPD to be approximately 155-160 K, as characterized by an estimate of the initial rise of the monolayer peak. The variation in the decomposition temperature can be attributed to the differences in the heating rates used in the XPS and TPD experiments. The XPS

heating rate varied from 0.4 to 1.1 K/s and was not necessarily linear with time. The XPS heating rate was 20 to 30 times slower than the TPD heating rate of 15 +/- 2 K/s. The analysis put forth by Redhead was used to model the decomposition kinetics for a heating rate of 0.7 K/s, characteristic of the XPS experiments, assuming an order of 1, a preexponential factor of 10^{13} s^{-1} and an activation energy of 40 kJ/mol, consistent with the peak temperature observed in the TPD experiments.[26] The initial rise of the modeled thermal desorption peak agrees with the XPS experimental value for the onset of decomposition.

C. RESULTS

1. XPS Results

Figure 4.1a-c shows the multilayer C(1s) spectra, for the three model perfluorinated ethers, adsorbed onto 100 K, polycrystalline iron surfaces. As can be seen from Figure 4.1, the C(1s) binding energy increases with increasing electronegative substitution and carbon atoms, with differing numbers of electronegative substituents, can be resolved using XPS. The two C(1s) peaks, in the mPFAE1 spectrum of Figure 4.1a, correspond to CF_3O and CF_3/CF_2O. An additional peak is observed in the C(1s) spectrum for mPFAE2 (Figure 4.1b), which corresponds to CFO. The two carbon peaks in the mPFAE3 spectrum of Figure 4.1c, correspond to

a) Perfluoro-1-methoxy-2-ethoxy ethane,

$CF_3OCF_2CF_2OCF_2CF_3$ mPFAE1

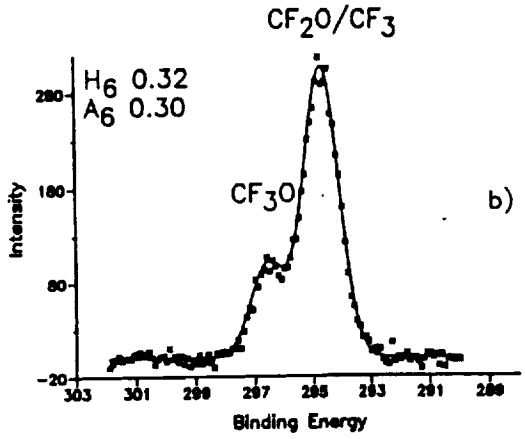

b) Perfluoro-1-methoxy-2-ethoxy propane,

$CF_3OCF_2\underset{CF_3}{CF}OCF_2CF_3$ mPFAE2

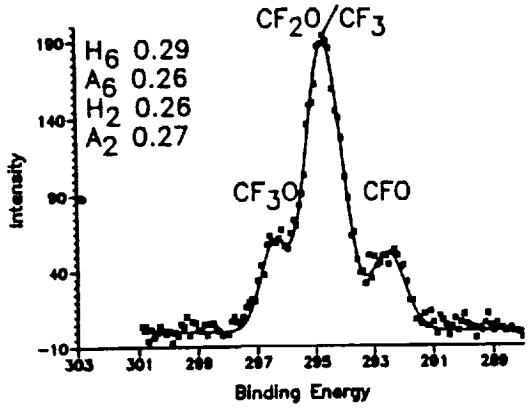

c) Perfluoro-1,3-diethoxy propane, mPFAE3

$CF_3CF_2OCF_2CF_2CF_2OCF_2CF_3$

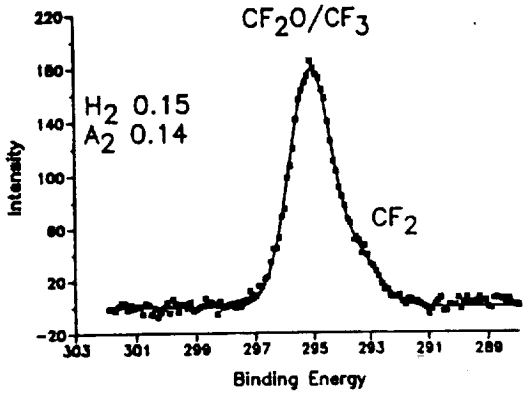

Figure 4.1 C(1s) spectra and the fits to the C(1s) spectra of the model fluorinated ethers adsorbed on a 100 K, clean polycrystalline iron surface: **a)** perfluoro-1-methoxy-2-ethoxy ethane, mPFAE1 **b)** perfluoro-1-methoxy-2-ethoxy propane, mPFAE2 **c)** perfluoro-1,3-diethoxy propane, mPFAE3. Listed next to each spectra are the intensity ratios, height (H) and area (A), calculated from the fits.

CF_3/CF_2O and CF_2. Using a 20 eV pass energy, the CF_3/CF_2O and the CF_2/CFO pairs are not resolvable, when both species of the pair are present on the surface. The CF_2/CFO pair can be differentiated, when only one species of the pair is present on the surface, as with mPFAE2 (CFO) and mPFAE3 (CF_2).

Also shown in Figure 4.1, are the Gaussian fits to the model fluorinated ether C(1s) spectra, with asterisks representative of the raw data, and the solid lines the fits to the raw data. Two computer programs were used to fit the two peaks in the mPFAE1 and mPFAE3 C(1s) spectra. The first program was limited to five adjustable parameters: the height and center of each peak and a single peak width, fitting a maximum of two peaks. The second routine allowed for independent variation of all parameters, the height, center and width for each peak, allowing for fits to spectra with two or more peaks. Only the second program was used to fit the three peaks in the mPFAE2 C(1s) spectra. Good agreement was found between the two fitting procedures. The 296 (CF_3O)/ 294 (CF_3/CF_2O) and 292 (CF_2/CFO)/ 294 (CF_3/CF_2O) height (H_6 and H_2, respectively) and area (A_6 and A_2, respectively) ratios, calculated from the Gaussian fits to the multilayer spectra, are listed next to each spectrum in Figure 4.1. The intensity ratios were used to monitor the changes in the adsorbed layer, as a function of increasing

TABLE 4.I

Comparison of the theoretical and experimental C(1s) area and height intensity ratios for the three model perfluoroalkylethers. I_T and I_E are the theoretical and experimental values, respectively. I_6/I_4 is the 296 eV (CF_3O) / 294 (CF_3/CF_2O) intensity ratio. I_2/I_4 is the 292 (CF_2/CFO) / 294 (CF_3/CF_2O) intensity ratio.

		mPFAE1		mPFAE2		mPFAE3	
		I_T	I_E	I_T	I_E	I_T	I_E
I_6/I_4	Area	0.25	0.30	0.25	0.26		
	Height	0.25	0.32	0.25	0.29		
I_2/I_4	Area			0.25	0.27	0.17	0.14
	Height			0.25	0.26	0.17	0.15

temperature. Given in Table 4.I, are the theoretical C(1s) intensity ratios for each of the model fluorinated ethers, as well as, the experimental intensity ratios calculated from the fits to the multilayer (100 K) C(1s) spectra.

Carbon, oxygen and fluorine binding energies, characteristic of the mPFAEs, are listed in Table 4.II. The binding energies, given in Table 4.II, were obtained from the Gaussian fits to C(1s) spectra, at monolayer coverages, for mPFAE1, mPFAE2 and mPFAE3 adsorbed on polycrystalline iron substrates. As the coverage decreased in going from the multilayer, shown in Figure 4.1, to the monolayer, listed in Table 4.II, a rigid shift of 0.7 eV to lower binding energy, was observed. The carbon, oxygen and fluorine binding energies, for mPFAE1 at monolayer coverages on cooled, inert gold, were equivalent to the binding energies on the iron substrates. The carbon and oxygen binding energies for $(CH_3CH_2)_2O$[27] and the fluorine binding energy for FeF_x are also listed in Table 4.II.

Upon warming from 100 K to a temperature below the reaction temperature, an overall decrease in the carbon, oxygen and fluorine intensities, in the stoichiometric ratio of the parent, was observed. In this temperature range, the mPFAEs molecularly desorb from the polycrystalline iron surface, with the carbon, oxygen and fluorine peak shapes and ratios and the 296/294 and 292/294 carbon ratios

TABLE 4.II

Comparison of Binding Energies (eV) for Fluorinated and Nonfluorinated Compounds

	C(1s)	O(1s)	F(1s)
mPFAE			
CF_3O	296.0 eV	535.5 eV	689.0 eV
CF_3/CF_2O	294.1 eV	535.5eV	689.0 eV
CF_2	293.0 eV		689.0 eV
CFO	292.0 eV	535.5 eV	689.0 eV
Diethyl ether[27]			
CH_3C	285.0 eV		
CCH_2O	286.6 eV	533.2 eV	
Iron Fluoride			
FeF_x			684.0 eV

unaltered from the unreacted, 100 K, C(1s) XPS spectra shown in Figure 4.1a-c.

At the individual reaction temperatures of the three model fluorinated ethers, several changes were observed in the carbon, oxygen and fluorine spectra as a function of increasing temperature, which could not be ascribed to molecular desorption. Figures 4.2a, 4.3a and 4.4a show the C(1s) spectra and the fits at the reaction temperature for the three mPFAEs. Figure 4.2a shows the mPFAE1, perfluoro-1-methoxy-2-ethoxy ethane C(1s) spectrum and fit at 138 K. At this temperature, the 296/294 height (H_6) and area (A_6) ratios decreased, with respect to the unreacted mPFAE1, signifying loss of CF_3O relative to CF_3/CF_2O. Also observed was a small increase in intensity at 292 eV, characteristic of CFO. Figure 4.3a shows the mPFAE2, perfluoro-1-methoxy-2-ethoxy propane C(1s) spectrum and fit at 142 K. At this temperature, the 296/294 height (H_6) and area (A_6) ratios decreased relative to the unreacted mPFAE2, signifying loss of CF_3O relative to CF_3/CF_2O and the 292/294 height (H_2) ratio increased relative to the unreacted mPFAE2, signifying a gain in CFO relative to CF_3/CF_2O. Figure 4.4a shows the mPFAE3 C(1s) spectrum and fit at 155 K. At this temperature, the 292/294 height (H_2) and area (A_2) ratios increased relative to unreacted mPFAE3, signifying a gain in CF_2/CFO relative to CF_3/CF_2O. Also observed was an increase

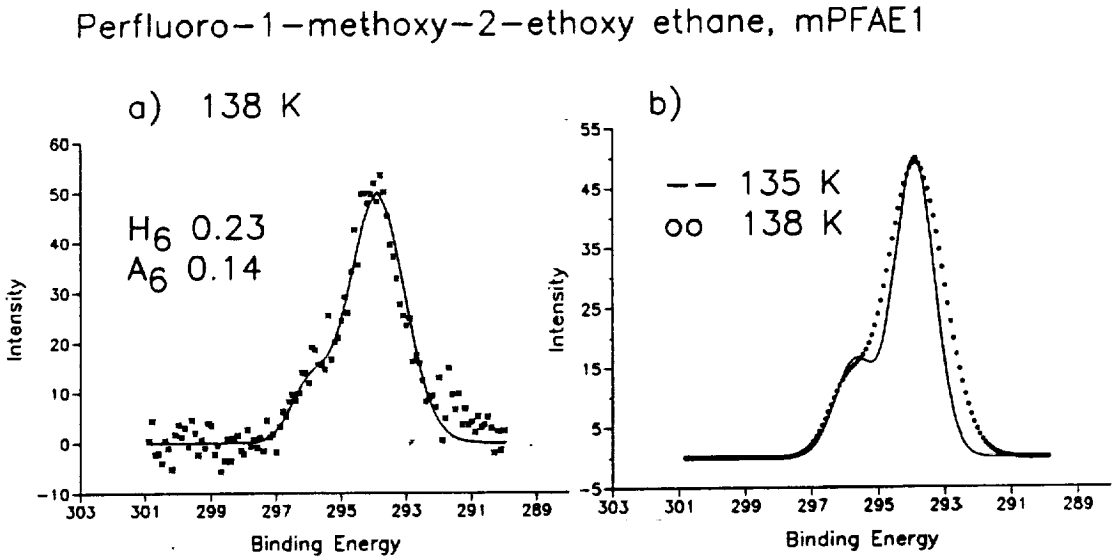

Figure 4.2 **a)** C(1s) spectrum and the fit to the C(1s) spectrum at the reaction temperature for perfluoro-1-methoxy-2-ethoxy ethane, mPFAE1. Peak area (A) and height (H) ratios are given. **b)** The fits to the mPFAE1 C(1s) spectra at 135 and 138 K were overlaid to illustrate the changes with increasing annealing temperature.

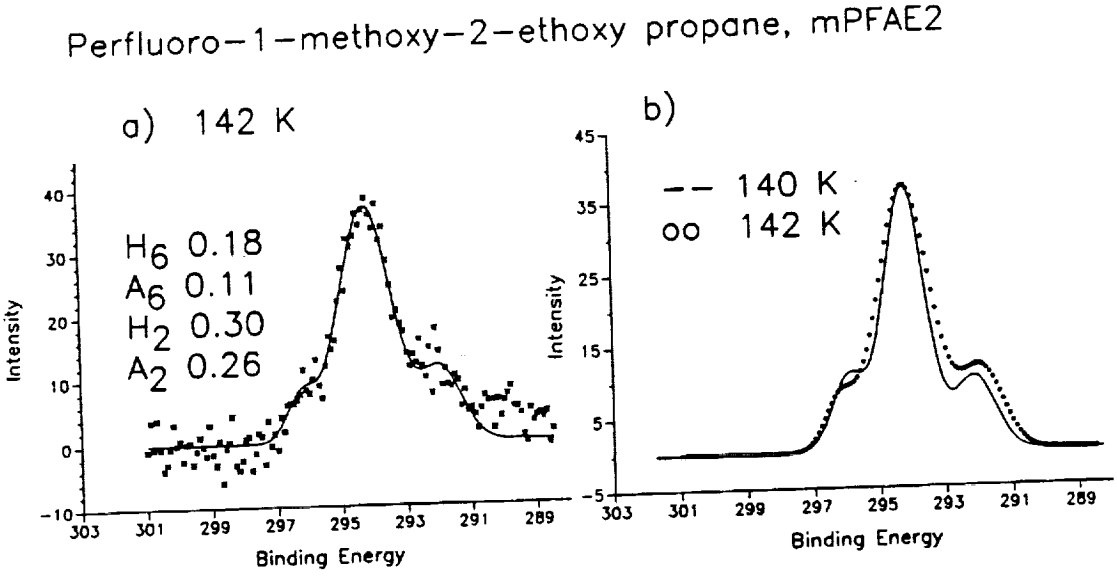

Figure 4.3 **a)** C(1s) spectrum and the fit to the C(1s) spectrum at the reaction temperature for perfluoro-1-methoxy-2-ethoxy propane, mPFAE2. Peak area (A) and height (H) ratios are given. **b)** The fits to the mPFAE2 C(1s) spectra at 140 and 142 K were overlaid to illustrate the changes with increasing annealing temperature.

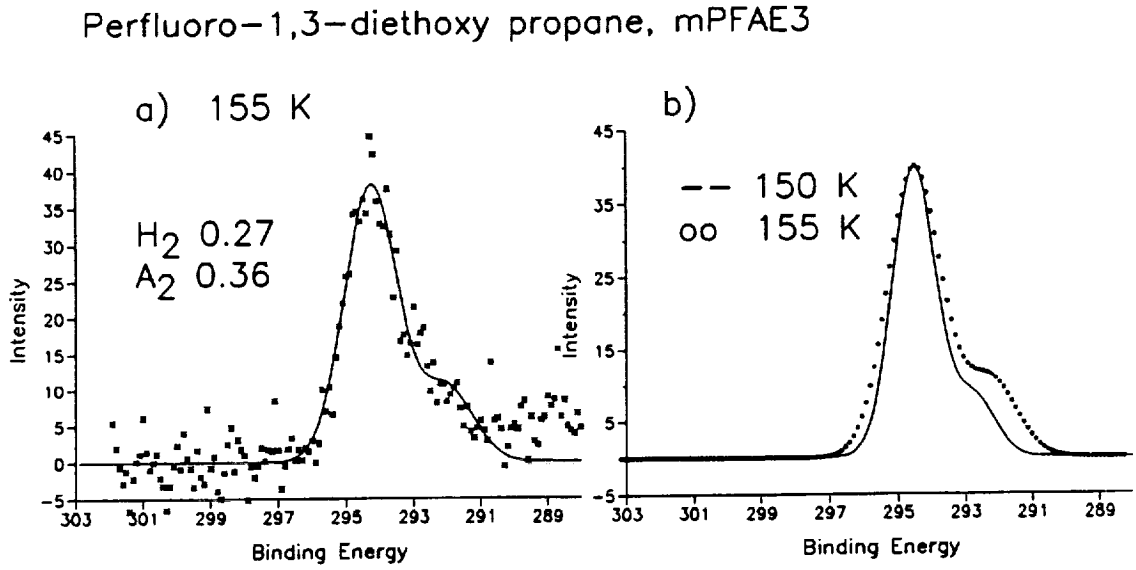

Figure 4.4 **a)** C(1s) spectrum and the fit to the C(1s) spectrum at the reaction temperature for perfluoro-1,3-diethoxy propane, mPFAE3. Peak area (A) and height (H) ratios are given. **b)** The fits to the mPFAE3 C(1s) spectra at 150 and 155 K were overlaid to illustrate the changes with increasing annealing temperature.

in intensity at 289 eV, characteristic of CF. In Figures 4.2b, 4.3b and 4.4b the height normalized fits to the reacted and unreacted C(1s) spectra have been overlaid to further illustrate the changes in the C(1s) spectra at the reaction temperature.

The changes in the C(1s) spectrum, with increasing annealing temperature, were not simply a consequence of reduced mPFAE coverage due to desorption. Overlaid in Figure 5, are the height normalized fits to the mPFAE1 C(1s) spectrum for a submonolayer carbon coverage at 100 K and for a submonolayer carbon coverage at 138 K, the mPFAE1 reaction temperature. The coverage on the 100 K, low exposure surface is approximately 1/2 of the carbon coverage at the reaction temperature. Broadening of the 294 eV peak and a decrease in the 296 eV peak height observed at the reaction temperature, were not observed for submonolayer carbon coverages at low temperatures. The low coverage, low temperature, C(1s) peak shape is identical to the spectrum at multilayer coverage, within experimental accuracy. Moreover, the carbon, oxygen and fluorine area ratios, the peak shapes and the 296/294 and 292/294 carbon ratios at the submonolayer coverage, were unaltered from the multilayer spectra at 100 K, indicating that the adsorption of the mPFAEs was molecular at 100 K.

At the reaction temperature and above, reaction

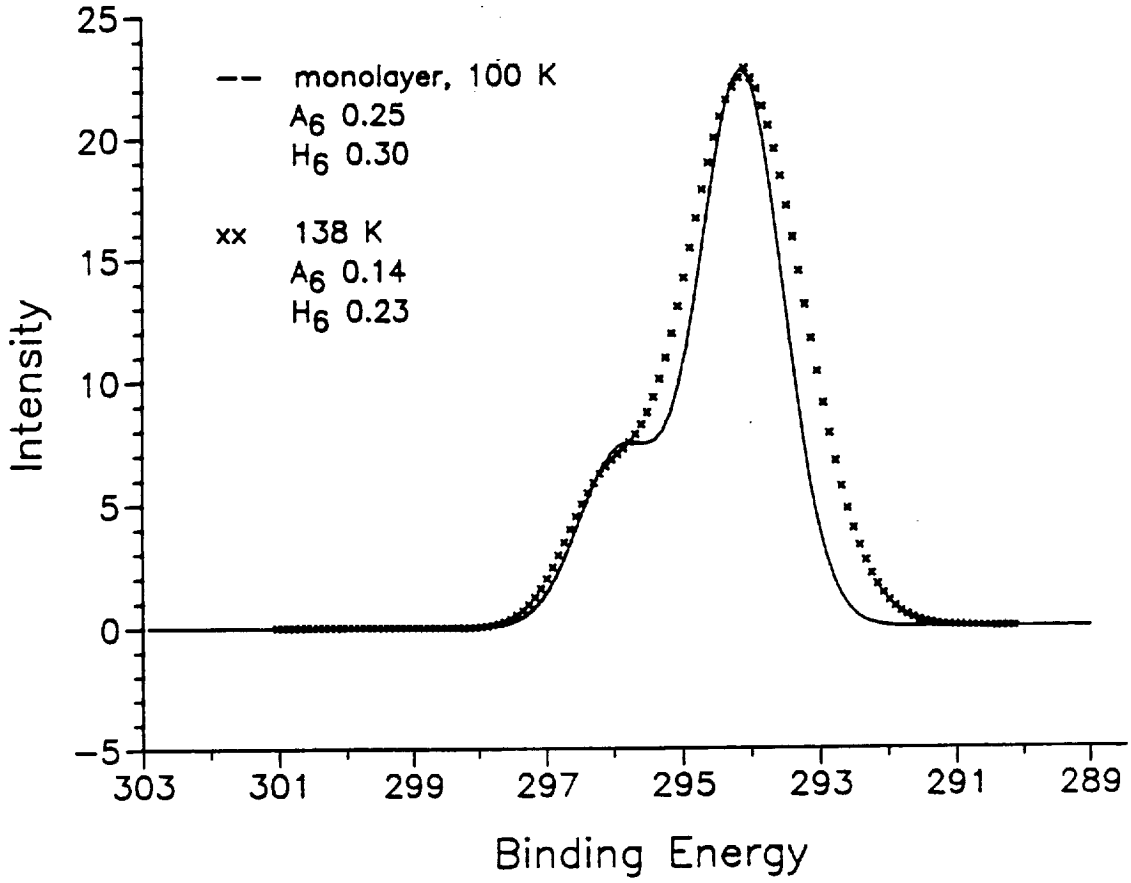

Figure 4.5 The fits to the mPFAE1 100 K, C(1s) spectrum at submonolayer coverages and the mPFAE1 C(1s) spectrum at the reaction temperature of 138 K have been overlaid. The carbon coverage at 100 K is 1/2 of the carbon coverage at the reaction temperature of 138 K.

products were observed on the polycrystalline iron surface. Figure 4.6a-c shows the growth in low XPS binding energy carbon, oxygen and fluorine species, as a function of increasing temperature for mPFAE1. Shown in Figure 4.6d are the carbon, oxygen, fluorine peak area ratios for the total (T), low binding energy (L) and high binding energy (H) components at each temperature. In the carbon XPS spectra, a small growth in intensity is observed at 292 eV, characteristic of CFO, as well as, growth in a broad peak centered at 285.8 eV. The growth in carbon intensity at 292.0 eV can be seen more clearly in Figure 4.2a. In the oxygen XPS spectra, growth in a broad peak centered at 532.4 eV is observed. In the fluorine XPS spectra, growth in intensity is observed at 684.0 eV, characteristic of iron fluoride. The low binding energy reaction products are indicative of carbon-fluorine bond breaking in the model fluorinated ethers, accompanied by C-O and C-C bond scission at the higher temperatures.

The carbon, oxygen, fluorine peak area ratios, shown in Figure 4.6d, deviate from the mPFAE1 parent stoichiometric ratio of 2.5 : 1 : 6.0, progressively with increasing temperature. At 138 K and 165 K, the high binding energy carbon, oxygen and fluorine and the low binding energy carbon and oxygen ratios show minimal deviation from the

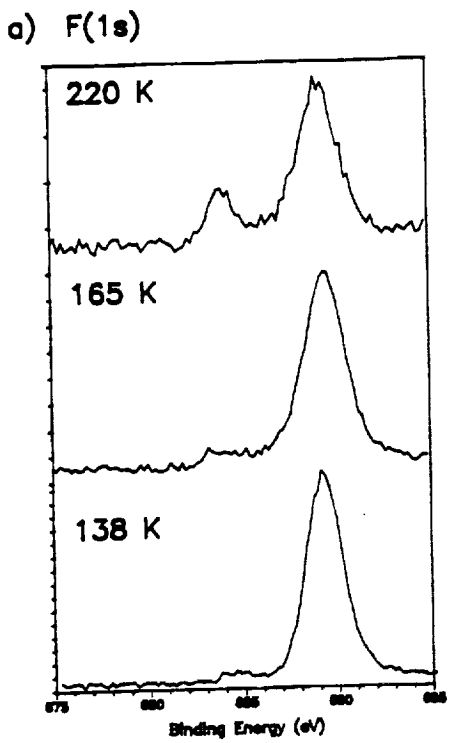

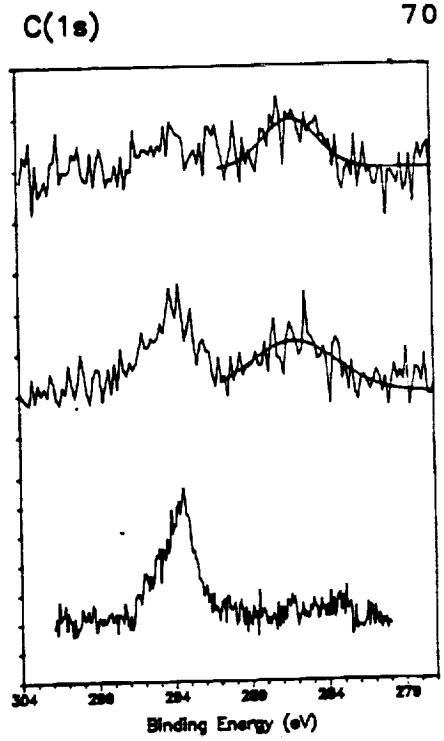

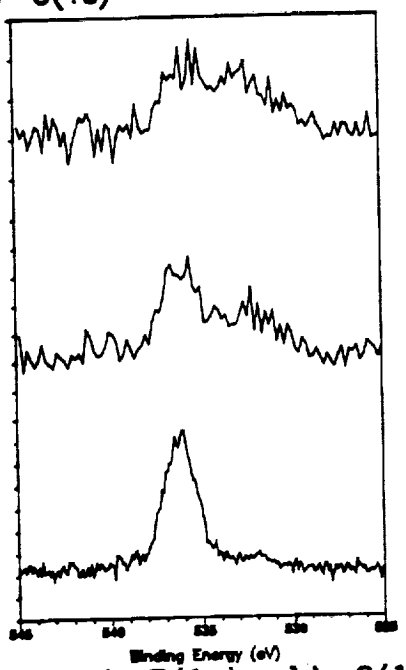

d)

220 K

$C_H:O_H:F_H$	1.8 : 1 : 4.2
$C_L:O_L:F_L$	1.8 : 1 : 1.3
$C_T:O_T:F_T$	1.8 : 1 : 3.0

165 K

$C_H:O_H:F_H$	2.4 : 1 : 5.8
$C_L:O_L:F_L$	1.8 : 1 : 1.0
$C_T:O_T:F_T$	2.35 : 1 : 3.6

138 K

$C_H:O_H:F_H$	2.4 : 1 : 5.9
$C_L:O_L:F_L$	2.33 : 1 : 1.3
$C_T:O_T:F_T$	2.4 : 1 : 5.0

Figure 4.6 **a)** F(1s), **b)** C(1s) and **c)** O(1s) mPFAE1 XPS spectra at three annealing temperatures of 138, 165 and 220 K. **d)** A comparison of the carbon, oxygen and fluorine high binding energy (H), low binding energy (L) and total (T) ratios at the annealing temperature. F(1s) tick mark=200, C(1s) and O(1s) tick mark=50

parent ratio. In contrast, at 138 and 165 K, the low binding energy carbon, oxygen and fluorine ratio is extremely deficient in fluorine when compared to the parent. At 220 K, deficiencies are observed for both carbon and fluorine in the high and low binding energy ratios. The same trends are observed in the mPFAE2 and mPFAE3 carbon, oxygen and fluorine XPS spectra, at the appropriate reaction temperature and above. Growth in a low binding energy carbon+oxygen layer, in the stoichiometric ratio of the parent, but deficient in fluorine, was also observed when an iron surface was held at 165 K and exposed to mPFAE1.[20] Covalently bonded fluorine was not observed, on the 165 K surface, until 1 ML of a carbon+oxygen passivating layer formed on the surface.

2. TPD Results

TPD spectra following perfluoro-1-methoxy-2-ethoxy ethane, mPFAE1, exposure at 115 K are shown in Figure 4.7. The spectra depicts mass 69, CF_3^+, an intense fragment of perfluoro-1-methoxy-2-methoxy ethane. The parent ion was not observed. Spectra at mass 31, CF^+, mass 47, CFO^+ and mass 50, CF_2^+ are identical. Mass 19, F^+ and mass 20, HF^+ were not detected. At the lowest exposure, two peaks of approximately equal intensity are observed at 185 and 148 K. The high temperature state shifted to 176 K as the exposure to mPFAE1 increased and saturated quickly at exposures below

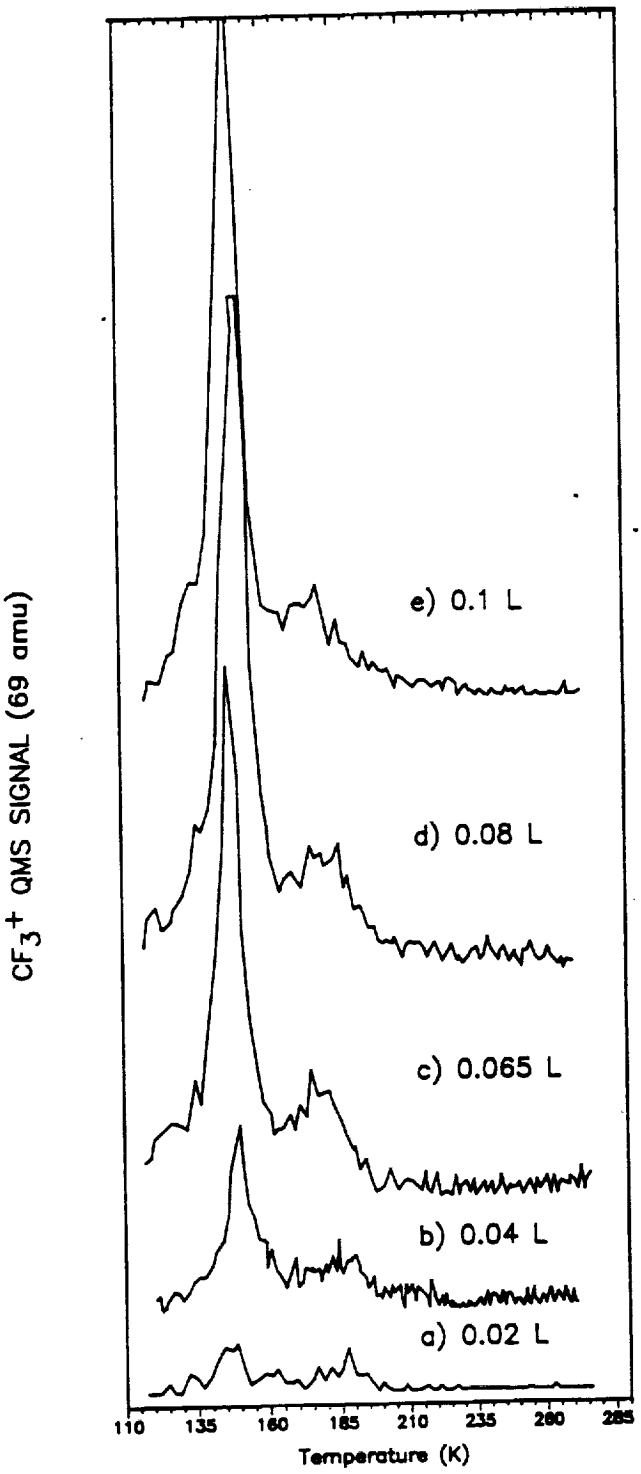

Figure 4.7 Line of sight TPD spectra for mPFAE1 at five exposures: **a)** 0.02 L, **b)** 0.04 L, **c)** 0.065 L, **d)** 0.08 L and **e)** 0.1 L.

0.065 L. The FWHM (full width at half maximum) of the high temperature peak is 25 K and does not vary significantly with increasing coverage. The low temperature state, at 149 K, does not saturate with increasing exposure, and is characteristic of sublimation from the multilayers.

Since the two peaks in the TPD spectra are not baseline resolved, it is difficult to determine kinetic parameters by conventional analysis techniques.[28] A plot of ln N versus ln c, at constant temperature, where N is the desorption rate and c is the surface coverage, gives a straight line with slope of n, the order of the reaction.[28] Plots of ln N versus ln c, at constant temperature, for the high temperature peak yield slopes which vary from 0.6 to 2.0, for temperatures between 165 to 200 K. The variation in slope may be due to the contribution of the multilayer peak to the monolayer peak at low temperatures, the error inherent in the small coverages at the higher temperatures or a coverage dependent activation energy.[28] Consequently, a plot of ln N versus 1/T, at constant coverage, could not be used to determine the activation energy.[28] Given these constraints, a rough estimate of the activation energy can be calculated assuming an order of 1 and a preexponential factor of 10^{13} s^{-1}.[26] The desorption temperature of the high temperature state, 176 K, corresponds to an activation energy of 45 kJ/mol.

Shown in Figure 4.8 is a comparison of the peak height ratios for masses 31, 47 and 50 referenced to 69 for gas phase mPFAE1 leaked into the chamber (fragmentation), the low temperature desorption peak (multilayer) and the high temperature desorption peak (monolayer). The peak height ratios of the mass spectrometer fragment ions from the low temperature desorption peak are consistent with the fragmentation pattern of perfluoro-1-methoxy-2-ethoxy ethane, as measured by our mass spectrometer. The peak height ratios of the high temperature desorption peak differ from the mass spectrometer fragmentation pattern of mPFAE1. The 31/69 peak height ratio changes from 0.37 to 0.47, an increase of 27% and the 50/69 peak height ratio changes from 0.18 to 0.21, an increase of 17%, meaning that at 176 K, CF and CF_2 evolution increased with respect to CF_3. The 47/69 peak height ratio changes from 0.11 to 0.12, which is not considered to be significant due to the low desorption yield of mass 47.

Table 4.III gives the 31/69 area ratio calculated from the integrated area of the low and high temperature peaks at specific temperatures throughout the peaks. The area under the low temperature peak was found by integrating the area under both peaks, from the initial rise of the low temperature peak to the tail of the high temperature peak, followed by subtraction of the high temperature peak area.

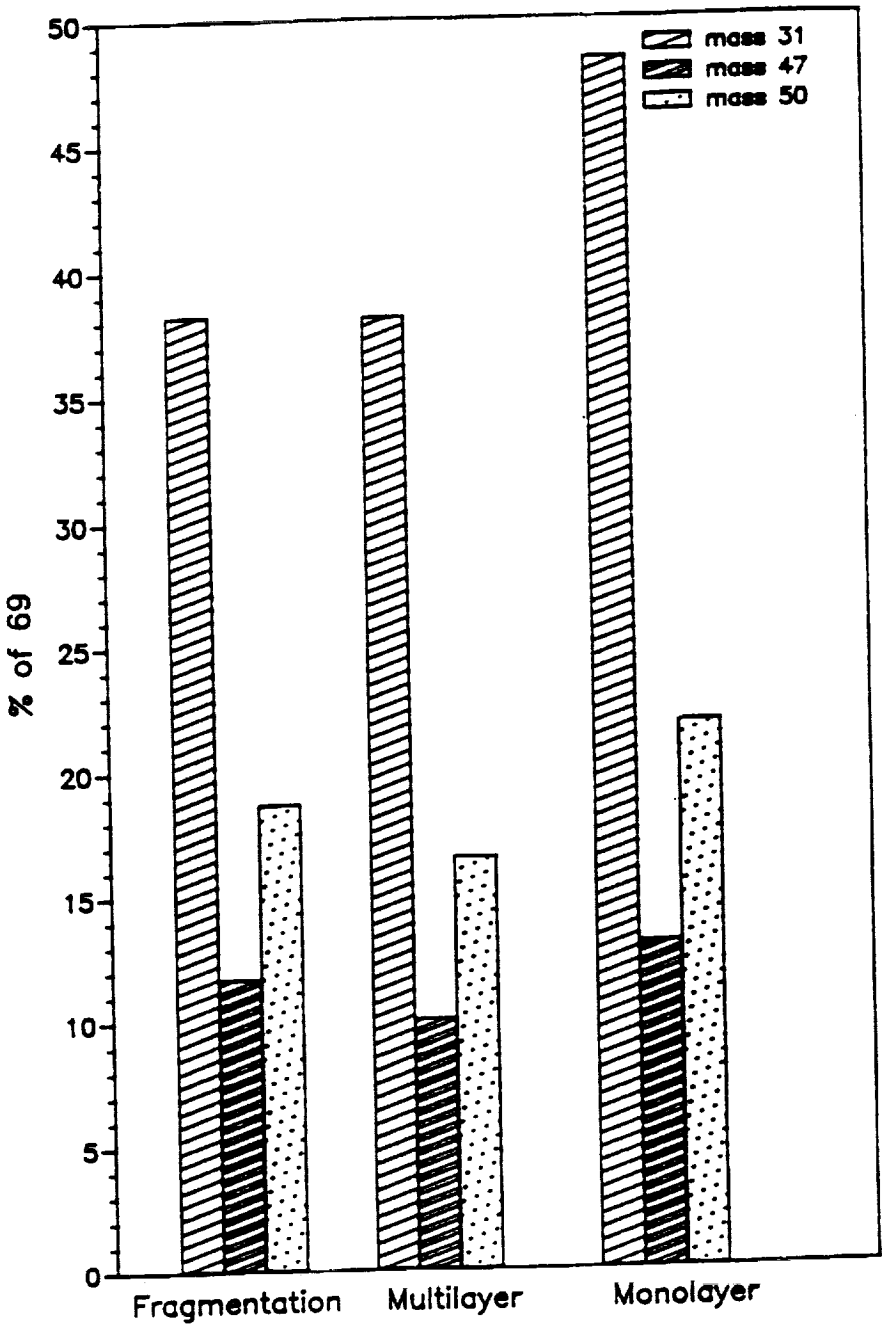

Figure 4.8 Comparison of the ratios of the peak heights for masses 31, 47, 50 referenced to 69, for mPFAE1 leaked into the chamber (fragmentation), the low temperature peak, (multilayer) and the high temperature peak (monolayer).

TABLE 4.III

Comparison of low and high temperature 31/69 peak area ratios at several temperatures for each peak.

Low Temperature Peak				High Temperature Peak		
Temp. K	Ave. %	S. Dev.		Temp. K	Ave. %	S. Dev.
140	39.5	4.5		165	47.1	3.7
145	38.3	5.0		170	46.6	2.1
150	39.5	2.6		175	46.0	3.8
155	39.0	5.0		180	51.0	4.7
				185	56.3	6.4

The 31/69 area ratios at four temperatures in the low temperature peak are equivalent to the unreacted mPFAE1 fragmentation pattern. The 31/69 area ratios at five temperatures in the high temperature peak are greater than the 31/69 ratio for the unreacted mPFAE1. The 31/69 ratio increased with increasing temperature above 175 K, indicating an enhanced reaction rate or possibly additional C-F bond scission. The enhanced rate or the additional C-F bond breaking may also be contributing to the changing reaction order of the high temperature peak. Due to the lower coverages at the high temperatures, more error is introduced into the ratios calculated at temperatures above 175 K.

D. DISCUSSION

X-ray photoelectron spectroscopy (XPS) was used to investigate the interaction of three model fluorinated ethers, perfluoro-1-methoxy-2-ethoxy ethane (mPFAE1) perfluoro-1-methoxy-2-ethoxy propane (mPFAE2) and perfluoro-1,3-diethoxy propane (mPFAE3), with clean polycrystalline iron surfaces. Temperature programmed desorption (TPD) was used to investigate the interaction of one model fluorinated ether, perfluoro-1-methoxy-2-ethoxy ethane, mPFAE1, with clean polycrystalline iron surfaces. The initial low temperature adsorption of the model fluorinated ethers was

molecular.

A change in the C(1s) line shape, the appearance of low binding energy carbon and oxygen species and iron fluoride, and an increase in the desorption yield of CF and CF_2 relative to CF_3 at the reaction temperature, are all indicative of decomposition of the adsorbed mPFAE. A detailed reaction pathway cannot be established on the basis of the present data alone. However, several features of the reaction are evident from the data and are schematically shown in Figure 4.9. The decrease in the C(1s) 296 (CF_3O) to 294 (CF_3/CF_2O) ratio in the mPFAE1 and mPFAE2, signifies preferential decomposition of the terminal CF_3O group in these molecules. The increase in the C(1s) 292 (CF_2/CFO) to 294 (CF_3/CF_2O) ratio in the mPFAE3, signifies preferential decomposition of the CF_3/CF_2O groups. The preferential site of attack, for the three model fluorinated ethers, suggests that the reaction initiates at the end groups of the adsorbed mPFAE. This may simply be due to the terminal groups having better accessibility to the surface. Accessibility may only be one factor though, as evidenced by the higher decomposition temperature for mPFAE3 compared to mPFAE1 and mPFAE2, and the preference for reaction at CF_3O compared to CF_3CF_2 in mPFAE1 and mPFAE2. This suggests two possibilities, either nucleophilic attack, by the surface,

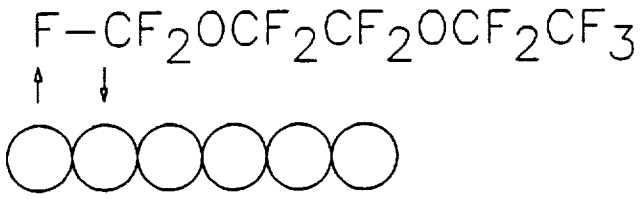

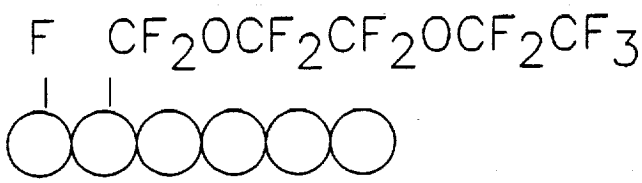

Figure 4.9 Reaction pathway proposed for model fluorinated ether decomposition. The circles represent the iron surface.

at the most electron deficient carbon in the molecule or fluorine abstraction at the weakest C-F bond. The appearance of iron fluoride, for all three model compounds and the increase in the desorption yield of CF and CF_2 compared to CF_3 for mPFAE1, at the onset of reaction, are consistent with C-F bond dissociation as a primary step in the decomposition. Broadening on the low binding energy side of the CF_3/CF_2O C(1s) is consistent with formation of $Fe-CF_2O$ or possibly $Fe-CF_3$ generated, respectively, from C-F dissociation or C-O dissociation at the CF_3O group. Between these two possibilities, the former is preferred, in light of the fact that C-F bond breaking is known to occur. Broadening on the high binding energy side of the CF_3/CF_2O C(1s) peak could be due to the formation of a CF_3O-Fe species due to dissociation of the C-O bond adjacent to the CF_3O group, or, more likely to a structural transition associated with the reaction, which shifts the terminal CF_3 group away from the surface.

By way of comparison, CCl_2F_2 has been reported to decompose on the Fe(110) surface, through selective interaction with fluorine at surface defect sites, with FeF_2 formation and $:CCl_2$ desorption.[18,29] Contrary to the results on iron, fluorinated ethers do not decompose on Ru.[30-32] The difference between Ru and Fe can be understood from bond

energy considerations. The bond energy for Ru-F calculated from $\Delta H_f(RuF_5)$ is 256 kJ/mol, significantly lower than either the Fe-F bond energy of 480 kJ/mol for FeF_3 or the C-F bond energy of 491 kJ/mol for CF_4.[33,34] C-F bond scission with PFAE or halogenated hydrocarbon decomposition is approximately thermoneutral on iron, but endothermic on Ru. This comparison implies that for decomposition of the halogenated hydrocarbons or oxygenated halocarbons on transition metals, the driving force may be the formation of the metal fluoride. On Ru, the combination of the reduced chemisorption bond strength of the fluorinated diethers compared to the hydrocarbon diethers and the lower Ru-F bond energy resulted in desorption rather than decomposition.[30-32]

Most oxygenated hydrocarbons dehydrogenate at low pressures on Group VIII transition metal surfaces, forming adsorbed CO, C and H.[31,35-39] For example, the bond scission sequence for the decomposition of ethanol on Ni(111) has been determined to be the dissociation of the O-H bond, leading to the formation of a stable ethoxy intermediate followed by the scission of 1) the methylene (CH_2) C-H bond, 2) the C-C bond and 3) the methyl (CH_3) C-H bond.[40] Methylene C-H bond scission controls the rate of ethoxy decomposition on nickel.[40] Fluorinated ethers weakly bond to transition metal surfaces through the oxygen lone pairs,

forming an alkoxy-like intermediate.[30,31] Comparing the decomposition of fluorinated ethers to oxygenated hydrocarbons, the scission of the C-F bond with closest approach to the iron surface is postulated to be the rate controlling step.

The bonding configuration of mPFAE1 and mPFAE2 might provide an explanation for the propensity of attack at the C-F bonds of terminal CF_3O groups, as opposed to another site on the molecular chain. Diethers can theoretically bond to metal surfaces through both oxygen atoms, with each oxygen atom contributing approximately 40 kJ/mol.[30] Hydrogenated diethers bond to Ru surfaces 35% more strongly than do hydrogenated monoethers.[31,32] It is speculated that both oxygen atoms contribute to the bonding, but are weakened due to the high local electron density.[31,32] In contrast, fluorinated diethers bond to Ru surfaces only 12% more strongly.[31,32] The metal fluorine repulsion inhibits bonding of both oxygen atoms to the Ru surface.[31,32] For mPFAE1, bonding is most likely to occur through the methoxy oxygen, because there is less metal fluorine repulsion due to the shorter fluoroalkyl side chain. For mPFAE2, in addition to the reduced fluorine metal repulsion at the methoxy oxygen, the pendant perfluoromethyl group sterically hinders access to the second oxygen of mPFAE2, the oxygen of the terminal ethoxy group. The C-F bond of closest approach

to the iron surface would then belong to the terminal methoxy group.

The low binding energy carbon, oxygen and fluorine peak area ratios, shown in Figure 4.6d, are severely deficient in fluorine, when compared to the stoichiometric ratio of the parent. Fluorine desorbs only as part of the fluorocarbon species, which evolve from the surface. Neither F^+ nor HF^+ were detected and the desorption of iron fluoride does not occur until 720 K.[18] Since no gas phase fluorine containing species, other than fluorocarbons were detected, it would seem that for each carbon deposited on the surface, a minimum of two fluorines must also be deposited. Additionally, given the increase in CF and CF_2 TPD yield, it can be concluded that carbons are leaving the surface minus one or more fluorines, so that fluorine deposition might be expected to be even higher. The actual ratio of low binding energy carbon and fluorine is 2:1, indicative of significantly less fluorine deposition. The apparent fluorine loss, in the temperature regime of interest, appears to be due to a surface process and not desorption into the gas phase. Carbon-halogen bond scission and metal halide formation has been observed to occur preferentially at defect sites on metal surfaces.[9,11,13,29] Metal halides form via an island growth mechanism and desorb from the metal surface with zero order kinetics, suggesting desorption from

multilayers.[11,13,29] Clustering at defect sites would act to attenuate the halogen signal prior to desorption, due to shielding of the fluorine species in the cluster by the multilayers.

Attenuation of the fluorine signal may also be in part due to diffusion of fluorine into the bulk of the polycrystalline iron at defect sites and along grain boundaries. The migration of atoms and molecules to steps and defects sites upon adsorption and the propensity for incorporation into the lattice at these sites is well documented.[41,42] Grain boundaries provide an efficient path for atomic movement into the subsurface region of a solid.[43] The activation energy required for diffusion along the grain boundaries of polycrystalline materials is significantly less than that required for diffusion into the lattice of a single crystal.[43] Examples of halide diffusion into the bulk of metal crystals have been reported in the literature.[11,15,16,44] Br atoms diffuse into the bulk of V(100) at ambient temperature and above.[11] The attenuation of the fluorine signal, with dissociative chemisorption of $CFCl_3$ on iron at 90 K and ambient temperatures, was reported to be due to the incorporation of the fluorine into the subsurface regions of the iron crystal.[15,16] Adsorption of an electronegative modifier into an overlayer structure would

be expected to increase the surface work function of a metal, but for the case of fluorine adsorption on iron a decrease in the surface work function has been reported.[44] The decrease in the surface work function has been ascribed to diffusion of the fluorine into the bulk of the iron crystal.[44]

Freshly formed nascent metal surfaces have been found to be very reactive toward the adsorption and the decomposition of many organic molecules.[45,46] Benzene was found to decompose catalytically at room temperature on a freshly formed Ni surface,[46] whereas decomposition on a Ni(111) and Ni(110) was not observed until 100°C.[47] The enhanced activity is due to the removal of the passivating contaminant layer and the highly defective nature of these freshly formed metal surfaces. Defects on a surface exhibit enhanced reactivity, due to the lower coordination number of the respective surface atoms and are responsible for much of the chemistry occuring on surfaces.[41,42] Atomically clean surfaces, particularly polycrystalline surfaces, can be used to investigate the surface interactions of tribological systems.

It is interesting to note that model fluorinated ether decomposition was not observed on a stepped Ru(100) surface.[32] The introduction of higher energy stepped surface sites on the Ru surface did not alter the chemistry of the

fluorinated ethers, attesting to the importance of the metal halide bond strength as a driving force for the reaction.

CHAPTER V

MODEL FLUORINATED ETHERS ON IRON SURFACES CHEMICALLY MODIFIED WITH OXYGEN

A. INTRODUCTION

Micro-oxidation corrosion tests were used to evaluate the stability of the polymeric perfluoroalkylethers.[1-8] During the micro-oxidation corrosion tests the PFAE fluids were heated in the presence of metal coupons, which were covered with an oxide film due to room temperature atmospheric exposure. The decomposition of the PFAE fluids in the presence of the metal coupons was characterized by the evolution of reactive degradation products, weight change of the metal coupons and the formation of metal fluoride on the coupon surface.[3,4,6-8] Both metal fluorides and metal oxides are Lewis acids. The decomposition of polymeric perfluoroalkylether fluids in contact with Lewis acids at elevated temperatures has been reported to occur through cleavage of the ether carbon oxygen bond.[5,9-11]

The goal of this research was to investigate the Lewis acid assisted decomposition of fluorinated ether lubricants, using model compounds and polycrystalline iron surfaces modified with varying coverages of oxygen. The interaction of the model fluorinated ethers on oxidized iron surfaces was explored using X-ray photoelectron spectroscopy (XPS) and temperature programmed desorption (TPD). The interaction of the model fluorinated ethers on iron surfaces modified by an overlayer of oxygen was explored using XPS. The model compounds investigated were perfluoro-1-methoxy-2-

ethoxy ethane, $CF_3OCF_2CF_2OCF_2CF_3$, mPFAE1, perfluoro-1-methoxy-2-ethoxy propane, $CF_3OCF_2CF(CF_3)OCF_2CF_3$, mPFAE2, and perfluoro-1,3-diethoxy propane, $CF_3CF_2OCF_2CF_2CF_2OCF_2CF_3$, mPFAE3. The model compounds are monomer units of polymeric PFAE materials being considered for use as high temperature lubricants. These low molecular weight compounds have the same functional units as the polymeric materials, but yield results which are simpler to interpret.

Chemisorption of an oxygen overlayer lowered the reactivity of the surface to adsorption and decomposition of the model fluorinated ethers, by blocking the active sites on the metal surface. Incomplete coverage of the iron surface with chemisorbed oxygen results in a reaction, which resembles the defluorination reaction observed on the clean iron surface. Perfluoro-1-methoxy-2-ethoxy ethane reacts on the oxidized iron surface through a Lewis acid assisted cleavage of the carbon oxygen bond, with preferential attack at the terminal fluoromethoxy.

B. EXPERIMENTAL

The XPS measurements were conducted in a VG Scientific ESCALAB/SIMSLAB Mk.II, with a typical base pressure of $1x10^{-10}$ torr. The system was equipped with a twin anode x-ray source, Al Kα (1486.6 eV) and Mg Kα (1253.6 eV), an Al Kα monochromatic x-ray source, an Ar ion gun, a stainless steel

leak valve controlled doser and a sample manipulator.

The TPD experiments were conducted in a turbomolecular pumped, stainless steel UHV chamber, with a typical base pressure of $2x10^{-10}$ torr. The system was equipped with a water cooled, Ti sublimation pump, an apertured UTI-100C quadrupole mass spectrometer, an Auger spectrometer with retarding field energy analyzer and integral electron gun, an Ar ion gun, a bakeable glass/teflon gas handling system and a sample manipulator. The sample could be reproducibly positioned in direct-line-of-sight to the mass spectrometer aperture and ionizer, approximately 40 mm removed from the ionizer. The mass spectrometer ionizing region was open to the chamber.

To avoid electron induced damage of the adsorbed model fluorinated ether layer, the Al monochromatic source was exclusively used. AES was used only to check cleanliness of the iron surface prior to mPFAE exposure and never used to probe the adsorbed mPFAE layer.

The polycrystalline iron foils (10 mm x 10 mm x 0.5 mm) were polished, using standard metallographic techniques, to a surface finish of 0.3 μm, followed by ultrasonic cleaning in acetone to remove the polishing residue. The iron foils were atomically cleaned in UHV with cycles of Ar^+ bombardment and annealing. The iron surface was considered clean when contaminants, in particular carbon, oxygen,

sulfur and nitrogen, could not be detected using either XPS or Auger. In the XPS chamber, the sample could be cooled to 100 K, with liquid N_2 and heated to 900 K, by radiation from a 0.2 mm tungsten filament. In the TPD chamber, the sample could be cooled to 115 K, with liquid N_2 and heated linearly with time, through the temperature region of interest, up to 400 K. Typically a heating ramp of 15 +/- 2 K/s was used. The temperature was measured using a chromel-alumel, Type K thermocouple spotwelded to an edge of the front face of the sample.

The three perfluoroalkylethers investigated were obtained from Exfluor Research Inc. and used as received. A GC/MS analysis showed mPFAE1 and mPFAE2 to be at a minimum 98 % pure and mPFAE3 to be at a minimum 95 % pure, with higher molecular weight ethers present as impurities. Prior to introduction into the vacuum chamber, the mPFAEs were further purified by repeated freeze-pump-thaw cycles.

In both the XPS and TPD chambers, the fluorinated ether exposures were calculated from uncalibrated ion gauge readings and are reported in Langmuir (1 L = 1×10^{-6} torr sec). In the XPS chamber, adsorbate coverages were obtained by C(1s) and O(1s) XPS measurements calibrated using the known saturation coverage of CO on Fe(110).[12] The coverages reported in reference to the XPS data are approximate.

Prior to mPFAE exposure, the polycrystalline iron

surfaces were oxidized by exposure of a room temperature surface to approximately 400 L of oxygen. The approximate thickness of the oxide layer is 15 ML (monolayers), based on the O(1s) peak area. XPS spectra of unreacted mPFAE, shown in Figure 5.1 were obtained following exposure of an oxidized iron surface at 100 K to an undirected, nominal 3 L exposure of the model fluorinated ethers. The approximate coverage of the fluorinated ether on the 100 K, oxidized, iron surface, for the 3 L exposure, is 4 ML based on the C(1s) peak area. As a cross check on the oxide thickness and fluorinated ether coverage estimates, the approximate thickness of the oxide film and of the model fluorinated ether overlayer on the oxidized iron surface were calculated using the expression:

$$d=(\lambda/\cos\theta)\ln(I_o/I), \qquad (5.1)$$

where θ is the emission angle with respect to the surface normal (θ is near zero for our experiments), I is the substrate signal intensity, I_o is the substrate signal intensity in the absence of an overlayer and λ is the electron mean free path. I and I_o were obtained by measuring the Fe($2p_{3/2}$) signal intensity with the ether overlayer and in the absence of the overlayer, respectively. A published value was used to approximate the electron mean free path.[13] An upper limit to the fluorinated ether molecular diameter was estimated to be 4.7 Å, based on

carbon and fluorine atomic radii of 0.77 and 0.68 Å, respectively and a C-F bond length of 1.3 Å.[14] The fluorinated ether thickness, estimated by this procedure, is 3.2 ML and is in reasonable agreement with the coverage determined from the C(1s) peak area. The oxide thickness, based on an oxygen atomic radius of 0.7 Å, is estimated to be 17 ML and is in reasonable agreement with the thickness determined from the O(1s) peak area.

The ether overlayer and substrate were heated to a series of temperatures between 120 and 160 K, with no additional exposures to mPFAE, and immediately cooled using liquid N_2. The rate at which the final temperature was approached varied from 0.4 to 1.1 K/s and the ramps applied were not linear nor was any effort made to exactly reproduce the ramps from run to run. Detailed scans of the carbon XPS region were acquired, using both 20 and 50 eV pass energies, after each heat treatment. Detailed scans of the oxygen, fluorine and iron regions were also acquired, using a 50 eV pass energy.

The polycrystalline iron surfaces were oxidized prior to the TPD experiments, by exposure of the iron surface at 500 K to approximately 1000 L of oxygen. Because the progress of the oxidation could not be followed, the TPD oxidation conditions were more severe than were the XPS oxidation conditions. TPD spectra were acquired following

the exposure of an oxidized, 115 K polycrystalline iron substrate to a directed dose of mPFAE1. A linear temperature ramp was applied to the substrate and evolving species were detected as a function of increasing temperature. All mass spectra were obtained with the energy of the ionizing electrons set at 70 eV and the filament current at 2.0 mA. Prior to the start of each experiment, the iron substrate was cleaned by Ar^+ sputtering at 650 K for approximately 20 minutes and reoxidized by the procedure described above.

Slight temperature differences were noted in the onset of mPFAE1 decomposition based on the XPS and the TPD results. Onset of decomposition using XPS was found to be 138 K and using TPD to be approximately 155-160 K, as characterized by the initial rise of the monolayer peak. The XPS temperature ramp varied from 0.4 to 1.1 K/s and was not necessarily linear with time. The XPS temperature ramp was 20 to 30 times slower than the TPD temperature ramp of 15 +/- 2 K/s. The variation in the onset temperature for decomposition can be accounted for due to the difference in the heating rate for the XPS and TPD experiments. The analysis put forth by Redhead was used to model the decomposition kinetics, assuming an order of 1, a preexponential factor of 10^{13} s^{-1} and an activation energy of 40 kJ/mol, consistent with the peak temperature observed in

the TPD experiments and substituting in a heating rate of 0.7 K/s, characteristic of the XPS experiments.[15] The initial rise of the modeled thermal desorption peak agrees with the XPS experimental value for the onset of decomposition.

C. RESULTS

1. XPS Results

Figure 5.1a-c shows the multilayer C(1s) spectra for the three model perfluorinated ethers adsorbed onto 100 K, oxidized iron surfaces. As can be seen from Figure 5.1, the C(1s) binding energy increases with increasing electronegative substitution and carbon atoms, with differing numbers of electronegative substituents, can be resolved using XPS. The two C(1s) peaks, in the mPFAE1 spectrum of Figure 5.1a, correspond to CF_3O and CF_3/CF_2O. An additional peak is observed in the C(1s) spectrum for mPFAE2 (Figure 5.1b), which corresponds to CFO. The two carbon peaks in the mPFAE3 spectrum of Figure 5.1c, correspond to CF_3/CF_2O and CF_2. Using a 20 eV pass energy, the CF_3/CF_2O and the CF_2/CFO pairs are not resolvable, when both species of the pair are present on the surface. The CF_2/CFO pair can be differentiated, when only one species of the pair is present on the surface, as with mPFAE2 (CFO) and mPFAE3 (CF_2).

a) Perfluoro-1-methoxy-2-ethoxy ethane,

$CF_3OCF_2CF_2OCF_2CF_3$ mPFAE1

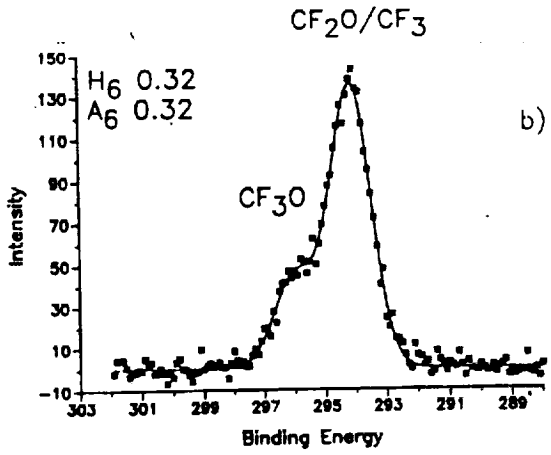

b) Perfluoro-1-methoxy-2-ethoxy propane,

$CF_3OCF_2\underset{CF_3}{CF}OCF_2CF_3$ mPFAE2

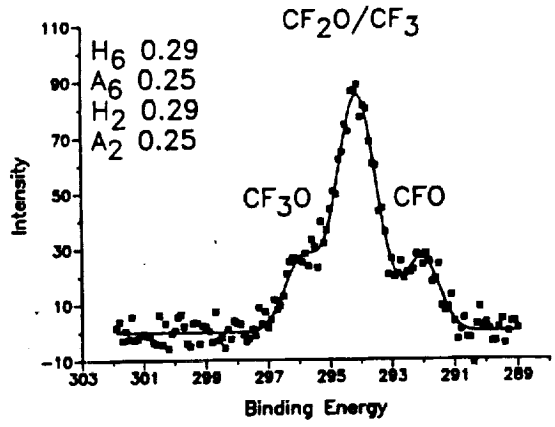

c) Perfluoro-1,3-diethoxy propane, mPFAE3

$CF_3CF_2OCF_2CF_2CF_2OCF_2CF_3$

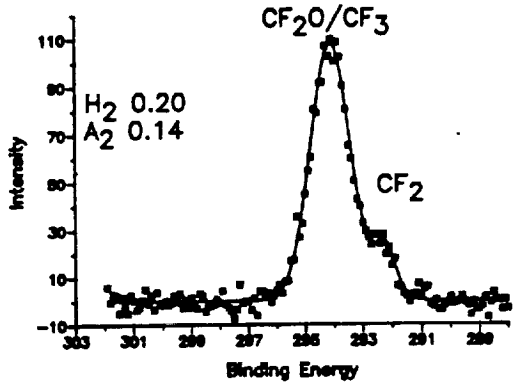

Figure 5.1 C(1s) spectra and the fits to the C(1s) spectra of the model fluorinated ethers adsorbed on a 100 K, oxidized polycrystalline iron surface: **a)** perfluoro-1-methoxy-2-ethoxy ethane, mPFAE1 **b)** perfluoro-1-methoxy-2-ethoxy propane, mPFAE2 **c)** perfluoro-1,3-diethoxy propane, mPFAE3. Listed next to each spectra are the intensity ratios, height (H) and area (A), calculated from the fits.

Also shown in Figure 5.1, are the Gaussian fits to the model fluorinated ether C(1s) spectra, with astericks representative of the raw data, and the solid lines the fits to the raw data. Two computer programs were used to fit the two peaks in the mPFAE1 and mPFAE3 C(1s) spectra. The first program was limited to five adjustable parameters: the height and center of each peak and a single peak width, fitting a maximum of two peaks. The second routine allowed for independent variation of all parameters, the height, center and width for each peak, allowing for fits to spectra with two or more peaks. Only the second program was used to fit the three peaks in the mPFAE2 C(1s) spectra. Good agreement was found between the two fitting procedures. The 296 (CF_3O)/ 294 (CF_3/CF_2O) and 292 (CF_2/CFO)/ 294 (CF_3/CF_2O) height (H) and area (A) ratios, calculated from the Gaussian fits to the multilayer spectra, are listed next to each spectrum in Figure 5.1. The intensity ratios were used to monitor the changes in the adsorbed layer, as a function of increasing temperature. Given in Table 5.I, are the theoretical C(1s) intensity ratios for each of the model fluorinated ethers, as well as the experimental intensity ratios calculated from the fits to the multilayer (100 K) C(1s) spectra.

Carbon, oxygen and fluorine binding energies, characteristic of the mPFAEs, are listed in Table 5.II. The

TABLE 5.I

Comparison of the theoretical and experimental C(1s) area and height intensity ratios of the three model perfluoroalkylethers. I_T and I_E are the theoretical and experimental values, respectively. I_6/I_4 is the 296 eV (CF_3O) / 294 (CF_3/CF_2O) intensity ratio. I_2/I_4 is the 292 (CF_2/CFO) / 294 (CF_3/CF_2O) intensity ratio.

		mPFAE1		mPFAE2		mPFAE3	
		I_T	I_E	I_T	I_E	I_T	I_E
I_6/I_4	Area	0.25	0.32	0.25	0.25		
	Height	0.25	0.32	0.25	0.29		
I_2/I_4	Area			0.25	0.25	0.17	0.14
	Height			0.25	0.29	0.17	0.20

TABLE 5.II

Comparison of Binding Energies (eV) for Fluorinated Compounds on Oxidized Iron and Nonfluorinated Compounds

	C(1s)	O(1s)	F(1s)
mPFAE			
CF_3O	295.8 eV	535.5 eV	689.0 eV
CF_3/CF_2O	293.8 eV	535.5 eV	689.0 eV
CF_2	292.6 eV		689.0 eV
CFO	291.8 eV	535.5 eV	689.0 eV
Diethyl ether[16]			
CH_3C	285.0 eV		
CCH_2O	286.6 eV	533.2 eV	
Iron Fluoride			
FeF_x			684.0 eV

binding energies, given in Table 5.II, were obtained from the Gaussian fits to C(1s) spectra, at monolayer coverages, for mPFAE1, mPFAE2 and mPFAE3 adsorbed on oxidized iron substrates. As the coverage decreased, in going from the multilayer, shown in Figure 5.1, to the monolayer, listed in Table 5.II, a rigid shift of 0.3 eV to lower binding energy, was observed. The carbon and oxygen binding energies, for $(CH_3CH_2)_2O$[16] and the fluorine binding energy for FeF_x, are also listed in Table 5.II.

a. *Oxidized Iron* Perfluoro-1-methoxy-2-ethoxy ethane, mPFAE1, was the only model fluorinated ether in the study observed to react on the oxidized iron surface. The progress of the mPFAE2 and mPFAE3 reactions could not be monitored because the majority of mPFAE2 and mPFAE3 desorbed prior to reaction. The use of the Al monochromatic source, coupled with the low atomic cross section for carbon, limits the detection sensitivity. The mPFAE1 experimental results will be discussed in detail.

Upon warming the mPFAE1 exposed, oxidized iron surface from 100 K to 134 K, an overall decrease in the high binding energy carbon, oxygen and fluorine intensities was observed in the stoichiometric ratio of the mPFAE1 parent. In this temperature range, mPFAE1 molecularly desorbs from the surface, with the carbon and fluorine XPS peak shapes and ratios and the 296/294 carbon ratio unaltered from the

measurements at 100 K. At the reaction temperature of mPFAE1, 138 K, a change was observed in the carbon spectrum as a function of increasing temperature, which could not be ascribed to molecular desorption. Figure 5.2a shows the mPFAE1 C(1s) spectrum and the fit at the reaction temperature, 138 K. At this temperature, the 296/294 height (H_6) and area (A_6) ratios decreased with respect to the unreacted mPFAE1, signifying loss of CF_3O with respect to CF_3/CF_2O. In Figure 5.2b, the height normalized fit to the unreacted (134 K) and the reacted (138 K) C(1s) spectra on the oxidized iron surface have been overlaid to further illustrate the changes in the C(1s) spectra at the reaction temperature. Notice that the only change evident, when comparing the reacted and the unreacted C(1s) spectra, is a decrease in the peak height and subsequent decrease in the area of the CF_3O peak. No increase in the peak width of CF_3/CF_2O is observed nor growth in low XPS binding energy carbon species.

No reaction was detected on the 100 K, oxidized iron surface upon exposure to the three model fluorinated ethers in the monolayer and submonolayer regimes. Overlaid in Figure 5.3 are the height normalized fits to the mPFAE1 C(1s) spectrum for a submonolayer carbon coverage at 100 K and for a submonolayer carbon coverage at 138 K, the mPFAE1 reaction temperature. The carbon coverage for the low

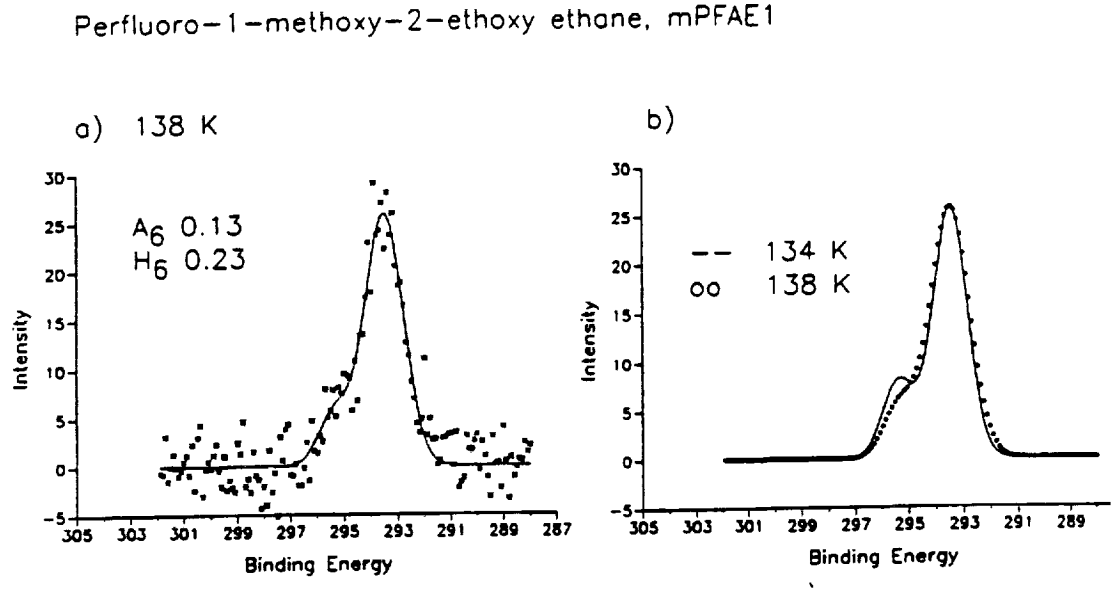

Figure 5.2 **a)** C(1s) spectrum and the fit to the C(1s) spectrum at the reaction temperature for perfluoro-1-methoxy-2-ethoxy ethane, mPFAE1 on oxidized iron. Peak area (A) and height (H) ratios, calculated from the fit at 138 K, are given. **b)** The fits to the mPFAE1 C(1s) spectra at 135 and 138 K were overlaid to illustrate the changes with increasing annealing temperature.

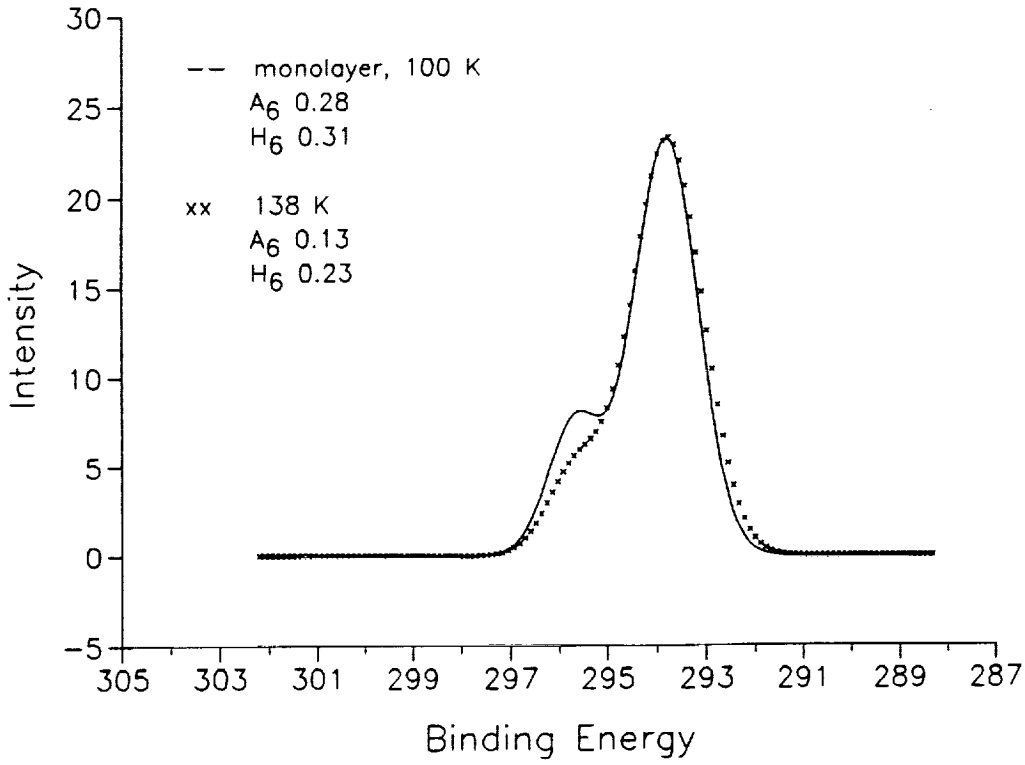

Figure 5.3 The fits to the mPFAE1 C(1s) spectra on an oxidized iron surface for submonolayer carbon coverages at 100 K and at the reaction temperature of 138 K, have been overlaid. The carbon coverage at 100 K is equal to the carbon coverage at the reaction temperature of 138 K.

temperature, low exposure oxidized iron surface is approximately equal to the carbon coverage at the reaction temperature. The decrease in the 296 eV peak height observed at the reaction temperature, was not observed for submonolayer carbon coverages at low temperatures. The low temperature, C(1s) spectrum at submonolayer coverages was identical to the high coverage spectrum, within experimental accuracy. The changes in the C(1s) spectrum, with increasing annealing temperature, is not due solely to heterogeneity in the binding site for the changing environment of mPFAE1 in the monolayer regime compared to the multilayer. Additionally, the carbon and fluorine ratios and peak shapes and the 296/294 carbon ratio at the submonolayer coverage were unaltered from the 100 K, multilayer XPS spectra. The initial low temperature adsorption of the mPFAEs was molecular.

The high binding energy carbon, oxygen, fluorine peak area ratio, at the reaction temperature of 138 K, was found to be 1.7 : 1 : 4.8. The ratio, at the reaction temperature, deviates from the parent stoichiometric ratio of 2.5 : 1 : 6.0 and the ratio for the adsorbed unreacted mPFAE1, at 134 K, of 2.3 : 1 : 5.7, with deficiencies in both fluorine and carbon. Additionally, at temperatures greater than 184 K, growth in a small fluoride peak at 684.0 eV, characteristic of iron fluoride, is observed for all

three model fluorinated ethers. A comparison of the fluoride growth on the clean iron and oxidized iron is shown in Figure 5.4. On the oxidized iron surface, iron fluoride is formed at a temperature at least 50 K above the reaction temperature, the temperature at which the changes in the C(1s) spectrum are first observed. The iron fluoride growth is significantly less on the oxidized iron surface. On the clean iron surface, iron fluoride formation and the changes in the C(1s) spectrum occur at the same temperature.

b. Chemisorbed Oxygen No detectable reaction was observed in the monolayer and submonolayer regime, at 100 K on an iron surface, modified with 1 ML of chemisorbed oxygen. The carbon, oxygen and fluorine ratios and peak shapes and the 296/294 and 292/294 carbon ratios were unaltered from the 100 K, multilayer XPS spectra. The initial low temperature adsorption on the iron surface modified with an oxygen overlayer was molecular.

Figures 5.5a, 5.6a and 5.7a show the C(1s) spectra and fits, at the clean iron surface reaction temperatures, for the three model fluorinated ethers adsorbed on iron surfaces, modified with approximately 1 ML of chemisorbed oxygen. At the oxygen exposures used, no iron oxidation was observed. Upon warming from 100 K to the clean iron surface reaction temperature, the mPFAEs desorb from the oxygen modified, polycrystalline iron surface, with the carbon,

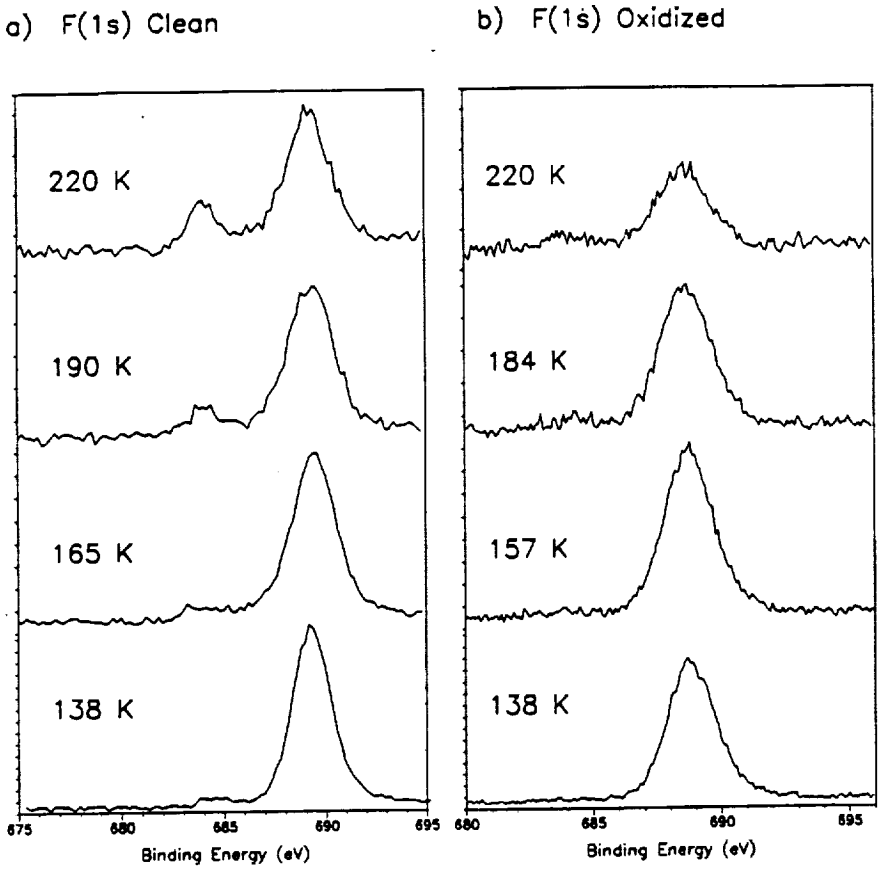

Figure 5.4 A comparison of the growth in metal fluoride on **a)** clean and **b)** oxidized iron surfaces with increasing annealing temperatures.

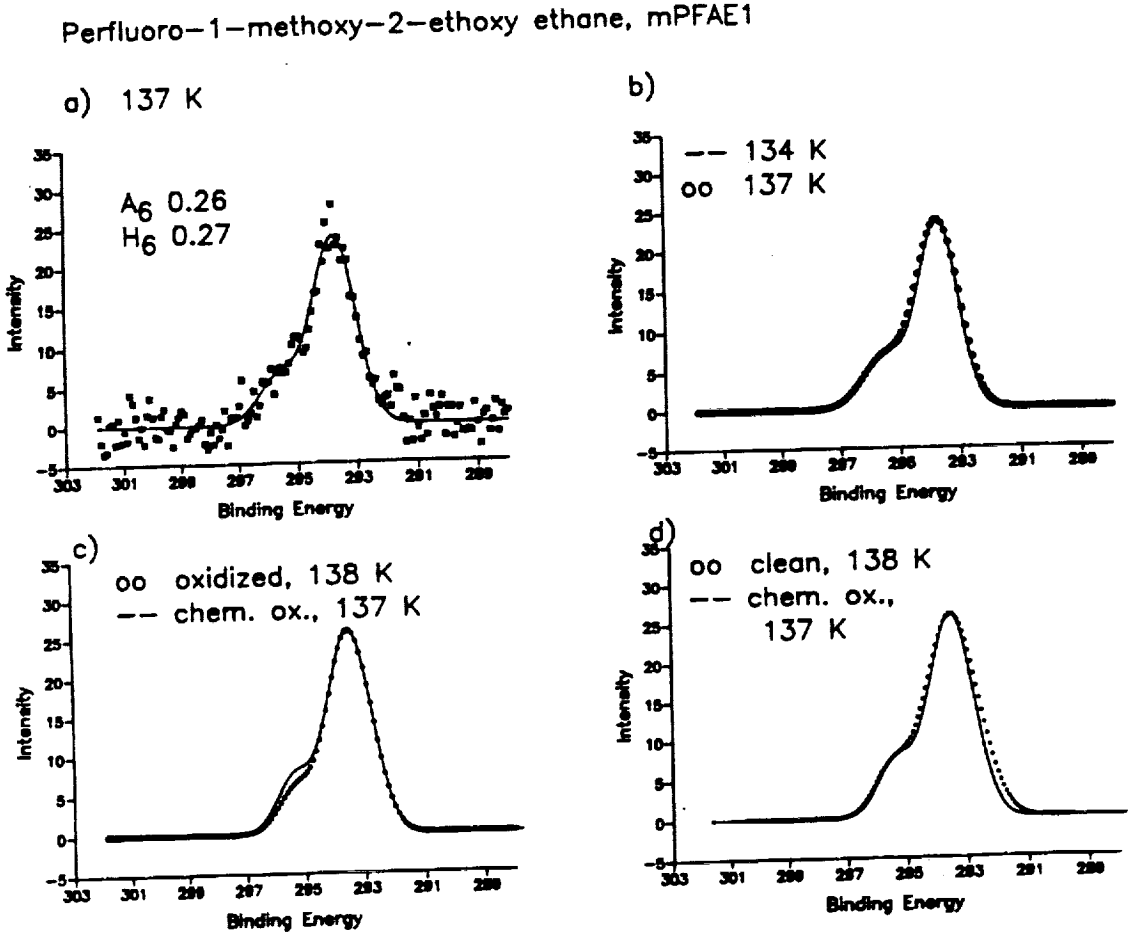

Figure 5.5 **a)** mPFAE1 C(1s) spectrum and the fit to the C(1s) spectrum at 137 K, the clean iron surface reaction temperature, on an iron surface modified with an overlayer of oxygen. Peak area (A) and height (H) ratios are given. **b)** The fits to the mPFAE1 C(1s) spectra at 134 and 137 K were overlaid to illustrate the lack of change in the C(1s) spectrum with increasing annealing temperature. Also shown is a comparison of the fit to the 137 K, C(1s) spectrum on oxygen modified surface to the reacted C(1s) spectra on **c)** an oxidized iron surface and **d)** a clean iron surface.

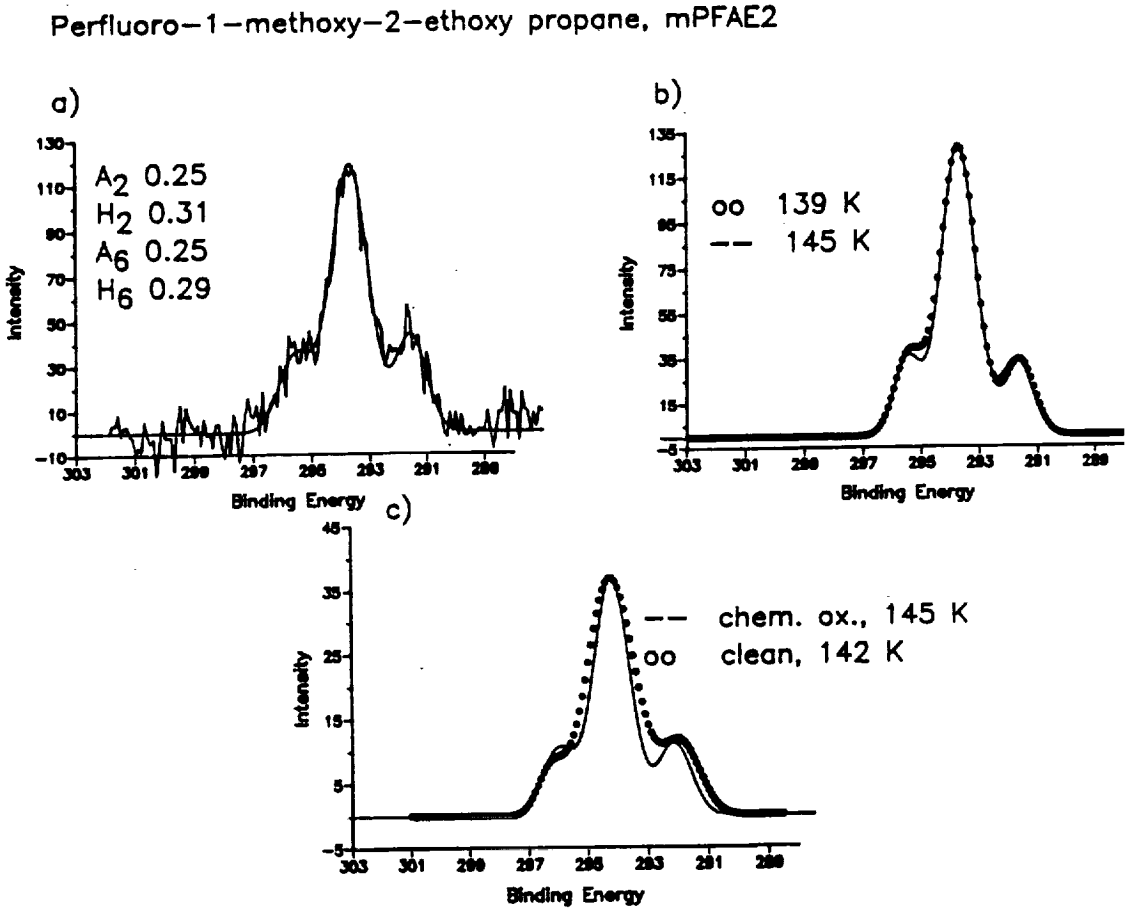

Figure 5.6 **a)** mPFAE2 C(1s) spectrum and the fit to the C(1s) spectrum at 145 K, the clean iron surface reaction temperature, on an iron surface modified with an overlayer of oxygen. Peak area (A) and height (H) ratios are given. **b)** The fits to the mPFAE2 C(1s) spectra at 139 and 145 K were overlaid to illustrate the lack of change in the C(1s) spectrum with increasing annealing temperature. **c)** Also shown is a comparison of the fit to the 145 K, C(1s) spectrum on oxygen modified surface to the reacted C(1s) spectra on a clean iron surface.

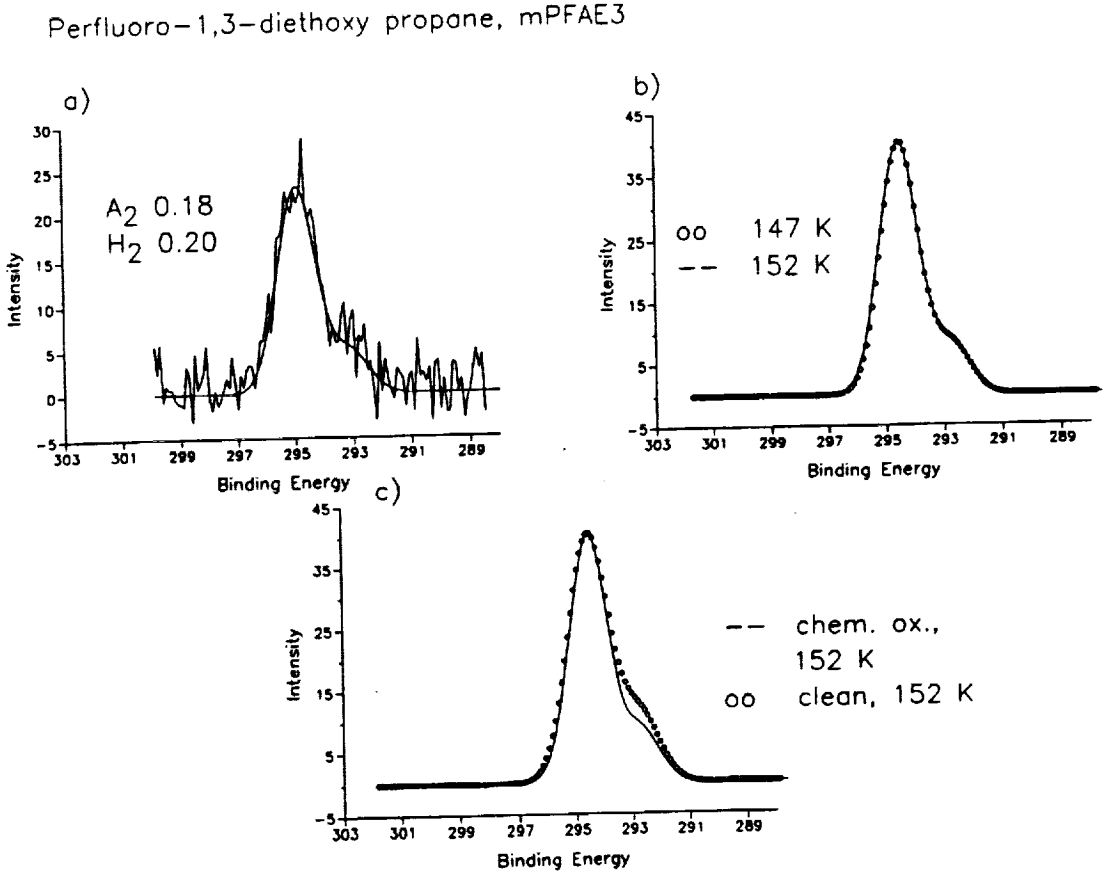

Figure 5.7 **a)** mPFAE3 C(1s) spectrum and the fit to the C(1s) spectrum at 152 K, the clean iron surface reaction temperature, on an iron surface modified with an overlayer of oxygen. Peak area (A) and height (H) ratios are given. **b)** The fits to the mPFAE3 C(1s) spectra at 147 and 152 K were overlaid to illustrate the lack of change in the C(1s) spectrum with increasing annealing temperature. **c)** Also shown is a comparison of the fit to the 152 K, C(1s) spectrum on oxygen modified surface to the reacted C(1s) spectra on a clean iron surface.

oxygen and fluorine ratios and peak shapes and the 296/294 and 292/294 carbon ratios undergoing only slight alterations when compared to the 100 K, multilayer XPS spectra. A comparison of the peak height and area ratios for the high temperature C(1s) spectra, given in Figures 5.5a, 5.6a and 5.7a, to the multilayer peak height and area ratios, shown in Figure 5.1a-c, reveals only slight decreases, which are significantly less than the decreases observed for the ratios on the clean iron surface at the reaction temperature. To further illustrate the absence of reaction on the chemisorbed oxygen surface, two sets of spectral overlays will be presented for each model structure. In Figures 5.5b, 5.6b and 5.7b, the height normalized fits to low temperature and high temperature C(1s) spectra, on the oxygen modified iron surface, have been overlaid to illustrate the lack of change on the oxygen modified surface, with increasing annealing temperature. In Figures 5.5c and d, 5.6c and 5.7c, the height normalized fits comparing reacted and unreacted C(1s) spectra have been overlaid. In Figure 5.5c and d, the high temperature, oxygen modified, mPFAE1 C(1s) is compared to the reacted C(1s) spectra on both the oxidized (Figure 5.5c) and the clean iron surface (Figure 5.5d). In Figure 5.6c and 5.7c, the high temperature, oxygen modified mPFAE2 and mPFAE3 C(1s) spectra, respectively, are compared to the reacted

mPFAE2 and mPFAE3 C(1s) spectra on the clean iron surface. The changes in the C(1s) spectra on the oxygen modified iron surfaces at the clean iron surface reaction temperature are not as significant as the changes in the reacted C(1s) spectra on the clean and oxidized surfaces.

Metal fluoride is observed, on the oxygen modified surface, at temperatures approximately 5 K above the clean iron surface reaction temperature. Figure 5.8 compares the temperature dependent fluoride growth on the clean iron surface and the iron surfaces modified with chemisorbed oxygen. The F / Fe (2p) ratio is calculated from the peak areas of the low binding energy fluoride peak observed at 684.0 eV and the $Fe(2p_{3/2})$ peak. In addition to the observed higher onset temperature for fluoride growth on the iron surface modified with an oxygen overlayer, the total amount of fluoride produced is significantly less on the oxygen modified surface than on the clean iron surface.

2. TPD Results

TPD spectra following perfluoro-1-methoxy-2-ethoxy ethane, mPFAE1, exposure of an oxidized polycrystalline iron surface at 115 K, are shown in Figure 5.9. The spectra are obtained by monitoring mass 69, CF_3^+, an intense fragment of perfluoro-1-methoxy-2-methoxy ethane. The parent ion was not observed. Spectra obtained, monitoring mass 31, CF^+, mass 47, CFO^+ and mass 50, CF_2^+, are identical. Mass 19, F^+

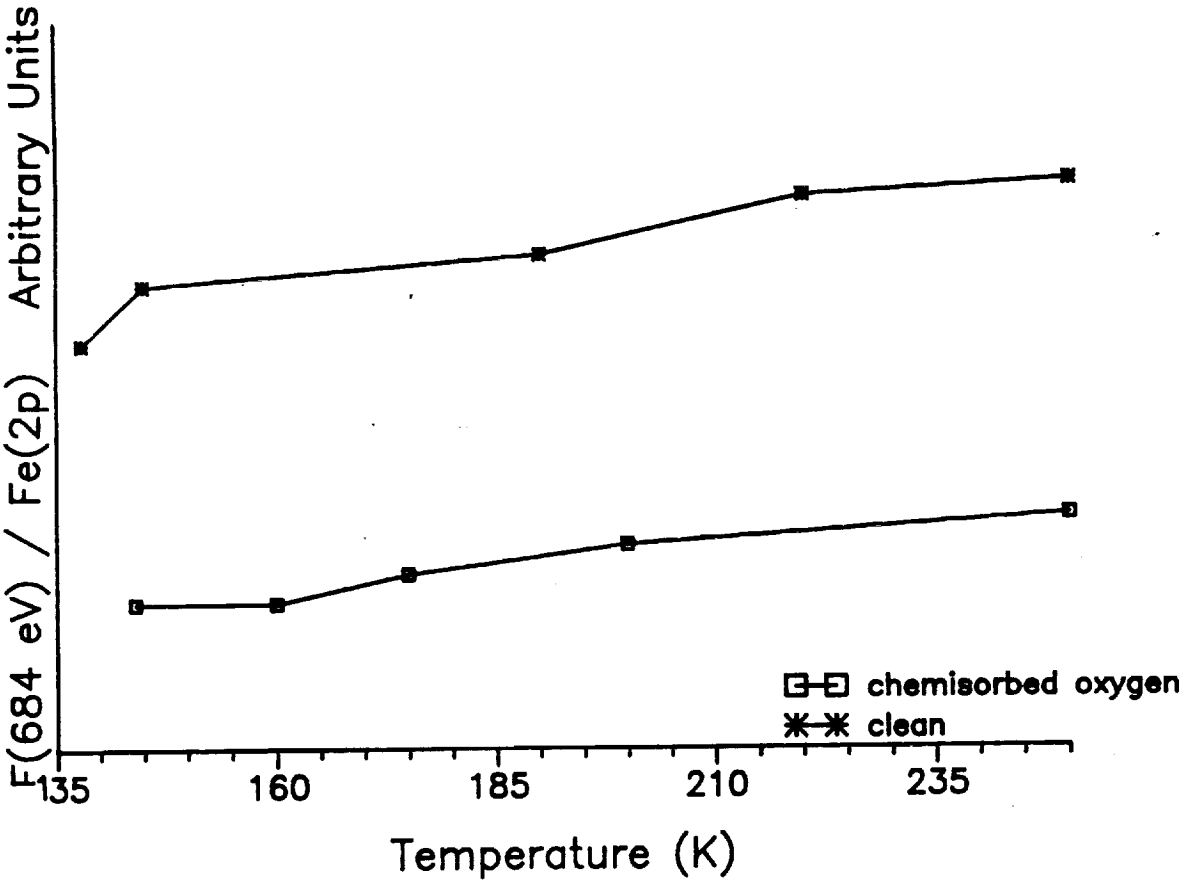

Figure 5.8 General trends in the fluoride growth on the clean iron surface and the iron surface modified with an overlayer of oxygen are compared.

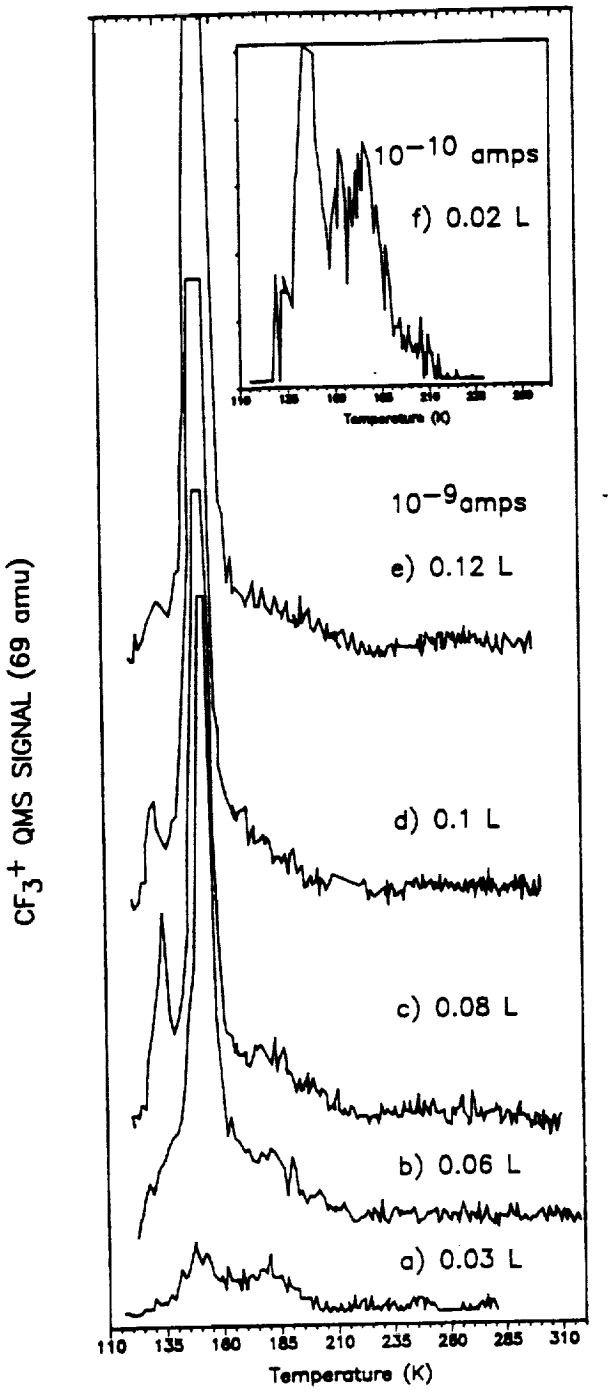

Figure 5.9 Line of sight TPD spectra for mPFAE1 at five exposures: **a)** 0.03 L, **b)** 0.06 L, **c)** 0.08 L, **d)** 0.1 L **e)** 0.12 L obtained using a sensitivity of 10^{-9} amps and **f)** 0.02 L obtained using a sensitivity of 10^{-10} amps.

and mass 20, HF^+ were not detected. At the lowest exposure, two peaks of approximately equal intensity are observed at 180 and 150 K. The high temperature state shifts to 175 K, as the exposure to mPFAE1 increased. The high temperature state is highlighted in the inset of Figure 5.9. The low temperature state, at 150 K, does not saturate with increasing exposure and is characteristic of sublimation from a multilayer.

The monolayer peak has a FWHM of 23 K at low exposures, which broadens with increasing exposure attaining a maximum value of 36-40 K. The broadening in the monolayer peak makes it difficult to determine the saturation exposure. Shown in Figure 5.10a are the TPD peaks at low and high exposures on the oxidized iron surface. The high temperature peaks, at both low and high exposures, have been fit to Gaussian peaks with FWHM of 23 K to illustrate the broadening observed with increasing exposures. Shown in Figure 5.10b is a comparison of TPD spectra on the clean and oxidized iron surfaces at similar exposures. Both of the TPD spectra, in Figure 5.10b, have been fit to Gaussians with FWHM of 25 K. The high temperature peak, on the clean iron surface, does not broaden to the same extent as the high temperature peak on the oxidized surface.

Since the two peaks in the TPD spectra are not baseline resolved, it is difficult to determine kinetic parameters by

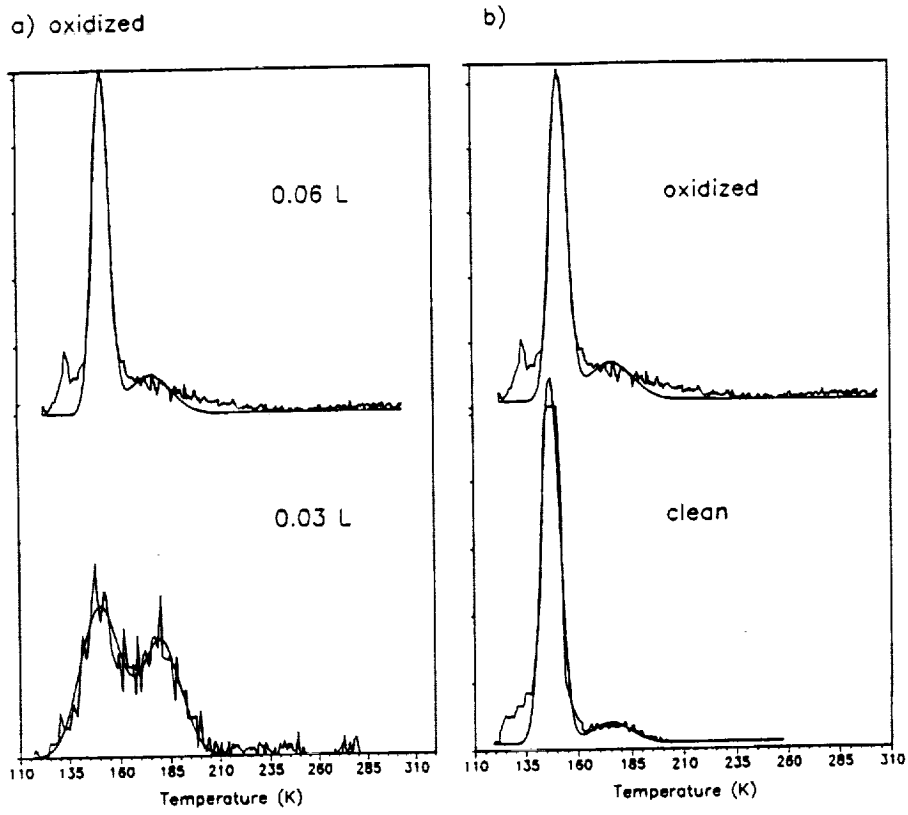

Figure 5.10 **a)** Illustrates the broadening in the monolayer peak on the oxidized iron surface, with increasing exposure. The high temperature peaks have been fit to Gaussians with a FWHM of 23 K. **b)** Comparison of the TPD spectra on the clean and oxidized iron surface at similar exposures. The high temperature peaks have been fit to Gaussians with a FWHM of 25 K.

conventional analysis techniques.[17] A plot of ln N versus ln c, at constant temperature, where N is the desorption rate and c is the surface coverage, gives a straight line with slope of n, the order of the reaction.[17] Plots of ln N versus ln c, at constant temperature, for the high temperature peak yield slopes which vary from 1.2 to 0.6, for temperatures between 165 and 200 K. The error in the desorption rate isotherms may be in part due to the contribution of the multilayer peak to the monolayer peak atlow temperatures, the error inherent in the small coverages at the higher temperatures, the peak width which increases with increasing exposure or a coverage dependent activation energy. Consequently, a plot of ln N versus 1/T at constant coverage cannot be used to determine the activation energy.[17] Given these constraints, a rough estimate of the activation energy can be calculated assuming an order of 1 and a preexponential factor of 10^{13} s^{-1}.[15] The desorption temperature of the high temperature state, 175 K, corresponds to an activation energy of 45.28 kJ/mol.

Shown in Figure 5.11 is a comparison of the peak height ratios for masses 31 (CF), 47 (CFO) and 50 (CF_2) referenced to 69 (CF_3), for gas phase mPFAE1 leaked into the chamber (fragmentation pattern), the low temperature desorption peak (multilayer) and the high temperature desorption peak (monolayer). The peak height ratios of the mass

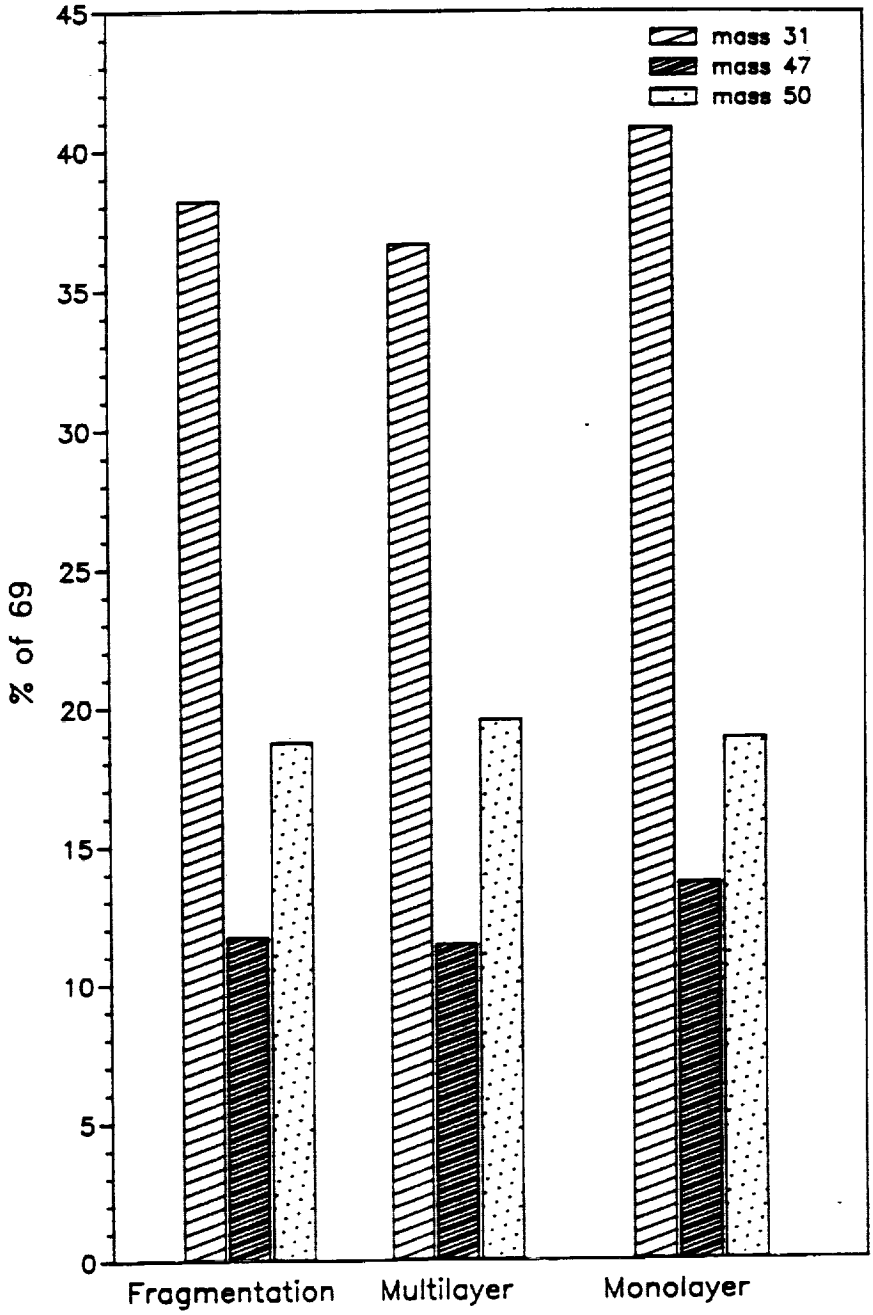

Figure 5.11 Comparison of the ratios of the peak heights for masses 31, 47, 50 referenced to 69, for mPFAE1 leaked into the chamber (fragmentation), the low temperature peak, (multilayer) and the high temperature peak (monolayer).

spectrometer fragment ions from the low temperature desorption peak are consistent with the fragmentation pattern of perfluoro-1-methoxy-2-ethoxy ethane, as measured by our mass spectrometer. The 31/69 and 50/69 peak height ratios from the high temperature desorption peak are consistent with the mass spectrometer fragmentation pattern of mPFAE1, whereas the 47/69 peak height ratio is 2 % higher. At 175 K, CFO evolution increased by 2 % with respect to CF_3. Due to the low desorption yield of CFO, mass 47, attaching any significance to the 2 % increase in the peak height of 47 when compared to 69 is questionable. As will be discussed below, the same trend was observed in the 47/69 area ratios for the monolayer peak, given in Table 5.III.

Table 5.III gives the 47/69 area ratio calculated from the integrated area of the low and high temperature peaks at specific temperatures throughout the peaks. The area under the low temperature peak was found by integrating the area under both peaks, from the initial rise of the low temperature peak to the tail of the high temperature peak, followed by subtraction of the high temperature peak area. The 47/69 area ratio at five temperatures in the low temperature peak are equivalent to the unreacted mPFAE1 fragmentation pattern. At temperatures below 180 K, the high temperature peak 47/69 area ratios are consistent with

TABLE 5.III

Comparison of low and high temperature 47/69 peak area ratios at several temperatures for each peak.

Low Temperature Peak				High Temperature Peak		
Temp. K	Ave.	S. Dev.		Temp. K	Ave.	S. Dev.
130	11.0	2.3		165	10.0	3.1
135	10.8	2.0		170	10.2	3.7
140	10.8	1.8		175	10.6	4.3
145	10.9	1.6		180	12.4	4.5
150	11.1	1.0		185	13.2	4.6
155	11.9	0.95		190	15.6	3.8
				195	15.0	5.5
				200	19.2	6.4

the unreacted mPFAE1 fragmentation pattern. At 180 K and above, the 47/69 area ratios increased with increasing temperature and are greater than the ratios for the unreacted mPFAE1. The increase in 47/69 ratio with increasing temperature above 180 K indicates an enhanced reaction rate or possibly additional bond scission. Table 5.IV shows the monolayer peak 47/31 and 31/69 area ratios. An increase in the oxygenated fluorocarbon fragments evolving from the surface was observed at 180 K and above, when compared to the non-oxygenated fluorocarbon fragments. Contrary to clean iron surface TPD results, no change was observed in the 31/69 ratio. The enhanced rate may also be contributing to the changing reaction order of the high temperature peak. Due to the lower coverages at the high temperatures, more error is introduced into the ratios calculated at temperatures above 180 K.

D. DISCUSSION

X-ray photoelectron spectroscopy (XPS) was used to investigate the interaction of three model fluorinated ethers, perfluoro-1-methoxy-2-ethoxy ethane, mPFAE1, perfluoro-1-methoxy-2-ethoxy propane, mPFAE2, and perfluoro-1,3-diethoxy propane, mPFAE3, with oxidized polycrystalline iron surfaces and polycrystalline iron surfaces modified with a chemisorbed oxygen overlayer. Temperature programmed

Table 5.IV

Comparison of the high temperature peak 47/31 and 31/69 peak area ratios.

Temperature (K)	47/31 Average	31/69 Average
160	23.6	37.9
165	23.7	38.6
170	24.4	38.7
175	24.8	37.0
180	25.8	39.1
185	27.0	39.4
190	27.3	41.0
195	31.8	39.7

desorption (TPD) was used to investigate the interaction of one model fluorinated ether, perfluoro-1-methoxy-2-ethoxy ethane, mPFAE1, with an oxidized polycrystalline iron surface. Low temperature adsorption, in the limit of low exposures, was molecular on both the oxidized iron surface and the iron surface modified with chemisorbed oxygen.

Chemisorbed oxygen was effective in reducing the reactivity of polycrystalline iron for chemisorption and decomposition of the model fluorinated ethers. The thickness of an ether layer, on a 100 K iron surface modified with chemisorbed oxygen, for a nominal 3 L exposure, is approximately one-half the thickness of the ether layer on the low temperature, clean iron surface for similar exposures. At the clean iron surface reaction temperature, the carbon and fluorine ratios and peak shapes and the 296/294 and 292/296 carbon ratios on the oxygen modified surface were virtually unaltered from the multilayer, 100 K XPS spectra. Iron fluoride formation, an additional indication of decomposition, was observed on the iron surfaces modified with an oxygen overlayer, at temperatures 5 K above the clean iron surface reaction temperatures. The amount of iron fluoride formed was significantly reduced when compared to the clean iron surface (Fig 5.6). The presence of an oxygen overlayer acts to significantly deactivate the iron surface toward PFAE

decomposition, presumably due to site blocking. Iron fluoride formation and the slight decrease in the carbon peak ratios, at temperatures near the clean iron surface reaction temperature, indicates that the decomposition detectable on the oxygen modified surfaces appears to proceed through the defluorination pathway operating on the clean iron surface. The residual decomposition can be attributed to incomplete oxygen coverage.

By way of comparison, passivation of Fe(110) toward CCl_4 decomposition, with preadsorbed oxygen, has also been reported.[18] Products from the mPFAE1 decomposition reaction, with an iron surface held at 165 K also passivated the iron surface and deactivated the decomposition reaction allowing for adsorption of molecular mPFAE1.[19]

Incorporation of an electronegative element, into a metal surface, produces localized Lewis acid and base sites on the surface.[20] On metal oxide surfaces the electron rich oxygen anions generally show basic, electron donating character and the electron deficient metal cations show acidic, electron accepting character. Lewis acids have been reported to cleave both the primary and secondary ether carbon oxygen bonds of polymeric perfluoroalkylethers.[5,9-11,21,22] The reactive degradation products, in particular COF_2, converted the metal oxides to metal fluorides. Metal halides are stronger Lewis acids than their corresponding

oxides and as a consequence are more reactive.[23] When $AlCl_3$ was used, the simultaneous replacement of α-fluorine with chlorine was also observed.[10]

A clean metal surface may act as either a Lewis acid or a Lewis base depending on the nature of the adsorbate.[20] The formation of localized Lewis acid and base sites through modification of a clean metal surface, with electronegative oxygen, would be expected to drastically alter the perfluoroalkylether, clean metal surface chemistry. On the clean iron surface, perfluoroalkylether decomposition proceeded through a defluorination pathway with formation of iron fluoride. Preferential attack occurred at the C-F bonds of the terminal fluoromethoxy of mPFAE1 and mPFAE2 and at the C-F bonds of CF_3/CF_2O of mPFAE3. The driving force of the reaction was proposed to be the formation of iron fluoride, a Lewis acid.

Perfluoro-1-methoxy-2-ethoxy ethane, mPFAE1, reacts on the oxidized iron surface via a pathway, similar to the pathways shown in Figures 1.2 and 1.3. This reaction pathway differs from the defluorination reaction observed on the clean iron surface. Just as on the clean iron surface, mPFAE1 reacts with loss of the methoxy intensity relative to CF_3/CF_2O. Contrary to the XPS results on clean iron, no increase in the 294 eV peak width nor growth in low binding energy CFO species at 292 eV and hydrocarbon-like species at

285 eV, was observed on the oxidized iron surface. On the oxidized iron surface the high binding carbon, oxygen and fluorine ratio of 1.7 : 1 : 4.8, at the reaction temperature, differs from the high binding energy ratio of 2.4 : 1 : 5.9 on the clean iron surface, at the reaction temperature and the mPFAE1 parent stoichiometric ratio of 2.5 : 1 : 6.0. The ratio on the oxidized iron surface indicates a deficiency in both carbon and fluorine and resembles the ratio expected for loss of CF_3, 2.0 : 1 : 4.5. The decrease in methoxy intensity and deficiencies in the high binding energy carbon and fluorine, with no corresponding increase in the low binding energy carbon and fluorine species on the surface, indicate fluorocarbon fragments, possibly CF_3, are leaving the surface with preferential attack again occuring at the terminal fluoromethoxy. Lewis acid assisted bond scission, of the carbon oxygen bond, has been reported to occur at both primary and secondary carbons of polymeric perfluoroalkylethers[9-11,21,22] and attack at the CF_3-O bond of mPFAE1 could account for the observed XPS results.

Several differences in the TPD results were also observed when comparing the clean and oxidized iron surfaces. At temperatures below 180 K, no change in the fragmentation pattern of the monolayer peak was observed when compared to the multilayer peak. At 180 K and above,

an increase in the oxygenated fluorocarbon fragment, CFO (mass 47), was observed when compared to CF (mass 31) and CF_3 (mass 69) with no change in the 31/69 fluorocarbon fragment ratio. On the clean iron surface, the opposite results were obtained with an increase in the CF (mass 31) and CF_2 (mass 50) relative to the CF_3 (mass 69) and no change in the 47/69 ratio. The increase in oxygenated fluorocarbon fragments from the high temperature region of the monolayer peak is also consistent carbon-oxygen bond breaking at CF_3-O, with the fluorocarbon species forming bonds to surface oxygen prior to evolution from the surface or carbon-oxygen bond breaking at CF_3O-CF_2. The second possibility contradicts the XPS results, which point to CF_3-O bond scission. However using XPS, only the early stages of the decomposition reaction are monitored and in this stage in which the 47/69 ratio is unchanged from the molecular fragmentation pattern, CF_3-O bond scission may be dominant. As the reaction proceeds, increases in the 47/69 ratio are observed and CF_3O-CF_2 bond scission may also occur.

The fact that iron fluoride is not observed on the surface at the reaction temperature and there is no significant change in the 31/69 ratio throughout the monolayer peak indicates that, at least initially, no C-F bonds are broken.

The peak width of the monolayer TPD peak on the

oxidized iron increases with increasing exposure, whereas on the clean iron surface the peak width is constant with exposure. The tailing or broadening of the monolayer peak on the oxidized iron surface and the increasing 47/69 and 47/31 ratios can be understood in terms of a surface which does not passivate, but becomes more reactive with time. The conversion of a metal oxide to the corresponding metal fluoride, a stronger Lewis acid, has been reported for Al_2O_3 and Fe_2O_3 in contact with polymeric perfluoroalkylethers.[9,21,22] In this work, a small amount of iron fluoride was observed using XPS at temperatures 50 K above the initiation of reaction.

Due to the repulsive interaction between the highly electronegative fluorines of the fluorinated ether and the highly electronegative oxygens on the surface, the mPFAE2 and mPFAE3 desorb prior to decomposition. Additionally the presence of the pendant perfluoromethyl group of perfluoro-1-methoxy-2-ethoxy propane, mPFAE2, may sterically hinder access to the ether carbon oxygen bond.

CHAPTER VI

MODEL FLUORINATED ETHERS ON "HIGH TEMPERATURE" METAL SURFACES

A. INTRODUCTION

In conjunction with the Air Force Office of Scientific Research, the summer of 1991 was spent at Wright Labs, Wright Patterson Air Force Base. X-ray photoelectron spectroscopy (XPS) was used to study the surface chemistry of two additional model fluorinated ether compounds on various metal surfaces. The two model perfluoroalkylethers (mPFAE) investigated were perfluorodimethoxy methane, $CF_3OCF_2OCF_3$, and its corresponding ring structure, perfluorodioxalane, $-CF_2OCF_2CF_2O-$. The model structures are monomer units of polymeric materials being considered for use as high temperature lubricants. These low molecular weight structures have the same functional units as the polymeric materials, but yield results which are simpler to interpret. The metal surfaces investigated were atomically clean polycrystalline nickel, iron and chromium and oxidized iron, held at a constant specified temperature between room temperature and 200°C.

Related "high temperature" experiments conducted at Northwestern University will also be discussed. The interaction of perfluoro-1-methoxy-2-ethoxy ethane, mPFAE1, with an atomically clean iron surface held at ambient temperatures and 165 K, and a 165 K iron surface, modified with 1 ML of chemisorbed oxygen, was investigated using XPS and Secondary Ion Mass Spectrometry (SIMS). mPFAE1 was

observed to defluorinate on the room temperature and the 165 K surface, with deposition of a carbon and oxygen layer in the stoichiometric ratio of the parent. The carbon and oxygen reaction products passivated the 165 K iron surface, allowing for adsorption of molecular perfluoro-1-methoxy-2-ethoxy ethane. Precoverage of the iron surface with an overlayer of chemisorbed oxygen, also deactivates the iron surface toward mPFAE1 decomposition.

B. EXPERIMENTAL

1. Wright Patterson

The XPS measurements were conducted in a Surface Science Instruments (SSI) small spot XPS, with typical base pressures of $4x10^{-10}$ torr. The XPS chamber was equipped with Al monochromatic x-ray source for sample analysis and a manipulator for positioning the sample. An attached side chamber, with typical base pressures of $5x10^{-9}$ torr, contained an Ar ion gun for sample cleaning and a stainless steel leak valve for controlled dosing.

The polycrystalline metal foils were polished, using standard metallographic techniques to a mirror finish, followed by ultrasonic cleaning in acetone to remove the polishing residue. The metal foils were atomically cleaned in vacuum, with cycles of Ar^+ bombardment and annealing. The metal foil surfaces were considered clean when

contaminants, in particular carbon, oxygen, sulfur and nitrogen, could not be detected using XPS. Heating and dosing of the metal foils was performed in the side chamber and then the foils were transferred into the XPS chamber for analysis. Gases were admitted into the side chamber, through a variable stainless steel leak valve with no directionality. The atomically clean iron foils were heated to 400°C and exposed to 200-400 L of room air to oxidize the surface. The fluorinated ether and room air exposures were calculated from uncalibrated ion gauge readings and are reported in Langmuir (1 L = $1x10^{-6}$ torr-sec). The XPS chamber had no facilities for sample cooling, heating or dosing and the side chamber had no facilities for cooling.

The two model perfluoroalkylethers investigated were synthesized and purified at Wright Labs. The initial purity was not available, but at the time the experiments were conducted the purity of both mPFAEs was estimated to be at a minimum 90 - 95 %. The purity of perfluorodiemthoxy methane was later found to be significantly less pure than originally estimated. Perfluorodimethoxy methane impurities consisted of CF_3OCF_3 and a hydrogen terminated structure, $CF_2HOCF_2OCF_3$. Prior to introduction into the vacuum chamber, the mPFAEs were further purified by repeated freeze-pump-thaw cycles.

Because of the lack of cooling, XPS spectra of the

unreacted fluorinated ethers could not be obtained. XPS spectra of the reacted mPFAEs were obtained following exposure of the clean metal and the oxidized metal surfaces, held at a constant, specified temperature, between room temperature and 200°C, to increasing exposures of mPFAE.

2. Northwestern University

The XPS and SIMS experiments were conducted in a VG Scientific ESCALAB/SIMSLAB Mk. II, with typical base pressures of $1x10^{-10}$ torr. The XPS experimental setup has been described in detail in the previous chapters.

The SIMS system was equipped with an Ar ion sputter gun, quadrupole mass analyzer and a sample manipulator. The iron surfaces were dosed with fluorinated ether in the XPS chamber and then transferred into the SIMS chamber for analysis. The samples could not be dosed or cooled in the SIMS chamber.

C. RESULTS

1. Ambient Temperature

At the time the experiments were conducted, the purity of the mPFAEs was estimated to be at a minimum 90 - 95 %. After these experiments had been completed, perfluorodimethoxy methane was found to be significantly less pure than originally estimated. Perfluorodimethoxy methane impurities consisted of CF_3OCF_3 and a hydrogen

terminated structure, $CF_2HOCF_2OCF_3$. The purity estimate of the perfluorodioxalane used for these experiments was not revised from the original estimate.

Exposure of clean polycrystalline nickel, chromium and iron surfaces to approximately $1X10^5$ L of perfluorodioxalane, the ring structure, at ambient temperatures and 200°C, results in the deposition of submonolayer to monolayer coverages of carbon and oxygen, observed at 285.0 and 532.0 eV, respectively and minimal growth in an inorganic fluoride, observed at 684.0 eV. No correlation was observed between the low binding energy carbon and oxygen ratio and the stoichiometric carbon and oxygen ratio of the parent molecule. Additionally, the amount of carbon and oxygen deposited could not be correlated to exposure. The carbon and oxygen layer was severely deficient in fluorine.

The following results were obtained using the impure perfluorodimethoxy methane material.

Shown in Figure 6.1a is the C(1s) spectrum for a room temperature, clean iron surface exposed to $1x10^5$ L of perfluorodimethoxy methane. The progression of carbon binding energies shown in Fig. 6.1a, corresponds to CF at 289.0 eV, CO at 286.1 eV and carbon at 284.8 eV and at 283.4 eV. Exposure of a clean iron surface, held at 80°C and 200°C, to perfluorodimethoxy methane results in a similar

a)

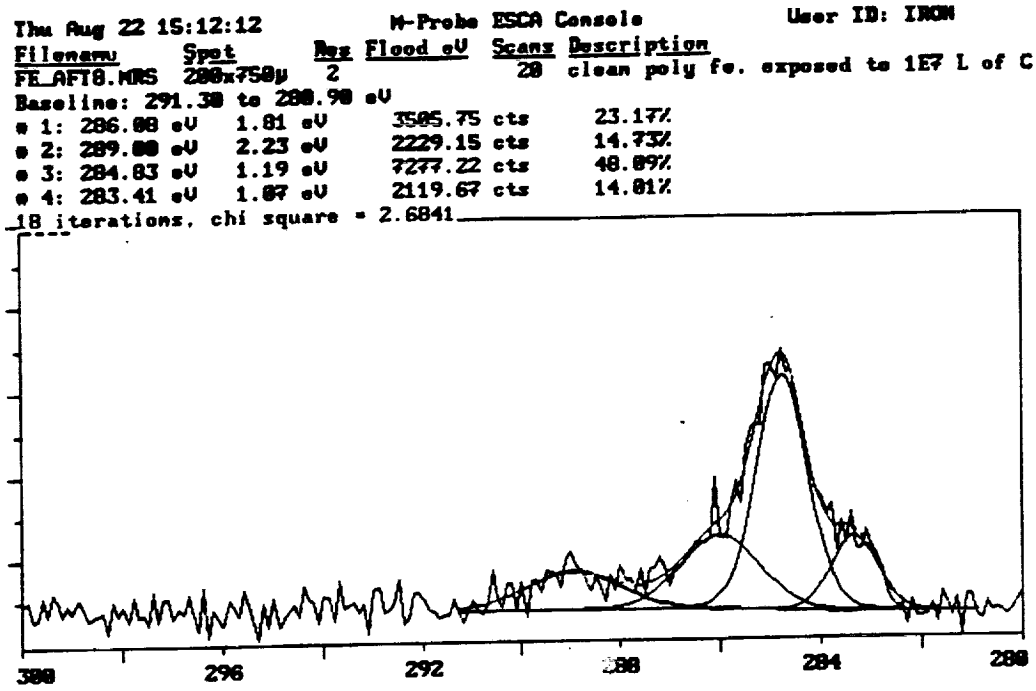

b)

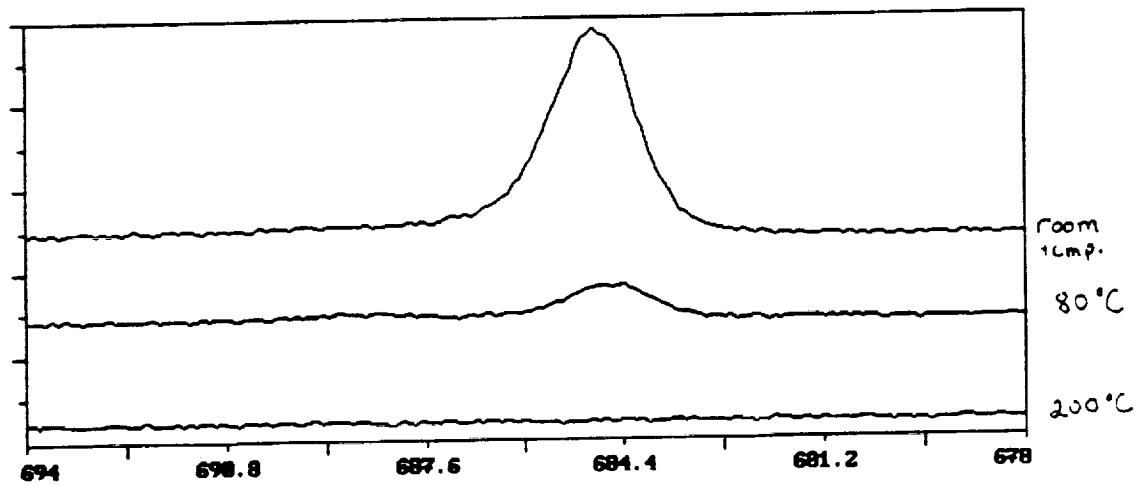

Figure 6.1 Perfluorodimethoxy methane exposed clean, polycrystalline iron surface. **a)** C(1s) spectrum at room temperature **b)** F(1s) spectra at room temperature, 80°C and 200°C.

progression of deposited carbon species. Shown in Figure 6.1b is the F(1s) spectra for a perfluorodimethoxy methane exposed clean iron surface held at ambient temperatures, 80°C and 200°C. The fluorine species at 684.0 eV corresponds to an inorganic fluoride, due to formation of a metal fluoride. At the higher temperatures carbon and fluorine deposition was reduced and at 200°C very little carbon and fluorine were deposited.

Shown in Figure 6.2a is the C(1s) spectrum for a room temperature oxidized iron surface, exposed to perfluorodimethoxy methane. The progression of carbon binding energies, shown in Fig. 6.2a corresponds to CF at 289.0 eV, CO at 287.0 eV and carbon at 284.8 eV. Carbon deposition on the clean iron surface is approximately three times greater than the carbon deposition on the oxidized iron surface. Exposure of an oxidized iron surface perfluorodimethoxy methane, held at 80°C, 150°C and 200°C, results in a similar progression of deposited carbon species. The F(1s) spectra for perfluorodimethoxy methane exposed oxidized iron surface, held at ambient temperatures, 80°C, 150°C and 200°C, are shown in Figure 6.2b. The fluorine species at 684.0 eV corresponds to an inorganic fluoride, due to formation of metal fluoride. As the temperature was increased carbon and fluorine deposition was reduced.

a)

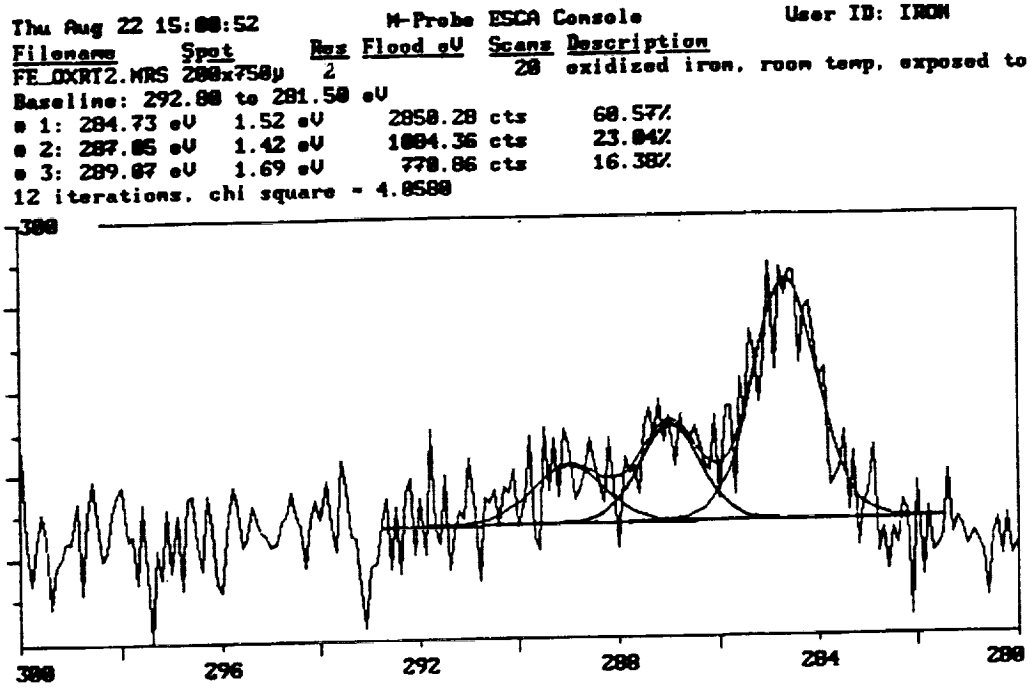

b)

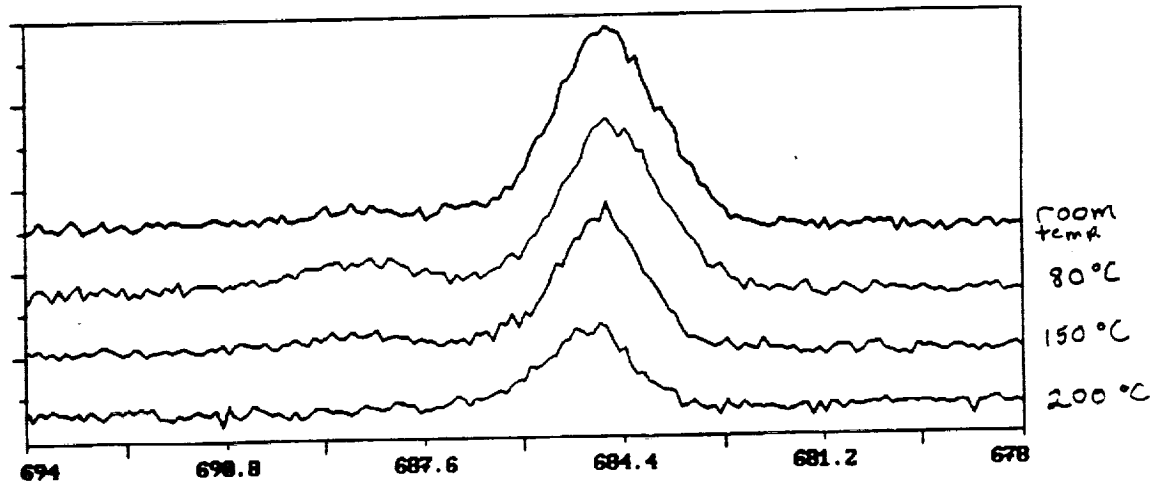

Figure 6.2 Perfluorodimethoxy methane exposed oxidized iron surface. **a)** C(1s) spectrum at room temperature **b)** F(1s) spectra at room temperature, 80°C, 150°C and 200°C.

Perfluorodimethoxy methane was purified, and the experiments described above for the clean metal surfaces were repeated by Wright Patterson personnel. The results obtained using the pure linear material are similar to the results observed for the ring structure. Exposure of clean, polycrystalline nickel, chromium and iron surfaces, held at ambient temperatures and 200°C, to $1x10^5$ L of the pure perfluorodimethoxy methane resulted in deposition of carbon and oxygen, observed at 285.0 and 532.0 eV, respectively and minimal growth in an inorganic fluoride. No correlation was found between the low binding energy carbon and oxygen ratio and the stoichiometric carbon and oxygen ratio of the parent molecule. The deposited carbon and oxygen layer was severely deficient in fluorine. The oxidized iron surface chemistry was not investigated using the pure material.

An atomically clean iron surface, held at ambient temperature, was exposed to a series of perfluoro-1-methoxy-2-ethoxy ethane, mPFAE1 exposures. Dissociative adsorption was observed on the room temperature iron surface, with deposition of low binding energy carbon and oxygen in the stoichiometric ratio of the parent and minimal growth in an inorganic fluoride. The low binding energy carbon and oxygen growth terminated at approximately 1 ML, with passivation of the iron surface toward further mPFAE1 decomposition. Covalently bonded fluorine and high binding

energy carbon and oxygen, characteristic of intact mPFAE1 were not observed.

2. 165 K

An atomically clean iron surface held at 165 K was exposed to a series of perfluoro-1-methoxy-2-ethoxy ethane exposures. Dissociative adsorption was observed on the 165 K, clean iron surface, with deposition of a low binding energy carbon and oxygen layer, in the stoichiometric ratio of the parent and minimal growth in an inorganic fluoride. Covalently bonded fluorine, characteristic of unreacted fluorinated ether, was observed to adsorb once a passivation layer, consisting of the carbon and oxygen reaction products, was formed. Shown in Figure 6.3a are the carbon, oxygen and fluorine spectra for a cumulative dose of 2.4 L, the total exposure at which covalently bonded fluorine was first observed. For doses larger than 2.4 L, very little growth is noticed in the carbon and oxygen peak area, attesting to the fact that the iron surface has been passivated. The strong temperature dependence of the mPFAE1 adsorption, the lower atomic sensitivities of carbon and oxygen and the reduced count rate using the Al monochromatic source, made it difficult to detect the high binding energy carbon and oxygen species.

The low binding energy carbon and oxygen layer grew in with increasing exposure until the surface was passivated,

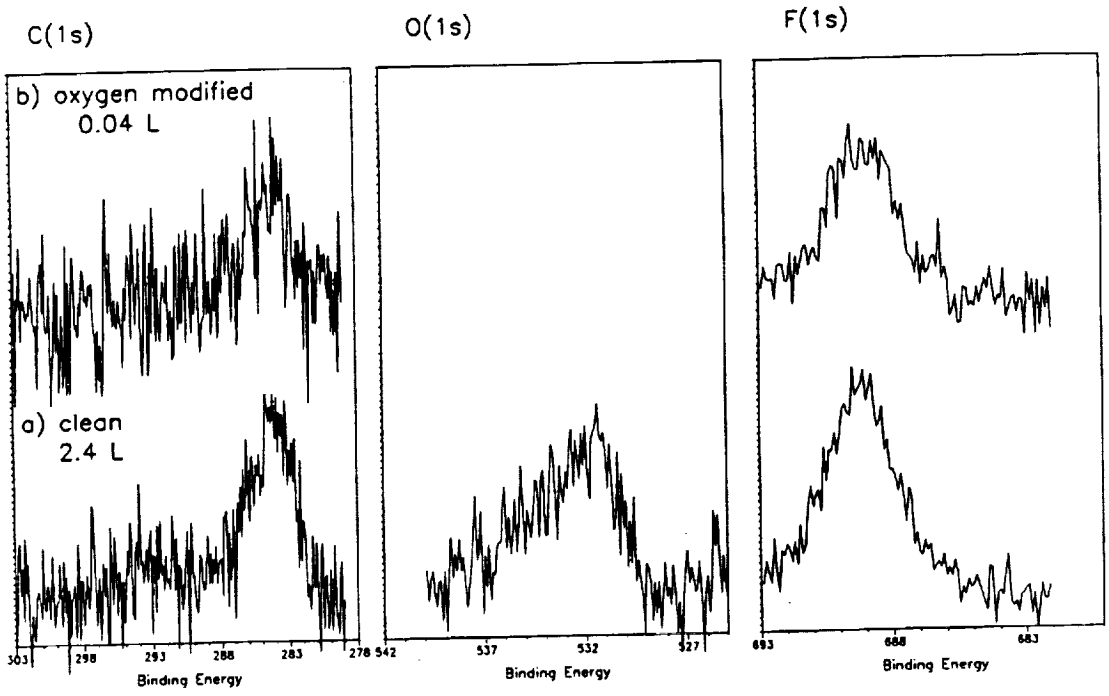

Figure 6.3 **a)** C(1s), O(1s) and F(1s) spectra for a 165 K, clean polycrystalline iron surface exposed to a 2.4 L cumulative dose of mPFAE1. **b)** C(1s) and F(1s) for an iron surface, chemically modified with oxygen, was exposed to a 0.04 L cumulative dose of mPFAE1. Oxygen acts to deactivate the iron surface toward mPFAE decomposition.

with only minimal growth in the low binding energy fluorine. This low binding energy carbon+oxygen layer was severely deficient in fluorine. SIMS has a significantly lower limit of detection than XPS and was used to detect the formation of iron fluoride. A positive SIMS analysis of the mPFAE1 exposed iron surface, detected signals at m/e=19 and 75, corresponding to F^+ and FeF^+. A negative SIMS analysis of the mPFAE1 iron surface, detected a very strong m/e=19 signal corresponding to F^-. The positive and negative SIMS analysis of FeF_3 pressed into In foil exhibited peaks for F^+, FeF^+, Fe^+, Fe_2^+ and F^-, consistent with the SIMS analysis of the mPFAE1 exposed iron surface. FeF_3 powders also exhibited a small signal for FeF_2^+, which was not observed on the mPFAE1 exposed iron surface. Iron fluoride is formed on the mPFAE1 exposed iron surface, but at relatively low levels. The SIMS instrument was not properly calibrated for quantitative depth profiling experiments, but an estimate for the monolayer lifetime was calculated to be 2.5×10^3 seconds.[1] Fluorine counts, m/e=19, were observed at sputter times in excess of 1.3×10^4 seconds. Fluorine is believed to exist in a subsurface region, where the signal may be partially attenuated by the carbon and oxygen reaction products.

Precoverage of the iron surface, with an overlayer of

oxygen deactivates the decomposition reaction. Shown in Figure 6.3b are the carbon and fluorine spectra for a cumulative dose of 0.04 L, the exposure at which covalently bonded fluorine was first observed on the oxygen modified surface. This exposure is significantly smaller than the exposure needed prior to the observation of covalently bonded fluorine on the clean iron surface.

D. DISCUSSION

Molecular adsorption of perfluorodioxalane should result in a C(1s) spectrum with two peaks; CF_2O_2 at 295.0 eV and CF_2O at 294.1 eV in a 1:2 ratio. Two peaks are also anticipated in the C(1s) spectra for molecular adsorption of perfluorodimethoxy methane; CF_3O at 296.0 eV and CF_2O_2 at 295.0 eV in a 2:1 ratio and for molecular adsorption of perfluoro-1-methoxy-2-ethoxy ethane; CF_3O at 296.0 eV and CF_3/CF_2O at 294.1 eV. Oxygen and fluorine binding energies expected for unreacted mPFAE are 535.5 eV and 689.0 eV, respectively. XPS spectra acquired for the model fluorinated ether, exposed metal surfaces at 165 K and ambient temperatures, are not the spectra described for the adsorption of the unreacted model fluorinated ethers. Shifts were observed in the carbon, oxygen and fluorine binding energies to lower than expected values, characteristic of C-F bond breaking and metal fluoride bond

formation.

Experiments performed at 165 K revealed that mPFAE1 fragmented on the iron surface, with deposition of low binding energy carbon and oxygen, in the stoichiometric ratio of the parent and formation of metal fluoride. The reaction observed is consistent with defluorination of the parent, with the carbon and oxygen from the fragmented molecule remaining on the surface. This reaction mechanism has been supported by additional low temperature experiments, which are discussed in detail in Chapter IV. The deposited carbon and oxygen layer is severely fluorine deficient. Using SIMS, fluorine species, possibly iron fluorides, were detected in the subsurface region. The fluorine deficiency may be due to attenuation of the fluorine signal by the carbon and oxygen reaction products on the surface. Attenuation of the fluorine signal may also be due to diffusion of fluorine into the bulk of the polycrystalline iron at defect sites and along grain boundaries. The migration of atoms and molecules to steps and defects sites upon adsorption and the propensity for incorporation into the lattice at these sites is well documented.[2,3] Grain boundaries provide an efficient path for atomic movement into the bulk.[4]

The perfluorodioxalane, perfluorodimethoxy methane and mPFAE1 room temperature, iron experiments are also

consistent with defluorination, with deposition of a low binding energy carbon and oxygen layer, deficient in fluorine. The ratio of the deposited carbon and oxygen layer for mPFAE1 was similar to the parent ratio, whereas the carbon and oxygen ratio for perfluorodioxalane and perfluorodimethoxy methane deviated significantly from the parent. The deviation in the carbon and oxygen ratio from the parent could be a result of evolution of reaction products at the higher surface temperatures. The surface chemistry observed for perfluorodioxalane and perfluorodimethoxy methane could also be due to impurities in the gas and unrelated to the main component. The exposures were large and the amount of carbon, oxygen and fluorine deposited small, so the observed chemistry, even of the relatively pure material, could be impurity controlled. The initial perfluorodimethoxy methane results shown in Figure 6.1 and 6.2, were clearly impurity driven. Because the surface could not be cooled to a low enough temperature to obtain a spectrum of the unreacted material, the reaction could not be followed and the reaction mechanism for perfluorodimethoxy methane and perfluorodioxalane could not be determined.

The $CF_3OCF_2OCF_3$ should be very reactive on both the clean metal and oxidized iron surfaces.[5-8] The terminal fluoromethoxy end group, CF_3O and the acetal unit, $O\text{-}CF_2\text{-}O$,

have both been reported to be vulnerable to attack.[5-11] Defluorination of the mPFAE1 on a clean iron surface was observed to proceed at low temperatures, 142 K and below, with preferential attack at the C-F bond of the terminal fluoromethoxy and formation of metal fluoride.[9-11] Fresh metal surfaces generated at a sliding contact were also very reactive toward polymeric perfluoroalkylether decomposition.[7,8] The polymeric materials, which contained the acetal unit, $O-CF_2-O$, readily decomposed under ambient sliding conditions, with evolution of COF_2 and saturated, low molecular weight fluorocarbons and formation of metal fluorides in the wear track.[7,8] Incorporation of an electronegative element into a metal surface produces localized Lewis acid and base sites on the surface.[12] Lewis acids have been reported to cleave both the primary and secondary ether carbon oxygen bonds of polymeric perfluoroalkylethers.[5,6,14-16] Lewis acid assisted cleavage of the carbon oxygen bond was observed at 138 K for perfluoro-1-methoxy-2-ethoxy ethane on oxidized iron surfaces, with preferential attack again occuring at the terminal fluoromethoxy, CF_3O.[17] Polymeric materials, containing an acetal unit, decomposed in the presence of Fe_2O_3 and Al_2O_3, with attack occuring preferentially at the acetal, $O-CF_2-O$, carbon oxygen bond.[5,6] Metal fluorides are stronger Lewis

acids than their corresponding oxides and as a consequence are more reactive, attacking polymeric fluorinated ethers with and without the vulnerable acetal unit.[14]

It is fairly clear that the perfluorodimethoxy methane should be reactive on the clean and oxidized metal surfaces. In addition to the other factors already discussed, the appearance of low reactivity or a reaction of questionable origin may be related to the relatively high temperature of the metal surfaces. Ethers weakly bond to metal surfaces through electron donation from an oxygen lone pair to the metal surface.[18] This interaction should contribute approximately 40 kJ/mol to the chemisorption bond strength, but will be weakened due to depletion of the electron density at the oxygen lone pairs due to fluorination.[18] Upon warming from 100 K, the majority of the fluorinated ethers desorb from the surface at temperatures well below ambient.[10,11] In a gas surface systems characterized by weak interactions, ΔH_{ads}<65 kJ/mol, a gas will have a short residence time on the surface.[19] The residence time necessary for mPFAE reaction is not known. On the 300 K surface, the residence time, especially for the smaller model compounds, may not be long enough to allow for a reaction to occur.

Comparing the impure perfluorodimethoxy methane results to the perfluorodioxalane results it was first thought that

the linear fluorinated ether was much more reactive on the clean metal surface than the ring structure. At that point in time, the ring structure was thought to be inherently more stable than the linear fluorinated ether. The experiments were repeated using the purified linear fluorinated ether and no differences were observed in the results for the linear and ring compounds on the clean, polycrystalline metal surfaces. The appearance of enhanced reactivity, for the perfluorodimethoxy methane was due to the two impurities, CF_3OCF_3 and $CF_2HOCF_2OCF_3$. The decomposition of three cyclic diethers, 1,3-dioxane, 1,4-dioxane and 1,3,5-trioxane, has been reported to proceed through a similar mechanism and to approximately the same extent as the corresponding linear hydrocarbon diethers on Ru(001).[20] The cyclization of the hydrocarbon ethers does not impart extra stability.[20] Extrapolating the results for hydrocarbon diether on ruthenium to the fluorinated diethers on iron, one would not expect the cyclic fluorinated ether to be any more stable than the linear. Whether this extrapolation is valid for the case of the cyclic fluorinated ethers is not known.

CHAPTER VII

SUMMARY

X-ray photoelectron spectroscopy (XPS) and temperature programmed desorption were used to study the adsorption and thermally activated decomposition of three model fluorinated ethers on atomically clean and oxidized polycrystalline iron surfaces and polycrystalline iron surfaces chemically modified with chemisorbed oxygen.

Before XPS could be used to investigate the surface chemistry of the model fluorinated ethers, it was necessary to study the effect of the probing photon beam. Perfluoro-1-methoxy-2-ethoxy ethane was observed to readily decompose upon exposure to the Al non-monochromatic x-ray source. Use of the Al monochromatic x-ray source eliminated the degradation over the experimental time frame by reducing the exposure of the adsorbed fluorinated ether layer to electrons, produced both internally and externally.

The model fluorinated ethers molecularly adsorb on the clean iron surface at 100 K. Defluorination of the model fluorinated ethers was observed at low temperatures, 155 K and below, on the atomically clean polycrystalline iron surfaces. Preferential attack occurred at the C-F bonds of the terminal fluoromethoxy of perfluoro-1-methoxy-2-ethoxy ethane, mPFAE1 and perfluoro-1-methoxy-2-ethoxy propane, mPFAE2 and at the C-F bond of CF_3/CF_2O of perfluoro-1,3-diethoxy propane, mPFAE3. Iron fluoride formation observed at the reaction temperature of the three model fluorinated

ethers is considered to be the driving force for the reaction. The reactivity of the iron surface toward mPFAE decomposition is due to the strength of the iron fluoride bond and the strong electron donating ability of iron.

Dissociative adsorption of the model fluorinated ethers was also observed on room temperature and 165 K, iron surfaces with deposition of low binding energy carbon and oxygen in the stoichiometric ratio of the parent, deficient in fluorine. The low binding energy carbon and oxygen growth terminated at approximately 1 ML, with passivation of the iron surface toward further mPFAE decomposition. Fluorine is believed to exist in the subsurface region, with the signal partially attenuated by the carbon and oxygen reaction products layer.

Chemisorption of an oxygen overlayer lowered the reactivity of an iron surface to adsorption and decomposition of the model fluorinated ethers, by blocking the active sites on the metal surface. Incomplete coverage of the iron surface results in a reaction, which resembles the defluorination reaction observed on the clean iron surface.

The model fluorinated ethers molecularly adsorb on an oxidized iron surface at 100 K. Perfluoro-1-methoxy-2-ethoxy ethane, mPFAE1 was observed to react on the oxidized iron surface via a pathway which differs from the

defluorination reaction observed on the clean iron surface. Perfluoro-1-methoxy-2-ethoxy ethane reacts on the oxidized iron surface through Lewis acid assisted cleavage of the ether carbon oxygen bond, with preferential attack at the terminal fluoromethoxy. The oxidized iron surface did not passivate, but became more reactive with time. Perfluoro-1-methoxy-2-ethoxy propane, mPFAE2 and perfluoro-1,3-diethoxy propane, mPFAE3 desorbed prior to the observation of decomposition on the oxidized iron surface.

References

References for Chapter I

(1) D. Sianesi, V. Zamboni, R. Fontanelli and M. Binaghi, Wear **18**, 85 (1971).

(2) C.E. Snyder, Jr. and R.E. Dolle, Jr., ASLE Trans. **19**, 171 (1976).

(3) W.R. Jones, Jr., K.J.L. Paciorek, T.I. Ito and R.H Kratzer, Ind. Eng. Chem. Prod. Res. Dev. **22**, 166 (1983).

(4) W.H. Gumprecht, ASLE Trans. **9**, 24 (1966).

(5) W.R. Jones, Jr., T.R. Bierschenk, T.J. Juhlke, H. Kawa and R.J. Lagow, NASA TM-87284 (1986).

(6) R.J. Lagow, U.S. Patent 4,523,039 (1985).

(7) K.J.L. Paciorek, R.H. Kratzer, J. Kaufman and J.H. Nakahara, J. Appl. Poly. Sci. **24**, 1397 (1979).

(8) C.E. Snyder, Jr., L.J. Gschwender and C. Tamborski, Lubr. Eng. **37**, 344 (1981).

(9) W.R. Jones, Jr., K.J.L. Paciorek, D.H. Harris, M.E. Smythe, J.H. Nakahara and R.H. Kratzer, Ind. Eng. Chem. Prod. Res. Dev. **24**, 417 (1985).

(10) T.N. Wittenberg, C.A. Svisco and W.E. Moddeman, Corrosion **36**, 517 (1980).

(11) W.L. Chandler, L.L. Llyod, M.M. Farrow, R.K. Burnham and E.E. Eyring, Corrosion **36**, 152 (1980).

(12) M.J. Zehe and O.D. Faut, Trib. Trans. **33**, 634 (1990).

(13) P.H. Kasai, W.T. Tang and P. Wheeler, Appl. Surf. Sci **51**, 201 (1991).

(14) D.J. Carre and J.A. Markowitz, ASLE Trans. **28**, 40 (1985).

(15) D. Sianesi and R. Fontanelli, Die Makromolekulare Chemie **102**, 115 (1967).

(16) G.V.D. Tiers, J. Am. Chem. Soc. **77**, 6703 (1955).

(17) S. Mori and Y. Imaizumi, Trib. Trans. **31**, 449 (1988).

(18) S. Mori, Appl. Surf. Sci. **27**, 401 (1987).

(19) C.M. Friend and E.L. Muetterties, J. Am. Chem. Soc. **103**, 773 (1981).

(20) G.A. Somorjai, Chemistry in Two Dimensions: Surfaces, (Cornell University Press, Ithaca, 1981), p.191.

(21) T.N. Rhodin and G. Ertl, The Nature of the Surface Chemical Bond (North Holland Publishing Company, Amsterdam, 1979), pp.342-346.

(22) S. Mori and W. Morales, Wear **132**, 111 (1989).

(23) S. Mori and W. Morales, Trib. Trans. **33**, 325 (1990).

(24) D.J. Carre, ASLE Trans. **29**, 121 (1986).

(25) D.J. Carre, Trib. Trans. **31**, 437 (1988).

(26) P.A. Dowben and R.G. Jones, Surf. Sci. **84**, 449 (1979).

(27) P.A. Dowben and R.G. Jones, Surf. Sci. **88**, 348 (1979).

(28) M. Grunze and P.A. Dowben, Appl. Surf. Sci. **10**, 209 (1982).

(29) R.Ch. Burshtein and N.A. Shurmovskaya, Surf. Sci. **2**, 210 (1964).

(30) D.R. Mueller, T.N. Rhodin and P.A. Dowben, J. Vac. Sci. Technol. A **4**, 1518 (1986).

(31) R. Mason and M. Textor, Proc. R. Soc. Lond. A. **356**, 47 (1977).

(32) R.G. Jones, Surf. Sci. **88**, 367 (1979).

(33) P.A. Dowben, M. Grunze, R.G. Jones and E. Illenberger, Ber. Bunsenges. Phys. Chem. **85**, 734 (1981).

(34) P.A. Dowben and M. Grunze, Ber. Bunsenges. Phys. Chem. **85**, 728 (1981).

(35) V.S. Smentkowski, C.C. Cheng and J.T. Yates, Jr., Surf. Sci. **220**, 307 (1989).

(36) V.S. Smentkowski, C.C. Cheng and J.T. Yates, Jr., Langmuir **6**, 147 (1990).

(37) V.S. Smentkowski and J.T. Yates, Jr., Surf. Sci. **232**, 92 (1990).

(38) V.S. Smentkowski and J.T. Yates, Jr., Surf. Sci. **232**, 102 (1990).

(39) M.M. Walczak, P.K. Leavitt and P.A. Thiel, J. Am. Chem. Soc. **109**, 5621 (1987).

(40) M.M. Walczak and P.A. Thiel, Surf. Sci. **224**, 425 (1989).

(41) M.M. Walczak, P.K. Leavitt and P.A. Thiel, Trib. Trans. **33**, 557 (1990).

(42) B.A. Sexton and A.E. Hughes, Surf. Sci. **140**, 227 (1984).

(43) K.D. Rendulic and B.A. Sexton, J. Catal. **78**, 126 (1982).

(44) R.T. Sanderson, Chemical Bonds and Bond Energy, 2^{cd} ed. (Academic Press: New York, 1976), p. 147.

(45) V.S. Smentkowski, M.D. Ellison and J.T. Yates, Jr., Surf. Sci. **235**, 116 (1990).

(46) V. Maurice, K. Takeuchi, M. Salmeron and G.A. Somorjai, Surf. Sci. **250**, 99 (1991).

References for Chapter II

(1) C.D. Wagner, W.M. Riggs, L.E. Davis, J.F. Moulder and G.E. Muilenberg, Handbook of X-ray Photoelectron Spectroscopy (Perkin Elmer Corporation, Eden Prairie, MN, 1979).

(2) G.A. Somorjai, Chemistry in Two Dimensions: Surfaces (Cornell University Press, Ithaca, NY, 1981).

(3) M. Briggs and M.P. Seah, Practical Surface Analysis by Auger and X-ray Photoelectron Spectroscopy (John Wiley and Sons, Chichester, 1983).

(4) D.T. Clark and H.R. Thomas, J. Polym. Sci. Polym. Chem. **16**, 791 (1978).

(5) R.J. Madix, in Chemistry and Physics of Solid

Surfaces, edited by R. Vanselow and S.Y. Tong (CRC Press, 1979), Vol. 2.

(6) P.A. Redhead, Vacuum **12**, 203 (1962).

(7) J.L. Falconer and R.J. Madix, J. Catal. **48**, 262 (1977).

(8) J.C. Vickerman, A. Brown and N.C. Reed, Secondary Ion Mass Spectrometry: Principles and Applications (Clarendon Press, New York, 1981).

References for Chapter III

(1) J.M. Ajello, T.W. Huntress, Jr. and P. Rayermann, J. Chem. Phys. **64**, 4746 (1976).

(2) R. Schumacher, H.-R. Sprunken, A.A. Christodoulides, and R.N. Schindler, J. Phys. Chem. **82**, 2248 (1978).

(3) S.D. Peyerimhoff and R.J. Buenker, Chem. Phys. Lett. **65**, 434 (1979).

(4) P.A. Dowben and M. Grunze, Ber. Bunsenges. Phys. Chem. **85**, 728 (1981).

(5) W.K. Fisher and J.C. Corelli, J. Polym. Sci. Polym. Chem. Ed. **19**, 2465 (1981).

(6) D.R. Wheeler and S.V. Pepper, J. Vac. Sci. Technol. **20**, 226 (1982).

(7) D.T. Clark and W.J. Brennan, J. Electron Spec. and Rel. Phenom. **41**, 399 (1986).

(8) D.R. Wheeler and S.V. Pepper, J. Vac. Sci. Technol. A **8**, 4046 (1990).

(9) R.R. Rye and N.D. Shinn, Langmuir **6**, 142 (1990).

(10) M. Briggs and M.P. Seah, Practical Surface Analysis by Auger and X-ray Photoelectron Spectroscopy (John Wiley and Sons, Chichester, 1983), p. 53.

References for Chapter IV

(1) W.H. Gumprecht, ASLE Trans. **9**, 24 (1966).

(2) C.E. Snyder, Jr., L.J. Gschwender and C. Tamborski, Lubrication Eng. **37**, 433 (1981).

(3) C.E. Snyder, Jr. and R.E. Dolle, Jr., ASLE Trans. **19**, 171 (1976).

(4) D. Sianesi, V. Zamboni, R. Fontanelli, and M. Binaghi, Wear **18**, 85 (1971).

(5) K.J.L. Paciorek, R.H. Kratzer, J. Kaufman, and J.H. Nakahara, J. Appl. Polym. Sci. **24**, 1397 (1979).

(6) W.R. Jones, Jr., K.J.L. Paciorek, T. Ito, and R.H. Kratzer, Ind. Eng. Chem. Prod. Res. Dev. **22**, 166 (1983).

(7) W.R. Jones, Jr., K.J.L. Paciorek, D.H. Harris, M.E Smythe, J.H. Nakahara, and R.H. Kratzer, Ind. Eng. Chem. Prod. Res. Dev. **24**, 417 (1985).

(8) W.L. Chandler, L.B. Lloyd, M.M. Farrow, R.K. Burnham, and E.M. Eyring, Corrosion **36**, 152 (1980).

(9) M. Grunze and P.A. Dowben, Appl. Surf. Sci. **10**, 209 (1982).

(10) K. Kishi and S. Ikeda, J. Phys. Chem. **78**, 107 (1974).

(11) A.P.C. Reed, R.M. Lambert and J.S. Foord, Vacuum **33**, 707 (1983).

(12) E. Bechtold and H. Leonhard, Surf. Sci. **151**, 521 (1985).

(13) D.R. Mueller, T.N. Rhodin and P.A. Dowben, J. Vac. Sci. Technol. A **4**, 1518 (1986).

(14) R. Mason and M. Textor, Proc. R. Lond. A. **356**, 47 (1977).

(15) P.A. Dowben and M. Grunze, Ber. Bunsenges. Phys. Chem. **85**, 728 (1981).

(16) P.A. Dowben, M. Grunze, R.G. Jones, and E. Illenberger, Ber. Bunsenges. Phys. Chem. **85**, 734 (1981).

(17) V.S. Smentkowski, C.C. Cheng and J.T. Yates, Jr., Langmuir **6**, 147 (1990).

(18) V.S. Smentkowski and J.T. Yates, Jr., Surf. Sci. **232**, 92 (1990).

(19) V.S. Smentkowski, C.C. Cheng and J.T. Yates, Jr., Surf. Sci. **220**, 307 (1989).

(20) M.E. Napier and P.C. Stair, J. Vac. Sci. Technol. A **9**, 649 (1991).

(21) M.E. Napier and P.C. Stair, J. Vac. Sci. Technol. A, accepted for publication.

(22) D.R. Wheeler and S.V. Pepper, J. Vac. Sci. Technol. A **8**, 4046 (1990).

(23) G. Broden, G. Gafner and H.P. Bonzel, Surf. Sci. **84**, 295 (1979).

(24) C.D. Wagner, W.M. Riggs, L.E. Davis, J.F. Moulder, G.E. Muilenberg, Handbook of X-ray Photoelectron Spectroscopy (Perkin Elmer Corporation, Eden Prairie, MN, 1979), p.5.

(25) R.T. Sanderson, Chemical Bonds and Bond Energy, 2^{cd} ed. (Academic Press, New York, 1976), pp.82 and 147.

(26) P.A. Redhead, Vacuum **12**, 203 (1962).

(27) D.T. Clark and H.R. Thomas, J. Polym. Sci. Polym. Chem. **16**, 791 (1978).

(28) J.L. Falconer and R.J. Madix, J. Catal. **48**, 262 (1977).

(29) V.S. Smentkowski, and J.T. Yates, Jr., Surf. Sci. **232**, 102 (1990).

(30) M.M. Walczak, P.K. Leavitt and P.A. Thiel, J. Am. Chem. Soc. **109**, 5621 (1987).

(31) M.M. Walczak and P.A. Thiel Surf. Sci. **224**, 425 (1989).

(32) M.M. Walczak, P.K. Leavitt and P.A. Thiel, Trib. Trans. **33**, 557 (1990).

(33) H.J. Eneleus and A.G. Sharpe, Advances in Inorganic Chemistry and Radiochemistry (Academic Press, New York, 1981), Vol. 24.

(34) H.A. Porter, E. Greenberg and W.N. Hubbard, J. Phys.

Chem. **69**, 2308 (1965).

(35) J.B. Benziger and R.J. Madix, J. Catal. **65**, 36 (1980).

(36) J.B. Benziger and R.J. Madix, J. Catal. **65**, 49 (1980).

(37) J.B. Benziger and R.J. Madix, J. Catal. **74**, 55 (1982).

(38) K.D. Rendulic and B.A. Sexton, J. Catal. **78**, 126 (1982).

(39) B.A. Sexton and A.E. Hughes, Surf. Sci. **140**, 227 (1984).

(40) S.M. Gates, J.N. Russell, Jr. and J.T. Yates, Jr. Surf. Sci. **171**, 111 (1986).

(41) T.N. Rhodin and G. Ertl, The Nature of the Surface Chemical Bond (North Holland Publishing Company, Amsterdam, 1979), pp.342-346.

(42) G.A. Somorjai, Chemistry in Two Dimensions: Surfaces (Cornell University Press, Ithaca, 1981), p.191.

(43) I. Kaur and W. Gust, Fundamentals of Grain and Interphase Boundary Diffusion (Ziegler Press, Stuttgart, 1989), pp. 1-18.

(44) R.Ch. Burshtein and N.A. Shurmovskaya, Surf. Sci. **2**, 210 (1964).

(45) S. Mori, Wear **132**, 111 (1989).

(46) S. Mori, Appl. Surf. Sci **27**, 401 (1987).

(47) C.M. Friend and E.L. Muetterties, J. Am. Chem. Soc. **103**, 773 (1981).

References for Chapter V

(1) W.H. Gumprecht, ASLE Trans. **9**, 24 (1966).

(2) C.E. Snyder, Jr., L.J. Gschwender and C. Tamborski, Lubrication Eng. **37**, 344 (1981).

(3) C.E. Snyder, Jr. and R.E. Dolle, Jr., ASLE Trans. **19** 171 (1976).

(4) D. Sianesi, V. Zamboni, R. Fontanelli, and M. Binaghi, Wear **18**, 85 (1971).

(5) K.J.L. Paciorek, R.H. Kratzer, J. Kaufman, and J.H. Nakahara, J. Appl. Polym. Sci. **24**, 1397 (1979).

(6) W.R. Jones, Jr., K.J.L. Paciorek, T. Ito, and R.H. Kratzer, Ind. Eng. Chem. Prod. Res. Dev. **22**, 166 (1983).

(7) W.R. Jones, Jr., K.J.L. Paciorek, D.H. Harris, M.E. Smythe, J.H. Nakahara, and R.H. Kratzer, Ind. Eng. Chem. Prod. Res. Dev. **24**, 417 (1985).

(8) W.L. Chandler, L.B. Lloyd, M.M. Farrow, R.K. Burnham, and E.M. Eyring, Corrosion **36**, 152 (1980).

(9) D.J. Carre and J.A. Markowitz, ASLE Trans. **28**, 40 (1985).

(10) G.V.D. Teirs, J. Am. Chem. Soc. **77**, 6703 (1955).

(11) D. Sianesi and R. Fontanelli, Die Makromolekulare Chemie **102**, 115 (1967).

(12) G. Broden, G. Gafner and H.P. Bonzel, Surf. Sci. **84**, 295 (1979).

(13) C.D. Wagner, W.M. Riggs, L.E. Davis, J.F. Moulder, G.E. Muilenberg, Handbook of X-ray Photoelectron Spectroscopy (Perkin Elmer Corporation, Eden Prairie, MN, 1979), p.5.

(14) R.T. Sanderson, Chemical Bonds and Bond Energy, 2^{cd} ed. (Academic Press, New York, 1976), pp.82 and 147.

(15) P.A. Redhead, Vacuum **12**, 203 (1962).

(16) D.T. Clark and H.R. Thomas, J. Polym. Sci. Polym. Chem. **16**, 791 (1978).

(17) J.L. Falconer and R.J. Madix, J. Catal. **48**, 262 (1977).

(18) V.S. Smentkowski, M.D. Ellison and J.T. Yates, Jr., Surf. Sci. **235**, 116 (1990).

(19) M.E. Napier and P.C. Stair, J. Vac. Sci. Technol. A **9**, 649 (1991).

(20) P.C. Stair, J. Am. Chem. Soc. **104**, 4044 (1982).

(21) M.J. Zehe and O.D. Faut, Trib. Trans. **33**, 634 (1990).

(22) P.H. Kasia, W.T. Tang and P. Wheeler, Appl. Surf. Sci. **51**, 201 (1991).

(23) K. Tanabe, Solid Acids and Bases (Academic Press, New York, 1970), pp. 45-80.

References for Chapter VI

(1) J.C. Vickerman, A. Brown and N.C. Reed, Secondary Ion Mass Spectrometry: Principles and Applications (Clarendon Press, New York, 1981), p. 10.

(2) T.N. Rhodin and G. Ertl, The Nature of the Surface Chemical Bond (North Holland Publishing Company, Amsterdam, 1979), pp. 342-346.

(3) G.A. Somorjai, Chemistry in Two Dimensions: Surfaces (Cornell University Press, Ithaca, 1981), p. 191.

(4) I. Kaur and W. Gust, Fundamentals of Grain and Interphase Boundary Diffusion (Ziegler Press, Stuttgart, 1989), pp. 1-18.

(5) M.J. Zehe, and O.D. Faut, Trib. Trans. **33**, 634 (1990).

(6) P.H. Kasia, W.T. Tang, and P. Wheeler, Appl. Surf. Sci. **51**, 201 (1991).

(7) S. Mori, Wear **132**, 111 (1989).

(8) S. Mori and W. Morales, Trib. Trans. **33**, 325 (1990).

(9) M.E. Napier and P.C. Stair, J. Vac. Sci. Technol. A **9**, 649 (1991).

(10) M.E. Napier and P.C. Stair, J. Vac. Sci. Technol. A., accepted.

(11) M.E. Napier and P.C. Stair, J. Am. Chem. Soc., submitted.

(12) P.C. Stair, J. Am. Chem. Soc. **104**, 4044 (1982).

(13) K.J.L. Paciorek, R.H. Kratzer, J. Kaufman, and J.H.

Nakahara, J. Appl. Polym. Sci. **24**, 1397 (1979).

(14) D.J. Carre and J.A. Markowitz, ASLE Trans. **28**, 40 (1985).

(15) G.V.D. Teirs, J. Am. Chem. Soc. **77**, 6703 (1955).

(16) D. Sianesi and R. Fontanelli, Die Makromolekulare Chemie **102**, 115 (1967).

(17) M.E. Napier and P.C. Stair, Appl. Surf. Sci., submitted.

(18) M.M. Walczak, P.K. Leavitt and P.A. Thiel, J. Am. Chem. Soc. **109**, 5621 (1987).

(19) G.A. Somorjai, Chemistry in Two Dimensions: Surfaces (Cornell University Press, Ithaca, 1981), p. 178.

(20) M.M. Walczak and P.A. Thiel, Surf. Sci. **238**, 180 (1990).

APPENDIX A

TEKNIVENT SOFTWARE

Software made and distributed by the Teknivent Corporation is available for the control, data collection and data analysis of a Balzers QM511 mass spectrometer. The Teknivent manual is available for in-depth review of the capabilities of the software package. This appendix will briefly outline steps to help a new user and to highlight problem areas.

A. INSTALLATION

1. Install the Vector/One diskette in drive A.
2. Type A:Install C
3. Change the autoexec.bat and the config.sys if necessary to accommodate needed file and buffer space.
4. Reboot computer

The installation creates a new directory called dataaq. To run the software type startup at the dataaq> prompt.

B. PCSPEC SOFTWARE

Typing startup at the dos prompt brings up the main menu. Option 1 and 6 are operational for our specific configuration. The other options listed are not applicable or are not functional. Option 6 is T-Plot which sets up plotting parameter files for mass spectrometer data. This is covered in the manual very clearly and in a straight forward manner and will not be repeated here.

Option 1, PCSPEC, is the heart of the software program and will be discussed in more detail. When option 1 is selected the following selections are presented,

0 Exit

1 Perform Mass Spec Calibration

2 Set Up Data Acquisition Request and Start

3 Process Already Acquired Data

9 Define Hardware/Spectrometer Configuration

Usually the hardware/spectrometer configuration setup, 9, is only run once when the software is first initiated for a given mass spectrometer. It is used to define the characteristics of the mass spectrometer and hardware so that it is controlled correctly.

1. Mass Calibration

During the calibration, two important parameters need to be adjusted, the settling times and the peak positions. The settling time is defined as the amount of time the mass spectrometer waits before sampling the next mass intensity. Three different step sizes need to be set, 10 amu, 1 amu and > 1 amu. This adjustment is quite critical. The procedure outlined in the Teknivent manual can be used reliably if it is understood that the suggested settling times are too small. The Balzers manual quotes a data collection speed, which is not realistic. It is based on the rise time of the peak and not the fall time, with the fall time being

significantly longer. The settling times suggested in the manual must be based on the rise time. If the data collection speed is not set slow enough you will see intensity leaking. Intensity from one mass will spill over into the next collected mass. The procedure that I found to work the best is to set the settling times to values of 5, 75, 100, for example. Set up a mass acquisition for a number of masses, an intense fragment followed by a mass where no intensity should be observed, which are separated by differing step sizes. If intensity is observed in the second mass, for the masses separated by 1 amu, then that settling time needs to be reset. The data collection speeds can also be slowed by setting a high filter time constant or increasing the integration time.

Peak positions are set in the mass calibration frame. The position of a mass is altered by using one of the mass/found at field pairs. A coarse calibration is done using a real time survey (50-500 amu) of a given mass range. A fine calibration is done using a real time sweep (2-20 amu) of a given mass range. Up to sixteen calibration points can be entered by listing under mass the nominal *m/e* value and under found at the actual location on the mass axis. I have found that when a new calibration file is set up the first mass/found at field pair given must be 511 = 255. I don't know why this is the case, other than to say

it is a glitch in the program. To generate a new calibration curve press the page down key. This internalizes the new mass/found at field pairs entered.

Several calibration files can be generated and stored for different uses, compounds etc. The specific calibration file to be used for a data acquisition only needs to be indicated prior to data collection.

2. Data Acquisition/Processing Acquired Data

Option 2, data acquisition defines the parameters that control how the data is acquired. Option 3, processing acquired data allows the user to view, process and obtain reports from the pcspec acquired data. The parameters are all well explained in the manual. The manual should be consulted for further description.

3. Miscellaneous

All special software keys are clearly defined in the Teknivent manual.

Currently the VM512 board is installed in the Balzers mass spectrometer. The Balzers manual provides a detailed description of the board and its functions. The VM512 board can be run in a 10 or 12 bit data format, selectable with jumpers. The 10 bit data format was selected. When the 12 bit format is selected the electrometer current can no longer be read on the console. Additionally, the board can be run at two scan speeds, 16 μs/measurement or 78

μs/measurement, selectable by jumpers. The slower scan speed was selected because of the improved filter action. To change any of these settings remove the board and follow the procedure outlined in the manual.